Surfaces and Interfaces 70 (2025) 106794

Contents lists available at ScienceDirect

Surfaces and Interfaces

journal homepage: www.sciencedirect.com/journal/surfaces-and-interfaces

A review on transparent superhydrophobic coatings for self-cleaning solar cell panels: Its fabrication, robustness and industrial implementation

Sagar S. Ingole [a,1], Rajaram S. Sutar [b], Pradip P. Gaikwad [a,1], Akshay R. Jundle [a,1], Rutuja A. Ekunde [a,1], Shanhu Liu [b,*], Sanjay S. Latthe [a,1,*]

[a] Self-cleaning Research Laboratory, Department of Physics, Vivekanand College (Empowered Autonomous), Kolhapur, 416003, India
[b] College of Chemistry and Molecular Science, Henan University, Kaifeng, 475004, China

ARTICLE INFO

Keywords:
Superhydrophobicity
Transparency
Solar cell cover glass
Solar cell efficiency
Self-cleaning coatings

ABSTRACT

Photovoltaic cells, which convert solar energy into electric energy through the photovoltaic effect, have emerged as a highly promising avenue for green and sustainable energy production. However, the accumulation of dust, bacterial growth, snow, and airborne particles on outdoor photovoltaic solar panels may impede solar light absorption and significantly reduce solar cell efficiency and power production. Therefore, regular cleaning is crucial for maintaining consistent solar cell output, but it can be a tedious process that diminishes the solar panel lifespan. To address this issue, transparent superhydrophobic coatings have the potential to provide self-cleaning abilities as well as transparency enable sunlight to reach solar cells. Understanding the fundamentals of synergistic effect of superhydrophobicity and transparency of coatings on the cover glass of solar cell panels is crucial for sustaining efficiency and longevity. This review provides an overview of the fundamentals of superhydrophobicity, self-cleaning properties, and transparency of coatings. It comprehensively explores various sophisticated techniques for fabricating transparent self-cleaning superhydrophobic coatings and summarizes different methods for testing their durability. It also overviews the advancements in applying transparent self-cleaning superhydrophobic coatings directly onto solar panel cover glass for potential real-world applications. Finally, the review concludes by addressing current challenges and offering recommendations for future research directions. This review offers valuable insights for those new to researching and creating transparent superhydrophobic coatings, particularly for safeguarding cover glass on photovoltaic solar cells.

1. Introduction

With the rapid advancement of economic and social development, renewable and green energy technologies have gained more attention [1,2]. Solar energy is a widely recognized renewable energy source, characterized by its cleanliness and eco-friendliness. The sun consistently emits photon energy in the form of electromagnetic radiation, providing a continuous and abundant energy supply to our planet [3]. Solar cells operate on the principle of the photovoltaic effect, where incoming photons from the sun are absorbed by semiconductor materials, leading to the generation of electricity [4]. The efficiency of solar cells relies on their ability to absorb sunlight. Solar cells are typically protected by cover glass to shield them from environmental damage. However, these cover glasses are prone to contamination from ubiquitous dust particles, which settle on the glass surface due to gravitational force. Moreover, bacterial growth, snow fall, and airborne particles on outdoor photovoltaic solar panels cover glass can hinder the solar light absorption, consequently reduces power generation [5,6]. Also, soiling is a significant concern in solar power research, particularly in arid regions with high solar irradiance. Water droplets, which accumulate on the soil contaminated glass surface of solar panels from rain or dew, present challenges for their efficiency. The impact of dew on soiling, in comparison to light rain, is still not well understood, despite the influence of factors like humidity [7].

Regular cleaning and maintenance of solar panels are essential for consistent performance. There are several manual cleaning methods have been used for frequently cleaning solar panels [8]. Fig. 1 provides a comprehensive overview of various manual and automatic cleaning methods for solar panels. As depicted in Fig. 1a, labourers utilize various materials such as mop, cloth, water, detergent or acid to manually clean

* Corresponding authors.
E-mail addresses: liushanhu@vip.henu.edu.cn (S. Liu), latthes@gmail.com (S.S. Latthe).
[1] Affiliated to Shivaji University, Kolhapur.

https://doi.org/10.1016/j.surfin.2025.106794
Received 13 March 2025; Received in revised form 15 May 2025; Accepted 23 May 2025
Available online 24 May 2025

the panels. These methods need a substantial trained man-force, not only to operate the cleaning equipment efficiently but also to ensure safety during the process. While this method offers several advantages in small scale, it also comes with notable drawbacks. A significant concern is that the use of hard brushes or excessive suction can scratch the glass surface of the panels, which in turn diminishes their sunlight absorption efficiency [9].

In contrast, the automatic cleaning methods shown in Fig. 1b involve robotic devices and automated cleaning systems that dispense water directly onto the solar panels [10]. Although these advanced technologies may initially offer an appealing solution, they require significant investment and ongoing maintenance expenses that can challenge the economic feasibility of implementation. Furthermore, these automated machines often consume large volumes of water and electricity to operate effectively [11]. During the cleaning process, they may not cover the entirety of the solar panels adequately, leading to areas that remain dirty and potentially diminishing overall energy output [12]. Consequently, the high operational costs associated with these automated methods could undermine the environmental and economic benefits that solar energy systems are intended to provide [13].

To address this challenge, the application of a transparent self-cleaning superhydrophobic coatings on solar cell panel cover glass proves to be reliable solution for mitigating the adhesion of dust particles [12], dew and rain [14], bacterial growth [15], snow [16], and airborne particles [17]. The application of such coatings not only improves the performance of solar panels but also increases their lifespan. Additionally, these coatings align with broader objectives such as transitioning to cleaner and more sustainable energy sources. In the realm of renewable energy systems, addressing the challenges posed by environmental contaminants on solar cell cover glass is essential to fully harness the potential of solar energy. The integration of self-cleaning technology onto solar cell cover glass is of significant interest in current research due to several reasons: (i) the growing global demand for solar energy necessitates the installation and development of new solar cells [18], (ii) the need to address challenges associated with manual cleaning processes [19], (iii) the reduction of efficiency losses resulting from environmental contaminants [20], and (iv) the potential energy savings and minimal environmental impact offered by self-cleaning technology through the reduction of manual cleaning processes [21].

In recent decades, superhydrophobic coatings have found various applications such as self-cleaning [22], anti-fogging [23], anti-icing [24], oil-water separation [25], and photothermal actuators [26]. Of particular interest is the development of transparent superhydrophobic self-cleaning cover glass for photovoltaic solar cell applications, which has garnered substantial attention. Numerous studies have applied transparent superhydrophobic coatings to photovoltaic solar cells and conducted thorough analyses of their performance in real-world outdoor conditions. Various advanced fabrication techniques, such as chemical vapor deposition (CVD), spin coating, dip coating, spray coating, electrospinning, laser deposition, lithography, sputtering, atmospheric plasma pressure spray and spray and wipe, have been extensively explored to engineer innovative surface structures with superhydrophobic properties. Each of these fabrication methods offers unique parameters for controlling the surface characteristics of the coatings. Additionally, ensuring the stability of the surface structure of the coatings is essential for their potential applications. As a result, researchers and industry professionals have developed several sophisticated mechanical testing methodologies to evaluate the durability and performance of these coatings in demanding environments [27]. These testing methods include the adhesive tape test [28], sandpaper abrasion test [29], water droplet impact test [30], sand particle impact test [31], pencil hardness test [32], chemical stability testing [33], cross-cut test [34] and cleanliness testing with dyne pens [35] all of which are widely documented in the literature and are employed to assess the quality and resilience of the coatings.

In this review, we conduct a detailed overview of superhydrophobic and transparent coatings for solar cell panel cover glass, focusing on their impact on enhancing photovoltaic solar cell performance. The existing reviews cover application of transparent superhydrophobic coatings for self-cleaning purposes, they often lack information on fabrication techniques and mechanical strength assessments [36–42]. Therefore, we discuss various fabrication techniques for preparing transparent self-cleaning superhydrophobic coatings and their corresponding mechanical strength testing methods. Additionally, we provide an overview on progress of the direct application of transparent superhydrophobic coatings for solar panel cover glass in outdoor settings, including an assessment of their real-world performance and durability. Finally, we identify current challenges in this field and propose potential directions for future research.

2. Fundamentals of transparent superhydrophobic coatings

2.1. Wetting phenomenon

The phenomenon of wettability refers to the interaction of liquid with a solid surface. This behaviour is affected by the chemical and microscopic surface structure of the solid materials, typically measured using the contact angle. A contact angle is determined by surface tension between solid, air, and liquid. Fig. 2 illustrate the different wetting state of solid surface based on the water contact angle which shows the

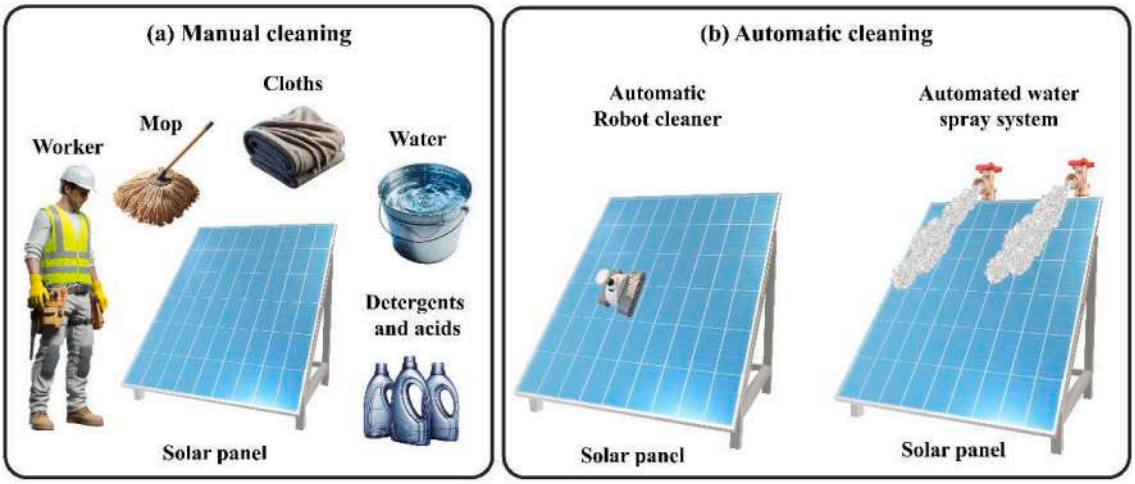

Fig. 1. (a) Manual and (b) automatic cleaning methods of solar panel.

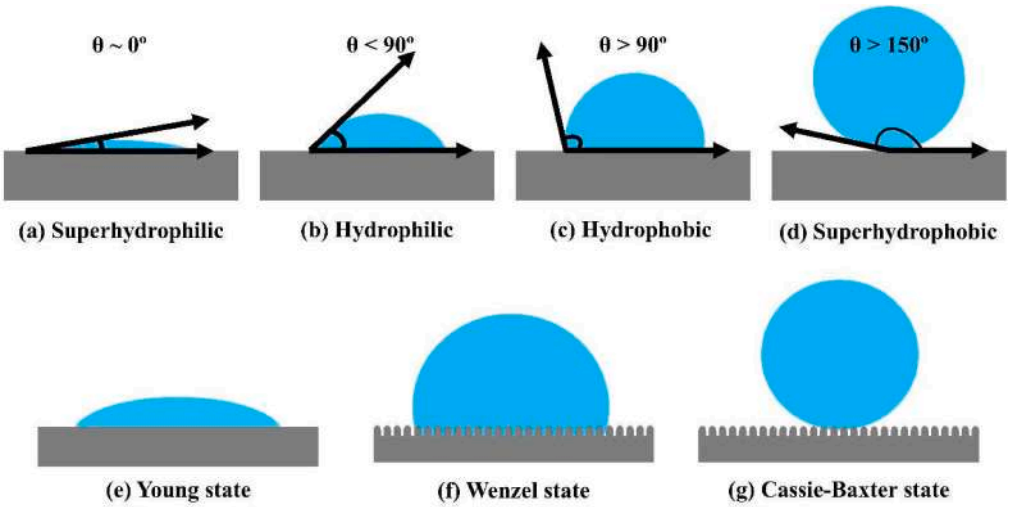

Fig. 2. Schematic representation of wetting behaviour of water droplet on solid surface defined as (a) superhydrophilic, (b) hydrophilic, (c) hydrophobic, and (d) superhydrophobic. Schematic depiction of the different wetting states namely, (e) Young, (f) Wenzel, and (g) Cassie-Baxter state.

interaction of water droplet to the solid surface. Fig. 2a depicts the complete wetting the solid surface and formation of thin film of water by spreading across the surface. This state of liquid form WCA close to 0° indicating superhydrophilic surface due to high affinity towards solid surface [215]. In hydrophilic state, the water droplet makes a water contact angle (WCA) less than 90°. The water droplet makes more rounded shape than superhydrophilic state on solid surface but still spread to some extent is depicted in Fig. 2b. The water droplet started to bead up rather than spreading if WCA is higher than 90° (Fig. 2c). The higher contact angle reduces the contact area between water and solid surface and leads towards to attain nearly spherical shape of water droplet. Fig. 2d depicts the water droplet formed almost spherical shape with negligible contact with solid surface. This state is known as superhydrophobic surface where surface exhibit extreme water repellence towards water droplets. Therefore, an interaction of water droplets lies within two extreme points of wetting state, complete wetting to repelling it [43].

A British physicist Thomas Young conducted groundbreaking research on surface wettability, specifically by measuring liquid contact angle. He introduced a theory known as Young's model, which focuses on the interaction between liquids and perfectly smooth solid surfaces. Young's model highlights the importance of low surface free energy in creating hydrophobic surfaces, with an emphasis on surface properties that repel water. However, it's essential to note that Young's theory is most relevant to idealized, uniform solid surfaces. The Young model is generally suitable for ideally smooth and uniform solid surfaces (Fig. 2e). However, in practical applications, solid surfaces tend to exhibit inherent roughness. Robert Wenzel addressed this issue by establishing the connection between solid surface roughness and contact angle. He observed that when a liquid comes into contact with a solid surface, it seeps into microscopic grooves, which increases the actual contact area beyond initially apparent contact area (Fig. 2f). This discovery prompted the adaptation of Young's model to account for surface roughness. Altering the surface roughness of a material can improve the hygroscopic properties of hygroscopic materials and enhance the liquid repellent property of materials [44].

However, in practical scenarios a liquid is unable to seep or only partially seep to the rough porous structures of a low surface energy solid surface. When a droplet interacts with a surface exhibiting a high degree of roughness, a layer of air becomes trapped between the liquid and the solid (Fig. 2g). This unique phenomenon was first reported by Cassie and Baxter, has significant implications for surface science and engineering applications. The contact angle of the hydrophobic material increases notably with increasing surface roughness in both the Wenzel and Cassie-Baxter models. However, there are significant differences in hysteresis angles between these two models. In the Wenzel state, the droplet fully seeps the small grooves of the rough surface, leading to a high hysteresis angle. Conversely, in the Cassie-Baxter state, the penetration of liquid droplets into the small grooves of the rough surface is prevented, resulting in a very small hysteresis angle. In the pursuit of developing superhydrophobic surface with self-cleaning capabilities, it is recommended to engineer surfaces that mimic the Cassie-Baxter model. The phenomenon of superhydrophobicity is characterized by WCA (θ) typically exceeds 150° along with rolling angle lower 10° [45]. The low sliding angle (θs) is particularly significant for self-cleaning behaviour, as it facilitates removal of dirt or dust particles by water droplets [46]. Development of a superhydrophobic surface relies on the presence of micro-nano scale rough structured surface topography [47, 48], along with low surface energy chemical composition of surface. Rough structured surface topography can effectively trap air in porous regions, resulting in minimize solid-liquid adhesion. Coatings with low surface energy materials containing hydrophobic groups that effectively repel water [49–51].

2.2. *Superhydrophobic self-cleaning mechanism*

The Nelumbo Nucifera lotus plant has been a subject of great interest in researchers due to its remarkable superhydrophobicity and self-cleaning properties, known as the "Lotus Effect" [52]. When a water droplet comes in contact with the surface of the lotus leaf, it does not adhere to surface and quickly roll down from the surface. As a result, the rolling water droplets gather and carry away dirt particles efficiently. Therefore, effectively cleans the surface itself. This natural self-cleaning ability has captured the attention of the scientific community and has the potential to inspire innovation in science and technology [53–56]. The superhydrophobicity of lotus leaf is attributed to micro-scale papillae and nano-scale hydrophobic epicuticular waxy materials [57]. The interaction between surface roughness and chemical composition requires for the development of an artificial superhydrophobic surface that mimics the water-repelling properties of lotus leaves. Hence, the synergy between the surface roughness and chemical composition requires to preparation artificial superhydrophobic surface which closely mimics like water-repellent nature of the lotus leaves [58–63]. Gravitation force on water droplets plays a pivotal role in self-cleaning process. During the self-cleaning process, it acts as a constant force to pull downward the spherical water droplet. The low adhesion property of the surface enables the rolling motion of water droplets downhill [64]. During the motion of the droplets, they entrain and encapsulate the dirt

particles present on the surface. The contaminated particles are effectively carried by water droplets and significantly enhance the self-cleaning capability as shown in Fig. 3.

2.3. Transparency, anti-reflection and superhydrophobicity

Optimizing both optical transparency and superhydrophobicity during the fabrication process is challenging. Optical transparency is the ability of a material to allow visible light to pass through without obstruction. However, to maintain superhydrophobic behaviour often require to produce a specific surface texture. On the other, while generation of rough texture it might possible that loss of transparency due to scattering of light. As a result, it can be quite challenging to design a surface that performs well in both areas at the same time [65]. Mie established a relationship between the scattering cross section (C_{SCS}) and the particle diameter (d) to quantify light scattering using the following Eq. (1) [66].:

$$Cscs = \frac{\pi d^2}{2} \sum_{n=1}^{\infty} (2n+1)(a_n + b_n) \quad (1)$$

Where a_n and b_n are the Mie coefficients of order n.

This equation indicates that the scattering cross-section is directly proportional to the square of the particle diameter, implying an upper limit for particle size. The particle diameter should be less than or equal to 100 nm. When this limit is exceeded, a rough surface can display superhydrophobicity but will also scatter incident light, diminishing surface transparency. Fig. 4 depicts the effect of light transmittance on a glass substrate with superhydrophobic coating fabricated via large particle size (greater than 100 nm) and small particle size (less than 100 nm). The scattering of incident light occurs when the deposited particle size is higher than 100 nm (Fig. 4a). In contrast, the deposition of less than 100 nm particles has a negligible impact on the incident light, allowing it to pass through the coated material (Fig. 4b). Hence, controlling the surface roughness by depositing small particle size particles is necessary to achieve higher transparency in superhydrophobic coating [67]. An elimination and/or reduction of the reflected light from the surface is known as anti-reflective surface. An elevation in the transmission light occurs through the rough surface. The micro-nano scale roughened surface lowering the refractive indices between solid as well as air interfaces of overall surface [68]. This property can be easily achieved by hierarchical rough structure of the superhydrophobic surface.

In the last decade, many efforts have been successfully achieved an excellent coating that exhibits optical transparency as well as superhydrophobicity simultaneously [69–74]. In-depth comprehension of light scattering on the rough surface is a pivotal aspect in the consideration of transparency and it is explained by Mie scattering [75]. The Mie scattering phenomenon becomes important when the microstructure of the coatings either approaches or surpasses the wavelength of visible light (400 - 700 nm) [76–78]. After several empirical investigations, it is revealed that the surface morphology (hierarchical structure) of less than 100 nm which is roughly one-quarter of a wavelength of visible light, offers the potential to coatings intermix the transparency with superhydrophobic property within the visible spectrum [67]. Cho et al. [66] studied the impact of surface roughness on the transparent superhydrophobic coating prepared via the spin coating technique. An elevation in surface roughness, there was no obvious reduction were observed to transmittance of coatings. Interestingly, the wetting behaviour was influenced by fractal nature of the coatings. Therefore, a comprehensive evaluation of the hierarchical surface can be represented by fractal dimension. Rather than simply elevating the surface roughness, a small sized nanoparticles can responsible to contribute higher WCA by producing complex structure to prepared coatings. Park et al. [79] used silica nanoparticles which exhibit a refractive index almost similar to air or transparent substrates can reduce the Mie scattering and maintain high transparency and superhydrophobicity. The high-water repellent property was achieved due to aggregation of the PDMS-coated silica nanoparticles and engineered hierarchical rough structure which can trap air pockets within it. This rough structure was confirmed with automic force microscope (AFM) analysis that reveals 189.1 nm rms value. Lin et al. [80] found that, in visible and near-IR spectrum the transmittance of the incident light was enhanced on the glass surface. This high transmittance occurred due to not only the formation of the small nanoparticles and nanorods via laser ablation but also the creation of smooth portions within micropits. The micropits topography enables the nanoscale roughness as well as

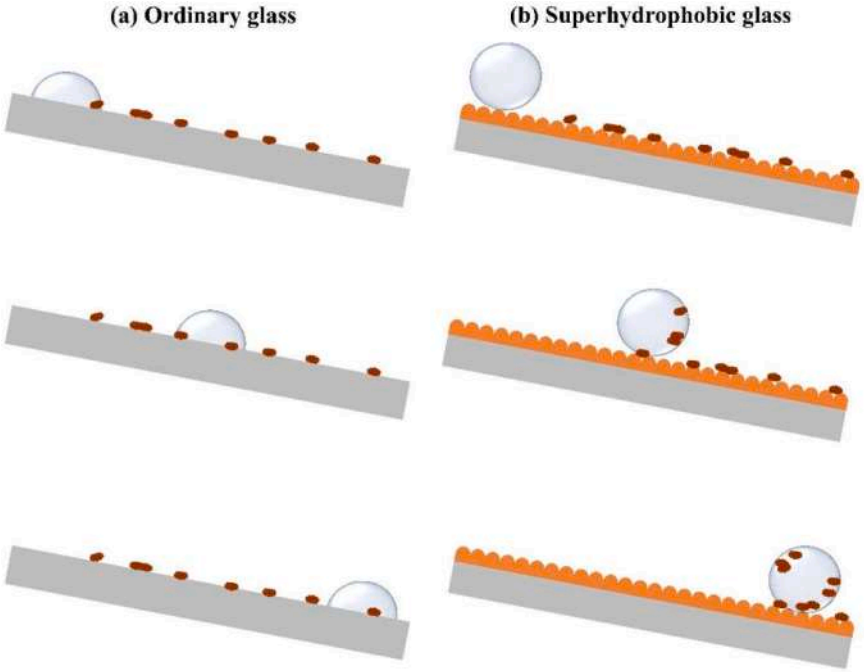

Fig. 3. Dynamic movement of water droplets on (a) ordinary and (b) superhydrophobic glass.

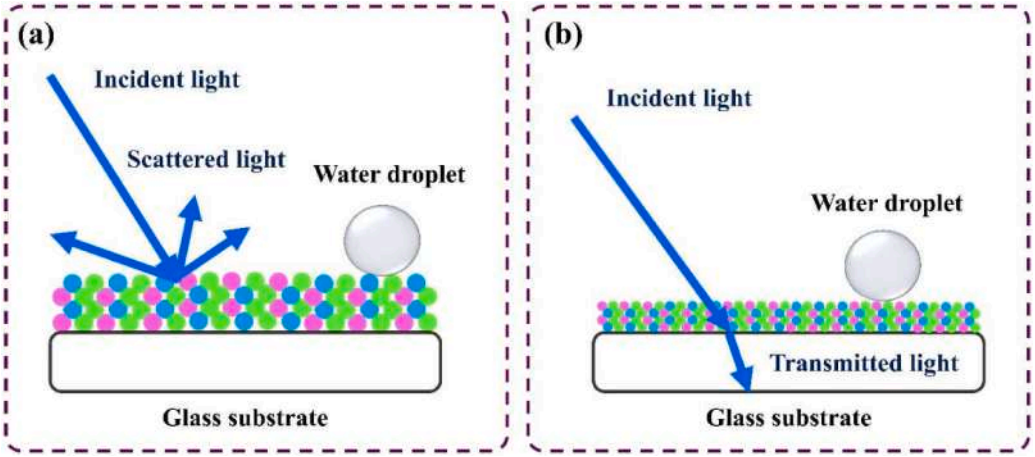

Fig. 4. Schematic representation of Mie scattering effect on rough surface created by (a) large and (b) small sized particles.

anti-reflection property which claims superhydrophobicity and transparency.

3. Fabrication techniques for transparent self-cleaning superhydrophobic coatings

The development of transparent superhydrophobic surfaces for commercial solar panels application necessitates the exploration of novel materials and fabrication methods. To achieve superhydrophobic surface mainly two steps are followed sequentially. A micro and nano rough structures are produced using nanomaterial-based composites followed by modification via low surface energy materials to enhance water repellent properties. In some cases, a hierarchical rough structure is developed on inherently hydrophobic materials to improve the water repellent properties [82–86]. Presently, most superhydrophobic coatings are produced through multi-step processes that roughen the material's surface, potentially compromising its transparency. Developing a simple, cost-effective, scalable, and environmentally friendly coating approach is essential. However, finding suitable materials, fabrication techniques, and cost-effective, durable, and eco-friendly superhydrophobic coatings for practical use continues to present significant challenges [87–90]. This section overviews the most promising fabrication techniques for transparent superhydrophobic coatings and their general overviews depicted schematically in Fig. 5.

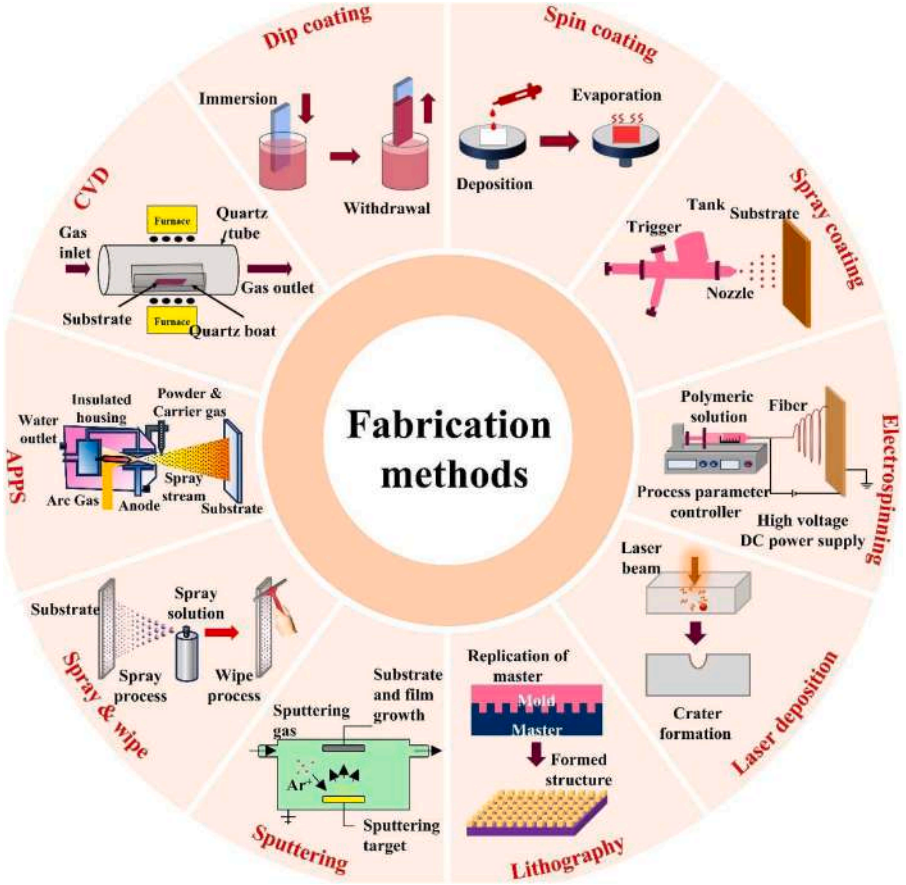

Fig. 5. Schematic illustrations of different fabrication methods for transparent superhydrophobic coating.

3.1. Chemical vapor deposition (CVD)

The process involves the interaction of gaseous molecules to substrate, resulting in the formation of a thin film on the substrate. When a low surface energy molecule in the vapor phase forms a fine structured surface, it leads to the creation of a hydrophobic or superhydrophobic surface. CVD is capable of producing well-defined nanostructures such as nanoparticles, nanotubes, nanofibers, nanorods, and nanobeads. An exhaust system is used to remove unreacted gaseous molecules from the chamber. However, challenges associated with CVD include achieving uniform coating, managing complex parameters (such as temperature, pressure, and gas flow rate) during large-scale applications, and the high expenses involved in equipment synthesis and maintenance [91–96,98].

Recently, Huang et al. [81] fabricated transparent superhydrophobic coating by the CVD method. In the fabrication process, the density of the formed nanocones of the coating was highly dependent on the

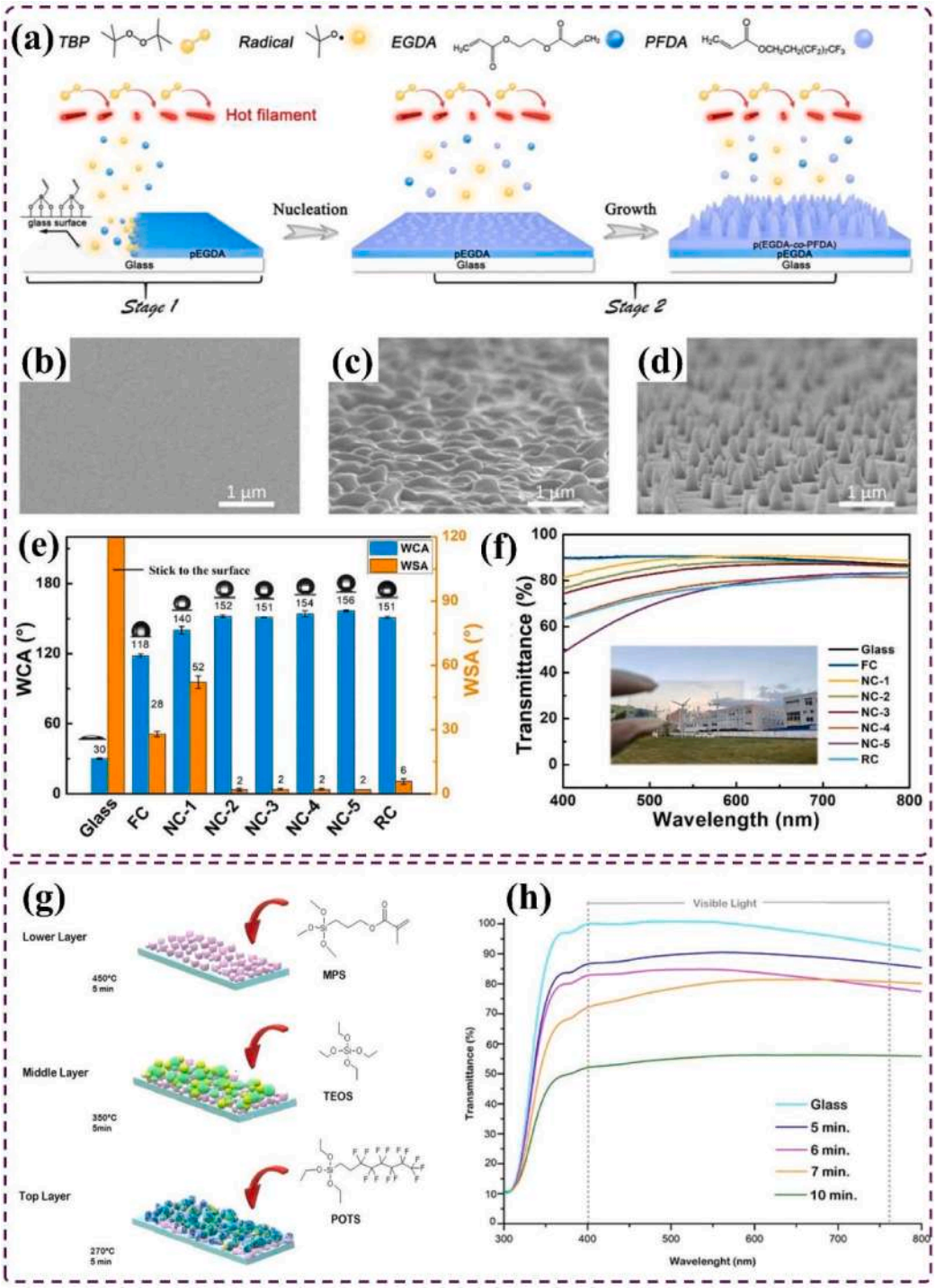

Fig. 6. (a) Schematic diagram of the growth of polymer nanocone array on the glass substrate and (b-d) their SEM micrographs. (e-f) Wettability and transmittance study of the pristine glass, FC-coated, RC-coated, and NC-coated samples. Reproduced from ref. [81] with permission from Elsevier, © 2023. (g) Schematic representation of the fabrication procedure of transparent superhydrophobic coating by CVD method. (h) Transmittance curves of different deposition times for each layer. Reproduced from ref. [99] with permission from Springer nature, © 2019.

monomer's saturation (P_m/P_{sat}) that leads to condensed monomer droplets which results in increased nanocore density. On the other hand, the height of the nanocone varied by deposition time (longer time leads to taller nanocones). The morphology of the higher nanocone resulted in a decrease in the transparency and vice versa. Therefore, for the achievement of high transmittance, the control on the nanocone parameter was highly important for better transparency as well as superhydrophobicity. The process involved feeding heated monomers into a custom-made reactor, where they condensed at the nanoscale and grew onto polymer nanocones (Fig. 6a). The alloy filament was heated to 220 °C, and the substrate temperature was maintained at 39 °C at a chamber pressure of 250 mTorr. The height and density of nanocones were controlled by adjusting deposition conditions such as flow rate and pressure with respect to stages and time of the monomers. The resulting nanocone array coating (NC) exhibited ordered nanocone arrays oriented vertically to the surface, displaying distinctive morphology compared to flat iCVD coating (FC) and rough iCVD coating (RC) as depicted in Fig. 6b-d. Wettability and transmission studies of pristine glass, FC, RC, and NC samples showed that the NC-coated samples exhibited higher WCAs due to increased roughness, except for the NC-1 sample, which had short and sparse nanocones. The increased density and height of nanocones caused a reduction in the transparency of NC-coated samples from NC-1 to NC-5 (Fig. 6e). An inset optical image in Fig. 6f depicts the visual transparency of the NC-3 sample.

Zhuang et al. [100] prepared a transparent superhydrophobic PTFE film via the single-step aerosol-assisted CVD method. The prepared films have showed extreme water repellence properties (WCA~168°) and maintained high optical transmittance greater than 90 %. A similar method was adopted by Tombesi et al. [99] for fabrication of transparent superhydrophobic layer with various layers on the glass surface. In this process, three layers of 3-methacryloxypropyltrimethoxysilane (MPS), tetraethyl orthosilicate (TEOS), and perfluorooctyltriethoxysilane (POTS) were applied to the glass surface at different temperatures with constant deposition time respectively (Fig. 6 g). The deposition time effects the transparency of the coating (Fig. 6h). The CVD method has been used in multiple iterations to create transparent superhydrophobic coatings. It's important to note that longer deposition times or denser nanostructures led to increased surface roughness, which compromised transparency. However, the single-step CVD method preserved both superhydrophobicity and transparency, eliminating the necessity for multi-step processes and allowing for large-scale production. In CVD-based fabrication process of superhydrophobic surfaces, perfluorocompounds such as POTS are commonly used due to their ability to lower surface energy as well as enhance water repellent properties. However, concerns about the safety and environmental persistence of fluorinated compounds can be raised. Their potential toxicity and long-term environmental impact have led to increased interest in developing fluorine-free alternatives for sustainable self-cleaning applications. Therefore, while perfluorosurfaces offer excellent performance a careful consideration of safety and regulatory aspects is important for real-world applications.

3.2. Sol-gel process

The sol-gel method is highly adaptable and user-friendly approach to create high-quality and multifunctional coatings with great control over their structure and properties all at relatively low temperatures and on various surfaces [101]. In this process, the molecular precursor transforms into a three-dimensional (3D) network within the aqueous solution through hydrolysis and polycondensation reactions [102]. Generally, the hydrolysis and condensation occur with metal alkoxides, where a water molecule react with it and replaces alkoxy groups by hydroxyl groups. This reaction can be catalysed by using acid or base. The reaction mechanism is shown as,

$$M(OR)n + nH_2O \rightarrow M(OH)n + nROH \quad (2)$$

Where, M is metal ion and R is organic group.

After hydrolysis, condensation reaction takes place where formation of M-O-M bonds occurred in 3D network. The reaction mechanism of condensation is given by,

$$M\text{-}OH + HO\text{-}M \rightarrow M\text{-}O\text{-}M + H_2O \quad (3)$$

The continuous network of metal oxide encases by solvent. The method exhibits several merits such as being environmentally friendly, cost-effective, operating in lower temperatures as well as enabling to crafting of a wide range of coatings and structures. Following the sol-gel method, techniques like dip [103], spin [104] and spray [105] coatings meticulously control the coating structure on the substrates. Furthermore, the sol-gel method can yield stable and transparent sol at room temperatures [106]. This stable sol can be used to coat the substrates via above mentioned techniques. Therefore, these techniques offer not only precision, and efficiency but also customization in the production of superhydrophobic coatings with exceptional properties. Hence, this method has vast use in fabricating superhydrophobic coatings with diverse nanostructures.

3.2.1. Dip coating

The dip coating technique consists of several steps: initially, the substrate is immersed in the coating solution. Subsequently, the substrate is lifted out of the solution, allowing any excess liquid to drip off, followed by the evaporation of the solvent [107]. Throughout this process, the thickness of the coatings can be regulated by adjusting the dipping and withdrawal speed [108]. A slow lifting of the substrate results in a thicker coating due to increased solvent evaporation, whereas rapid lifting leads to thinner coatings due to the combination of liquid adhesion and gravity [109–112]. The solution can be utilized until it completely evaporates from the container. Although this simple method has the potential for automation in the production process, it necessitates careful consideration of the physical and chemical properties of the solution to achieve the desired coating thickness.

Adak et al. [113] used a sol-gel process to produce a transparent superhydrophobic coating. They utilized a combination of acid and base-catalysed silica sol derived from TEOS precursor and applied it to a clean glass substrate using the dip coating technique (Fig. 7a). The speeds at which the coating was withdrawn ranged from 60 to 200 mm/min to assess the transmittance and wetting properties of the prepared samples. When optimized at 100 mm/min, the resulting sample demonstrated a high WCA of 150° and advancing contact angle hysteresis (CAH) of nearly 2° with a transmittance exceeding 91.8 % (Fig. 7b). Luo et al. [114] prepared a non-fluorinated superhydrophobic coating on glass surfaces by applying an anti-reflective solution using a dip coating technique, followed by modification with hexamethyldisilazane (HMDS) (Fig. 7c). The glass substrate was coated with an anti-reflective layer and annealed at 550 °C to produce samples with rough nanostructures (labelled as SSO sample). These samples were then treated to improve their self-cleaning capabilities, resulting in exceptional superhydrophobic and antireflective properties (labelled as SST sample). The resulting coating demonstrated significantly improved transparency compared to untreated glass. Fig. 7d and e depicts the static WCA of SSO and SST samples, respectively. The static WCA of the HMDS-modified sample was measured at 152° Furthermore, the coated sample exhibited self-cleaning properties, demonstrated by its ability to repel pencil shavings and methylene blue solution (Fig. 7f-h). These observations indicate exceptional superhydrophobic performance of the developed coating.

Xi et al. [115] developed transparent superhydrophobic coatings on glass surfaces by immersing multiple times in a mixture of acid-catalysed silica sol (binder) and hydrophobic silica nanoparticles (building blocks). This process created a 3D network-like nanostructured surface composition, enhancing the coating's durability while preserving 96.17 % transparency. Liu et al. [116] applied a layer of ethylene-vinylacetate

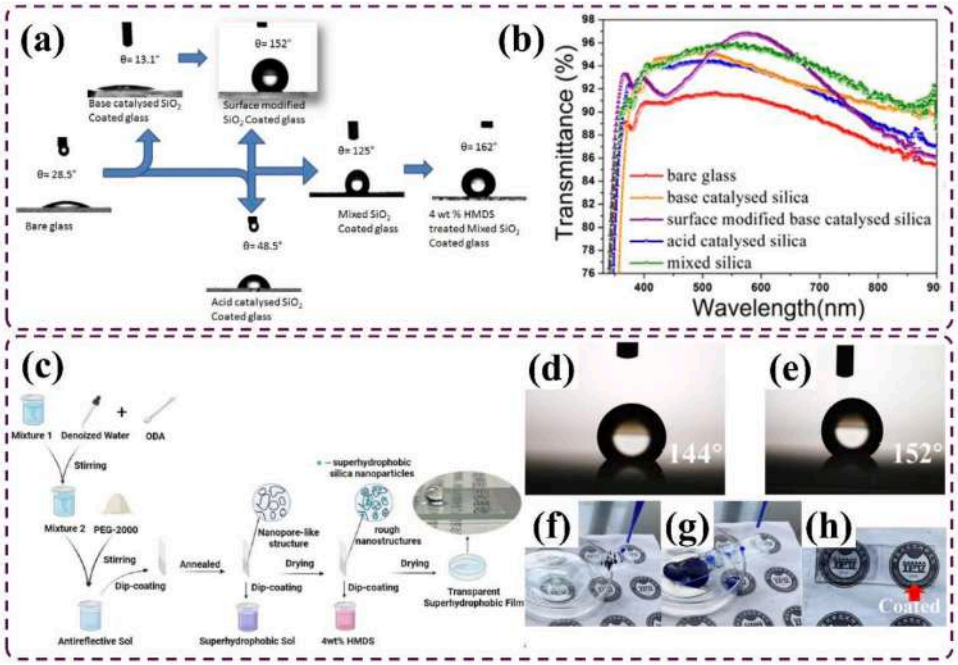

Fig. 7. (a) WCA images and (b) transmittance curves of prepared coatings from different silica sol on the glass surface. Reproduced from ref. [113] with permission from Elsevier, © 2020. (c) The schematic illustration of fabrication procedure of transparent superhydrophobic coating on glass surface. WCA of (d) SSO and (e) SST sample. (f-g) Self-cleaning test on SST sample against pencil shavings. (h) An optical image after self-cleaning effect on SST sample. Reproduced from ref. [114] with permission from Elsevier, © 2023.

copolymer (EVA) onto a glass substrate, followed by the deposition of a composite layer of SiO_2/3-methacryloxypropyltrimethoxysilane/polytetrafluoroethylene (SiO_2/KH-570/PTFE) to achieve transparent superhydrophobic coatings (refer to Fig. 8a). The authors have observed that the number of dipping cycles and the concentration of silica with PTFE influenced the wettability and transparency of the coatings, as illustrated in Fig. 8b-e.

3.2.2. *Spin coating*

The spin coating method involves the deposition of a solution onto a substrate attached to a rotating fixture [117]. The rotation spreads the solution uniformly across the substrate due to centrifugal force, creating a thin film [118,119]. The film thickness is influenced by the solution's concentration and the duration of rotation, and solvent evaporation occurs during the process [120]. Higher rotation speeds result in thinner, more uniform films, while lower speeds lead to thicker coatings [121].

Ji et al. [122] developed a transparent and superhydrophobic hybrid protective coating using a sol-gel/spin coating technology. Fig. 9a depicts experimental process of preparation of hybrid coating of self-designed resin and hydrophobic silica (G/Hs). The resulting hybrid coating of G/Hs-3(5) exhibits exceptional mechanical strength and durability, along with superior superhydrophobicity (WCA: 160.1 ± 1°, SA: 7 ± 1°), high transparency (average of 93.6 %), and a self-cleaning property. The graphite powder was evenly spread on the G/Hs-3(5) sample and water droplets were allowed to fall on the contaminated sample. Ultimately, the graphite powder was collected by water droplets and rolled off from the coating (Fig. 9b-e). Liang et al. [123] conducted a study where they used a spin coating technique to apply a composite of SiO_2 and PDMS to create a transparent superhydrophobic coating on glass surfaces. They found that the transparency of the coatings could be controlled by adjusting the concentration of PDMS in the composite. Specifically, they varied the PDMS concentration in the composite sol from 0 to 0.7 g and discovered that a 0.3 g PDMS-containing composite coating exhibited the high transparency than other coatings. They noted that increasing the amount of PDMS led to the aggregation of silica nanoparticles, which in turn reduced light transmission. In a similar way, Choi et al. [124] developed transparent self-cleaning coatings using a polyimide-fluorinated silica sol (PIFSS) nanocomposite and spin-coating technique. By adding varying quantities of silica sol, they achieved coatings with different levels of transparency. Subsequently, the spin-coated samples were treated with triethoxy-1H,1H,2H,2H-perfluorodecylsilane and dried in a vacuum oven at 200 °C for 3 h (Fig. 9f). They reported that coatings with silica sol concentrations of 5, 10, and 15 g exhibited transparency levels of 89 %, 88 %, and 82 %, respectively (Fig. 9 g).

Likewise, Li et al. [125] employed a sol-gel processed spin coating technique to fabricate a highly transparent superhydrophobic polymethylsiloxane (PMS) coating on glass surfaces. The resulting sample demonstrated a WCA of 164 ± 1° and a transparency of 89.35 %. Li et al. [126] developed a transparent superhydrophobic layer using a two-step spin coating method. First, they combined an epoxy resin with a curing agent and silica nanoparticles, and applied the mixture to the substrate. In the second step, they spin coated a suspension of silica nanoparticles mixed with 1H,1H,2H,2H perfluorodecyltrimethoxysilane onto the pre-treated sample. The prepared sample was then dried at 80 °C for 4 h. The resulting sample exhibited a WCA of 153.4° ±1.7° and a SA of 5.1° ±1.1°. During water dynamic testing, 6 μL water droplets were dropped from heights of 10 cm and 25 cm at speeds of approximately 1.41 m/s and 2.23 m/s, respectively (see Fig. 9h). Notably, a water droplet dropped from a height of 10 cm was observed to bounce off the coating surface, indicating excellent water droplet impact resistance even at relatively large heights.

3.2.3. *Spray coating*

Spray coating is a not only simple, flexible but also widely used technique to develop functional coatings on any surface especially transparent superhydrophobic coatings. During the fabrication process, a solution containing nanoparticles is atomized using compressed gas and allowed to spray onto a surface which able to form a thin and even layer [127]. This technique is much popular in both labs and industry, since it is readily applicable on large or uneven surfaces. The coating's

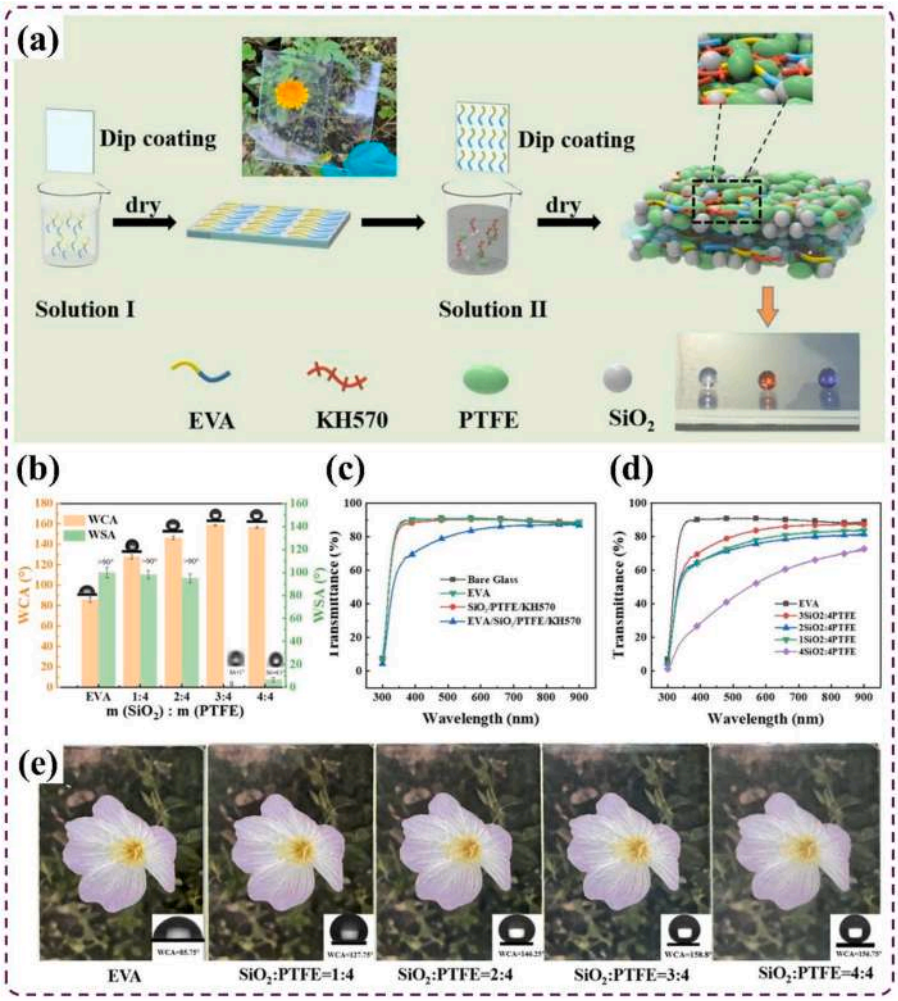

Fig. 8. (a) Schematic diagram of the fabrication procedure of EVA/SiO_2/PTFE/KH-570 film. (b) Wettability of composite coating prepared by varying concentration of silica to PTFE. (c) Transmission spectra of the as-prepared samples. (d) Transmission spectra and (e) optical images of various concentrations of silica to PTFE composite coatings. Reproduced from ref. [115] with permission from Elsevier, © 2023.

quality depends on several factors such as nozzle to substrate distance, pressure, solution concentration as well as drying conditions [128]. A precise control on these parameters, it's possible to control surface roughness and transparency to develop transparent superhydrophobic coatings. However, ensuring a uniform surface, avoiding nozzle clogging, and dealing with solvent fumes are still some of the practical issues. Though, due to its low cost and scalability, spray coating continuously preferred to develop advanced surface coatings.

Leão et al. [129] developed superhydrophobic coatings on glass substrates using a vulcanized (RTV) polysiloxane matrix and varying amounts of different commercial fumed silica (Aerosil R200, Aerosil R202, and Aerosil R805) along with organically modified silica (ORMOSIL) nanoparticles via the spray coating technique. Notably, the combination of Aerosil R202 with polysiloxane filler at 20 % and 25 % demonstrated superior superhydrophobicity and transparency. Specifically, sample R202.20 exhibited a water contact angle (WCA) of 157 ± 1°, a sliding angle (SA) of 10.1 ± 2.5°, and 77 % transparency. Meanwhile, sample R202.25 showed a WCA of 156 ± 3°, an SA of 1.8 ± 1.1°, and 78 % transparency. Hong et al. [130] have synthesized a hydrophobic binding agent (PMK) and combined it with hydrophobic silica nanoparticles to create a transparent superhydrophobic PMKS coating (see Fig. 10a). They achieved a precise combination in sample PKMS-0.08 (0.08 g of PKM, 10 mL of hydrophobic SiO_2 dispersion and 20 μL volumes of curing agent D-400), resulting in transparency (88 %) and superhydrophobicity (water contact angle of 162°). Increasing the amount of binding agent reduced transparency due to increased nanoparticle agglomeration. Sample PKMS-0.08 demonstrated excellent water adhesion resistance (see Fig. 10b). In water collision tests, water droplets from a 20 cm height exhibited various behaviors including striking, dispersing, bouncing, and rapid gathering before rolling off the coating's surface (see Fig. 10c). This confirmed the coating's outstanding non-infiltration properties for water droplets.

Yang et al. [132] produced transparent superhydrophobic coating for glass surfaces by applying 200 layers of waterborne superhydrophobic suspension using 0.7 MPa pressure at a distance of 10–20 cm. The resulting sample demonstrated a high WCA of 156.1° and a SA of 2° with excellent transmittance. However, the transparency decreased from 90 % to 70 % when the spraying cycles were increased from 200 to 220. Ke et al. [133] created transparent superhydrophobic coating using a spray coating technique followed by rapid thermal processing of low melting-point glass powder (LMPGP) and SiO_2 nanoparticles. The composite solution was sprayed onto a pre-cleaned glass substrate at a pressure of 4.5 MPa and 40 cm distance. The transparency of the coating was influenced by the size of the silica nanoparticles, with transmittance decreasing from 88.8 % to 87.7 % as the particle size varied from 7 nm to 50 nm. Zhao et al. [131] developed transparent and durable superhydrophobic glass using a method known as sequentially reinforced additive coating (SRAC). The process involved combining silica sol and poly (furfuryl alcohol) (PFA) at varying proportions, with a constant concentration of silica sol and a variable concentration of PFA. The

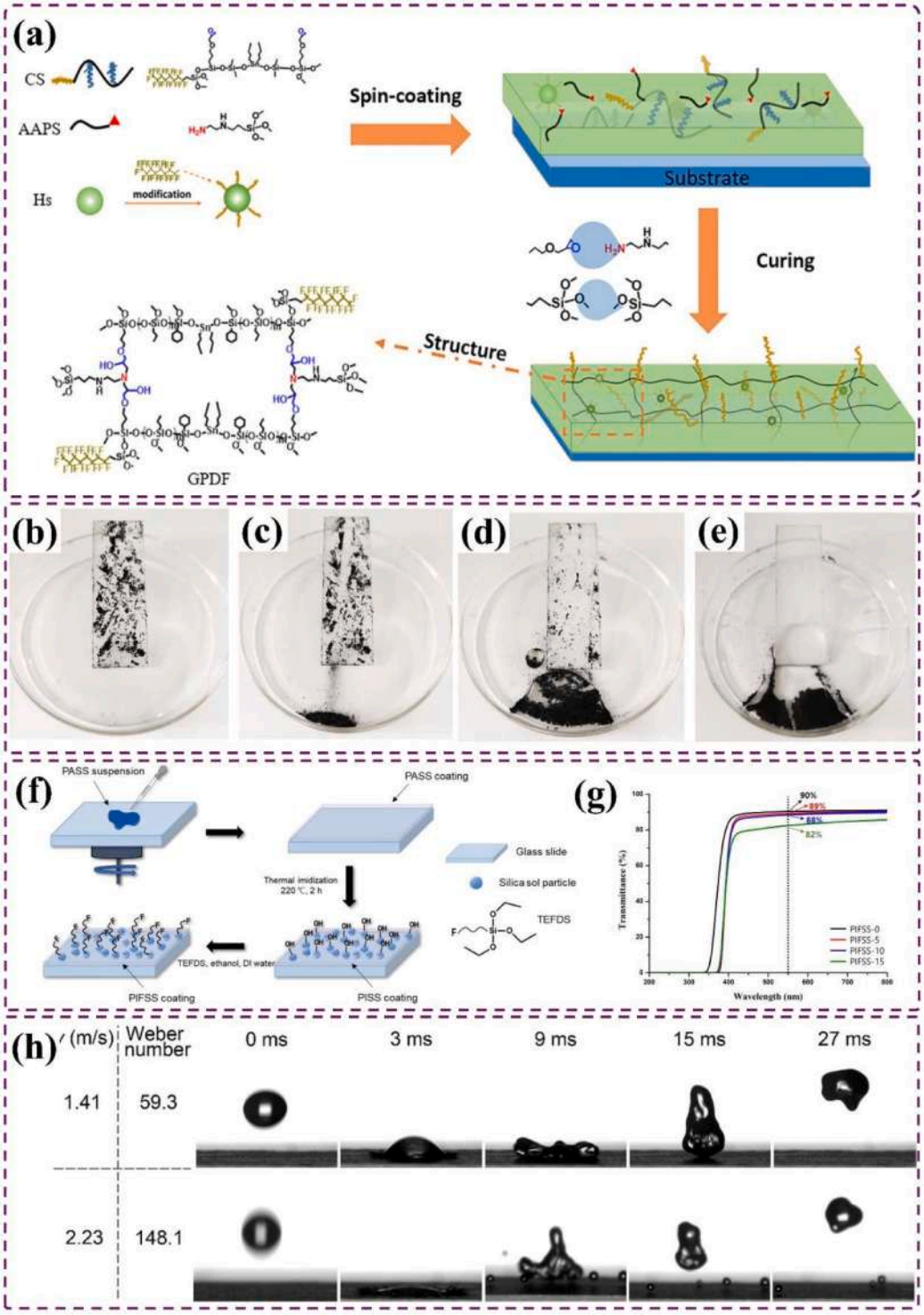

Fig. 9. (a) Schematic representation of the fabrication of superhydrophobic G/Hs coating. (b-e) Self-cleaning performance on the G/Hs-3(5) sample. Reproduced from ref. [122] with permission from Elsevier, © 2021. (f) Fabrication procedure of the self-cleaning PIFSS coating and (g) transmittance curves of the different PIFSS coatings. Reproduced from ref. [124] with permission from MDPI, © 2021. (h) A water droplet impact on the fabricated coating with different speed and weber number. Reproduced from ref. [126] with permission from Elsevier, © 2022.

combined solution was sprayed onto a glass substrate heated to 220 °C at a rate of 4 mL/min, followed by annealing at 520 °C for 1 h. The prepared samples were then dipped in a 1wt % PDMS-ethanol solution and dried for 30 s in air before being placed on a heating plate at 320 °C for 4 min. Samples with PFA concentrations of 0.5, 1, 1.5, 2, and 2.5 mL were further heated at 150 °C for 12 h and denoted as F1, F2, F3, F4, and F5, respectively. The hydrophobic nature of the coating increased with higher PFA concentrations is depicted in Fig. 10d. As shown in Fig. 10e and f, the transmittance decreased from 90 % to 70 %, and the best balance of transmittance and water contact angle was observed for the F3 samples, respectively. Optical photographs showed the repellent properties of the coating against various liquid droplets (Fig. 10 g). The application of the spray coating has led to reduced transparency of the samples due to increased surface roughness or thickness. This is caused

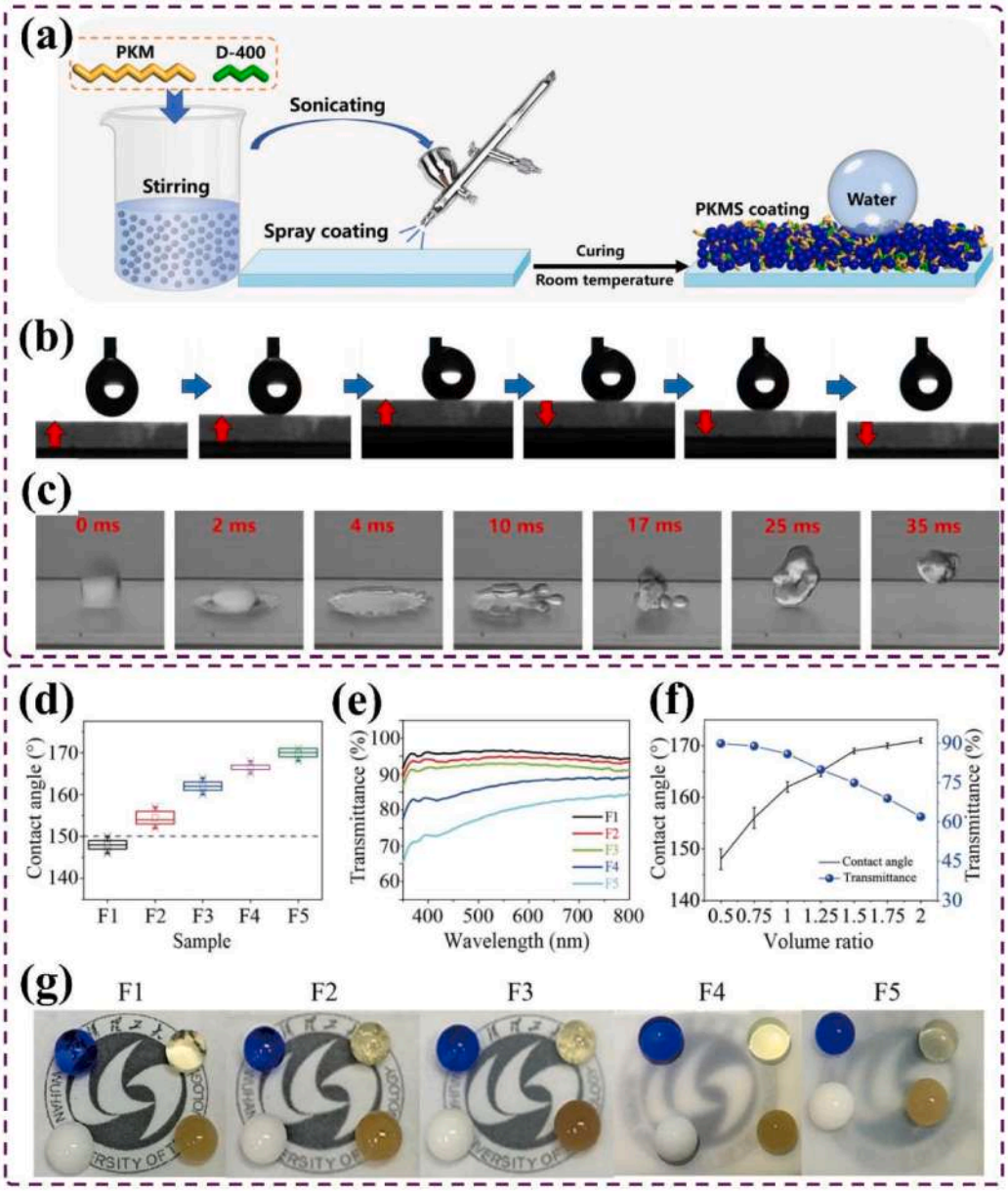

Fig. 10. (a) Schematic diagram of the fabrication of superhydrophobic PKMS coating. (b) Optical images of anti-water adhesion test and (c) first collision bounce of a water droplet on PKMS-0.08 superhydrophobic sample. Reproduced from ref. [130] with permission from Elsevier, © 2023. (d) The WCA and (e) transmittance of F1, F2, F3, F4, and F5 samples respectively. (f) WCA and transmittance (at 600 nm wavelength) of different samples by varying the concentration of PFA. (g) Optical photographs of different liquid droplets on F1, F2, F3, F4, and F5 samples. Reproduced from ref. [131] with permission from American Chemical Society, © 2018.

by the addition of multiple layers, changes in nanoparticle size, or adjustments in material concentration.

3.3. Electrospinning

The electrospinning method is widely used for producing continuous fibres of polymeric materials with diameters ranging from micrometres to nanometres [134]. The method involves several components including a high-voltage DC power supply, grounded collector, feeding system, and process parameter controller. The feeding system comprises a solution container, a spinneret, and a pump [135]. The process begins by applying high voltage to the needle and the grounded collector. This causes a droplet of the solution to appear on the tip of the needle due to surface tension, which then elongates into a conical shape known as the Taylor cone as a result of electric force. The charged particles within the solution then emerge from the Taylor cone with turbulent oscillatory motion due to the changing electric field [136,137]. Eventually, a mesh-like fibre structure starts to collect on the rotating collector as the solvent evaporates [138]. By adjusting parameters such as applied voltage, the distance between the needle and the collector, and the type of substrate, precise control can be achieved over the resulting surface morphology and fibre diameter.

Recently Kim et al. [139] have developed a self-cleaning coating on glass surfaces using PET (polyethylene terephthalate) derived from recycled Coca-Cola bottles. The coating was applied using a sequential deposition process involving electrospinning and electro-spraying methods (Fig. 11a). The efficacy of the self-cleaning coating was demonstrated through a test where graphite powder was spread on the coated surface and then removed using water droplets. The results showed that the powder was effectively captured by water droplets and subsequently rolled off the surface, leaving it clean (as shown in Fig. 11b). The self-cleaning capabilities were tested on small solar cells,

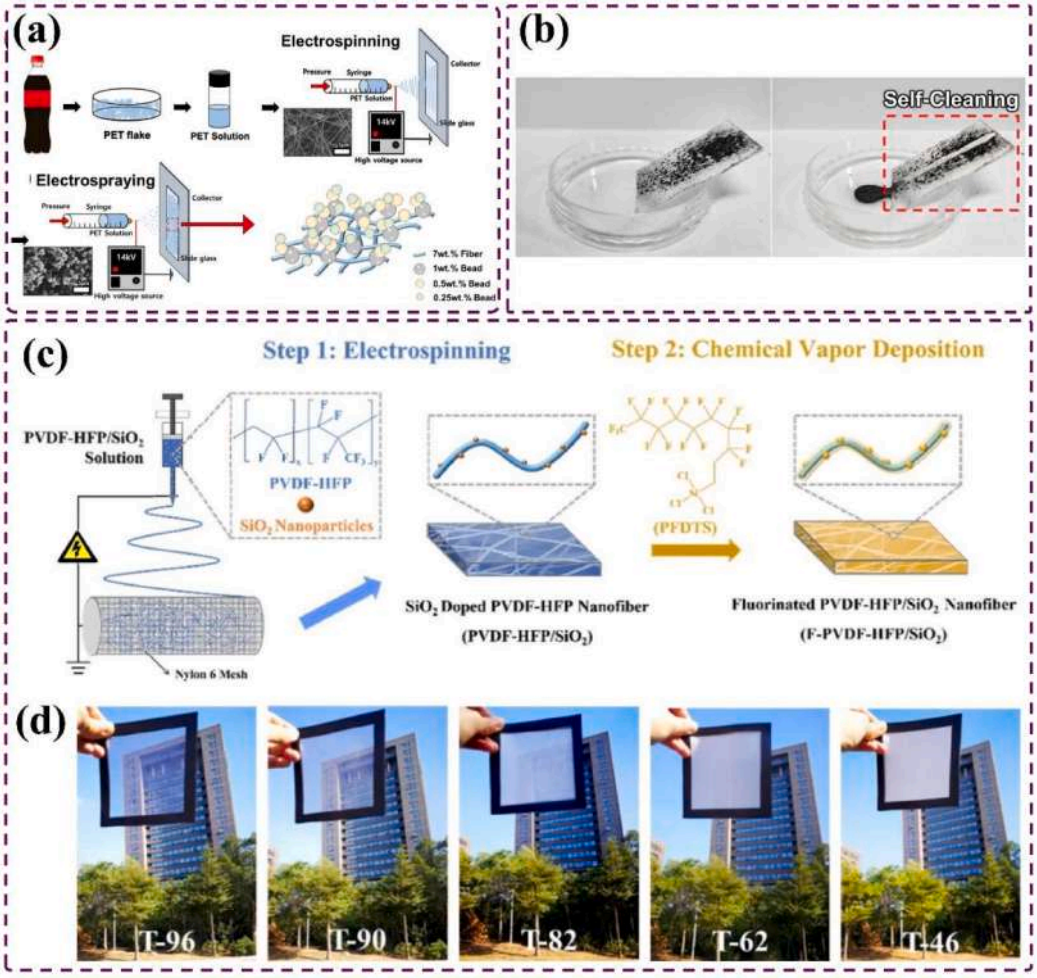

Fig. 11. (a) Schematic illustration of fabrication of the superhydrophobic coating by using waste bottles. (b) Self-cleaning behaviour of electrospun superhydrophobic sample. Reproduced from ref. [139] with permission from MDPI, © 2023. (c) Schematic diagram for the fabrication steps of the superhydrophobic F-PVDF-HFP/SiO_2 coating. (d) Optical photographs of F-PVDF-HFP/SiO_2 air filters with different transparency. Reproduced from ref. [140] with permission from Elsevier, © 2023.

demonstrating excellent efficiency under varying illuminance levels over a 14-day period. Chen and colleagues [140] created a hierarchical superhydrophobic structure on glass by combining electrospinning PVDF-HFP/SiO_2 suspension and vapor deposition of a fluorinated compound on a nylon 6 mesh (see Fig. 11c). They found that the optimal conditions were a flow rate of 1 mL/h, an applied voltage of 18 kV, and a distance of 15 cm, which resulted in 80 % transparency. However, increasing the electrospinning time reduced transparency, as seen for electrospinning times of 0.5, 1, 2.5, 3, and 4 h (see Fig. 11d). The labels T-96 and others indicate the actual transmittance values of the samples. By adjusting both the void size and fibre thickness, the authors were able to achieve transparency for light with wavelengths of 400–800 nm. Youn et al. [141] produced hydrophobic transparent nanofiber scaffolds using polystyrene (PS) by electrospinning a PS solution at 25 kV and a flow rate of 0.1 mL/h in both random and aligned configurations. They manipulated the deposition time (from 10 s to 40 s) to control fibre thickness and studied the transparency of the resulting structures. They found that as deposition time increased, transparency decreased due to higher PS fibre density. They also observed an increase in WCA as the distance between fibres decreased, resulting in water droplets being unable to penetrate the structure and instead resting on the surface. The WCA for random and aligned structures increased from 73° to 126° and from 77° to 142°, respectively, with longer deposition times. In studies on electrospinning, it was observed that transparency of the prepared samples decreased as the deposition time increased. This decrease in transparency could potentially limit the use of the prepared samples in applications that require high levels of transparency.

3.4. Laser deposition method

The laser deposition method utilizes highly energetic laser pulses from an excimer to emit UV radiation towards the targeted area of the sample material [142]. This process causes ablation and vaporization, leading to the formation of micro-nanostructures on the surface, which contributes to the material's hydrophobic properties [143]. The material undergoes localized heating, phase transition, and eventually vaporization, resulting in the ejection of material in vapor form. At very intense laser energy, the vaporized components convert into plasma, comprising ions and electrons, which influence the deposition dynamics on the material. Precise control of laser energy parameters, selection of the target material, and optimization of laser characteristics are critical for the optimization. Additionally, the energy of the laser, pulse duration, and repetition rate play crucial roles in controlling the ablation and deposition process [144,145].

Wang et al. [146] utilized picosecond laser pulses to create groove-shaped microstructure arrays on a glass surface (Fig. 12a). The surface was rendered hydrophobic by applying 1H, 1H, 2H, 2H-perfluorodecyltriethoxysilane, resulting in a hierarchical micro-nano structure. To achieve periodic microstructures, the laser beam was directed onto the substrate 50 times at a scanning speed of 300 mm/s. Each pulse had a

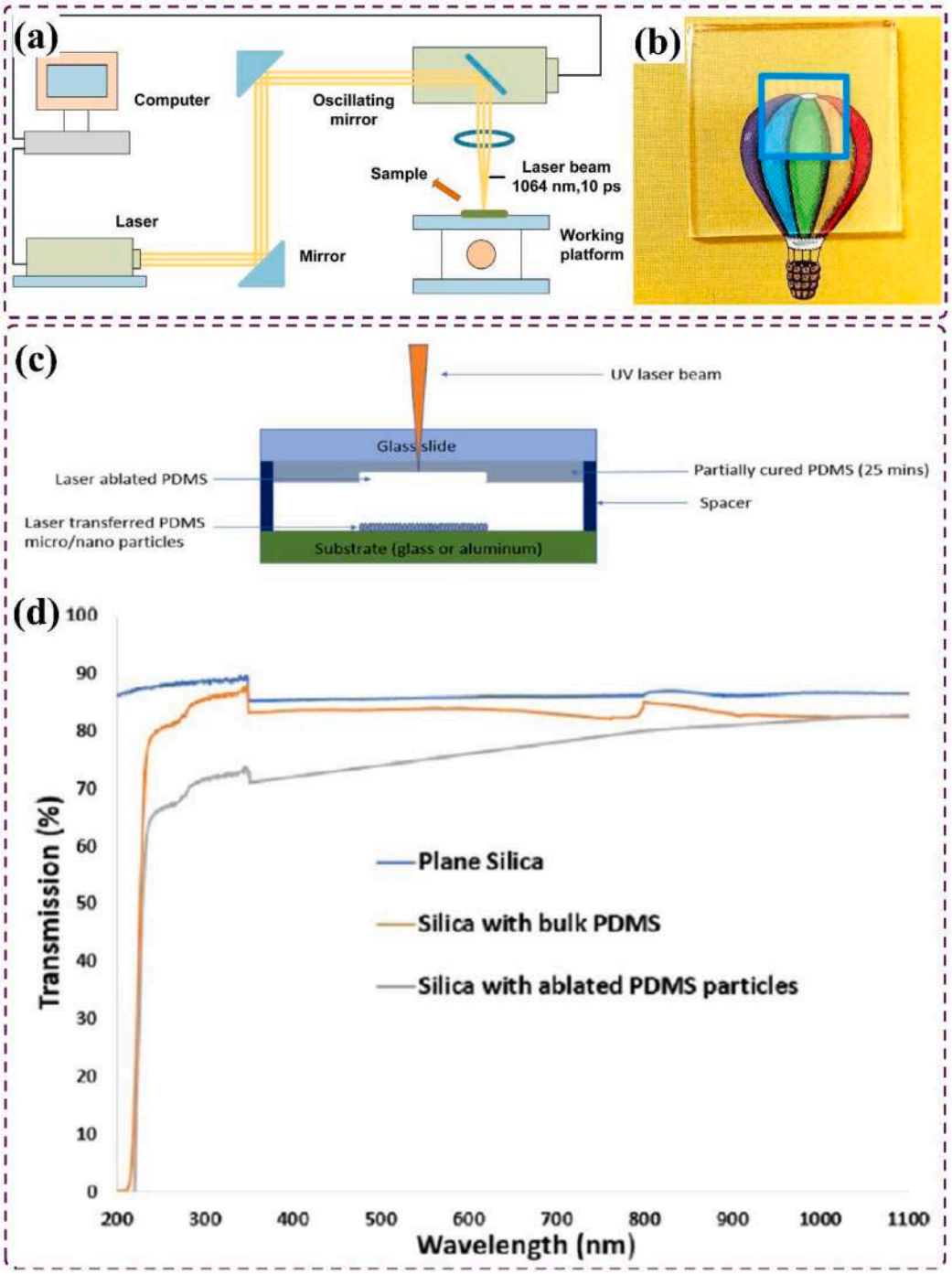

Fig. 12. (a) Schematic diagram of laser deposition system and (b) optical image of the sample prepared at 75 μm laser line interval. Reproduced from ref. [146] with permission from Elsevier, © 2017. (c) A schematic of PDMS transferring process onto different surface via pulsed laser ablation. (d) Transmittance curves of different silica films. Reproduced from ref. [147] with permission from American Chemical Society, © 2023.

mean energy of 35 μJ and a spot size of approximately 20 μm. The transmittance decreased from 87 % to 78.62 % as the laser line interval decreased from 75 μm to 55 μm. Fig. 12b depicts the optical image of the sample prepared at a 75 μm laser line interval, with the blue squared portion representing the laser-structured area and the rest being unstructured by the laser treatment. Chakraborty and colleagues [147] developed a transparent superhydrophobic surface using a 355 nm wavelength nanosecond pulsed laser to ablate a PDMS coating on a glass surface (Fig. 12c). The pulse width was 20 ns, and the scan rate during fabrication was maintained at 200 mm/s. They experimented with varying the laser fluences from 1.1 to 2.3 J/cm^2 to achieve superhydrophobic behavior, observing the onset of superhydrophobicity after surpassing 2 J/cm^2. Despite a 15 % reduction in transmittance compared to plain silica, the laser-ablated PDMS surface exhibited a high WCA of 153.8 ± 1.7° (Fig. 12d).

Zhao et al. [148] utilized laser-induced plasma-assisted ablation to generate a precisely roughened surface on quartz glass, resulting in a transparent superhydrophobic surface. The laser used had a wavelength of 1064 nm, a pulse width of approximately 12 ps, and an average power of 60 W. The rough surface was created by exposing the glass to a laser with a power density of 2.4 MW/cm^2 and a frequency of 2 MHz, using two different patterns: line and cross-type, with a spot diameter of

around 20 μm. Subsequently, the surface was treated with a 1H, 1H, 2H, 2H-perfluorodecyltriethoxysilane solution to confer superhydrophobic properties. The transmittance of both line and cross-patterned samples exceeded 90 % at all scanning speeds, with transmittance increasing with the scanning speed of the laser beam.

Lin et al. [80] used a fs laser to create a transparent and durable superhydrophobic coating on glass surface. By directing 800 fs pulses with a 1030 nm wavelength, a 200 kHz repetition rate, and maximum power of 40 W, the authors achieved the desired level of roughness necessary to balance hydrophobicity and transparency in three different ways. The laser beam produced micro-pits with a focused spot diameter of 35 μm. To enhance water-repellent properties, 1H, 1H, 2H, 2H-Perfluorodecyltriethoxysilane was applied using a chemical vapor deposition (CVD) process to modify the glass surface. The study also involved optimizing the interval of the micropit array, laser frequency, and micropit morphology to achieve both transparency and superhydrophobicity simultaneously.

3.5. Lithography

The lithography process involves creating a master pattern for producing micro-nano structures on a substrate [149]. A photosensitive material, known as a photoresist, is applied to the substrate and undergoes a transformation when exposed to UV radiation through an optical mask [150]. This results in an exact replica of the master pattern on the substrate. Additional surface treatments can yield superhydrophobic properties. This intricate process of developing a transparent superhydrophobic coating finds applications in optics [151] and

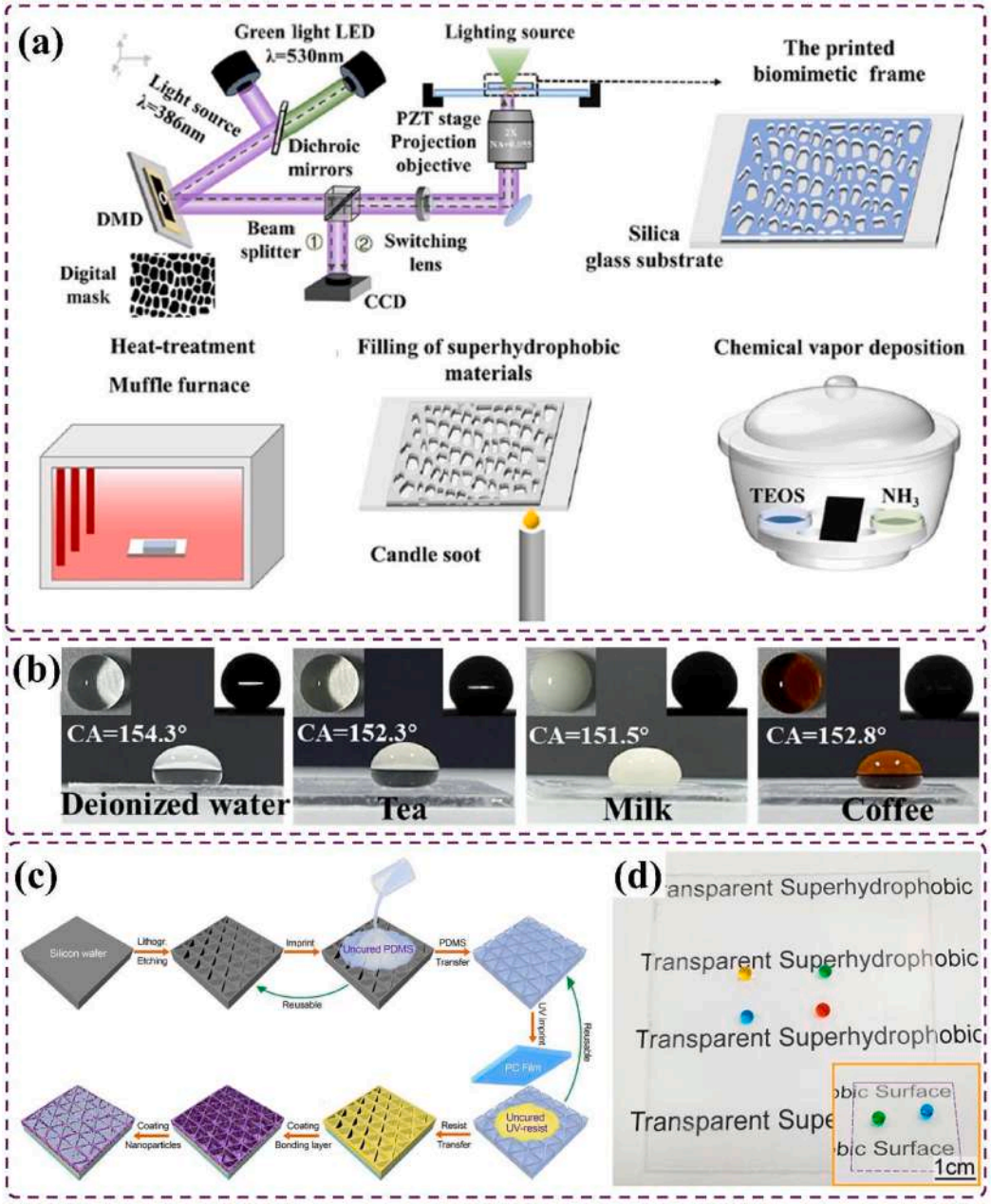

Fig. 13. (a) Schematic of the fabrication procedure of superhydrophobic coating. (b) Wettability of different droplets on BSSG sample. Inset images depicting top view and WCA image of the respective liquid droplet. Reproduced from ref. [159] with permission from American Chemical Society, © 2023. (c) A schematic representation of the step-by-step process of the fabrication of the transparent superhydrophobic coating. (d) A coloured water droplets placed on the M-SHS sample. Reproduced from ref. [160] with permission from American Chemical Society, © 2022.

self-cleaning technologies [152]. The technique encompasses various subclasses, including photolithography [153,157], soft lithography [154], electron-beam lithography [155], and nanolithography [156].

Yu et al. [158] have used photolithography to fabricate a flexible transparent superhydrophobic film by creating a mushroom-like microstructure of PDMS array. They initiated the process by depositing candle soot on the PDMS mushroom structure for 5 min, followed by a 24 h CVD process at 35 °C in a closed desiccator using TEOS and NH_4OH. This led to the formation of a silica shell on the candle soot through a hydrolysis and condensation reaction on TEOS. The PDMS mushroom structure was subsequently dried at 80 °C for 2 h. The nanosilica-coated PDMS mushroom structure was then modified by immersing it in a mixture of heptadecafluoro-1,1,2,2,-tetrahydrodecyl trichlorosilane (HDFS) and hexane for 24 h at 25 °C, followed by drying at 60 °C for 24 h. This treatment resulted in an enhancement of the roughness and improved the hydrophobicity of the film. Furthermore, fluorination using HDFS was performed to further augment the superhydrophobicity of the film. The prepared samples, namely PDMS mushroom microstructures (PM), nanosilica-coated PDMS mushroom microstructures (NS@PM), and fluorine-functionalized nanosilica--coated PDMS mushroom microstructures (FNS@PM), displayed water contact angles (WCAs) of 145°, 161°, and 166° and transparencies of 89 %, 77 %, and 76 %, respectively.

Zhang and colleagues [159] have developed transparent, highly water-repellent coatings on glass using micro stereolithography printing. They printed a biomimetic microstructure on the glass surface and applied heat treatment. Unwanted materials were removed in the presence of air, followed by debinding and sintering in a vacuum. Nanoparticles were then introduced into the printed frame through in situ deposition (see Fig. 13a). The resulting sample exhibited high transparency (90 %) and excellent robustness. If the frame structure was too tall, it would result in excessive filling of nanoparticles, potentially impacting the sample negatively. Conversely, if the frame structure was too small, it could compromise the robustness of the coating. Wettability of the prepared sample was tested by placing different liquid droplets on it (see Fig. 13b). Luo et al. [160] created inverted-pyramidal micro--cavities using photolithography and wet-etching techniques then transferred to hot-pressed glass. These cavities were then filled with silica nanoparticles (Fig. 13c). The use of photolithography was particularly significant in developing the micro-cavities on the silicon wafer. As a result of these fabrication processes, the transparency of polycarbonate (PC) and polyethylene terephthalate (PET) samples increased from 90.6 % and 88.3 % to 92.5 % and 90.7 %, respectively. Additionally, the prepared transparent samples exhibited excellent non-wetting properties, as evidenced by the spherical shape of the coloured droplets depicted in Fig. 13d. The nanoprint lithography presents several advantages for creating nanoscale surface structures. It is more cost-effective than traditional lithography and is well-suited for advanced nanotechnology applications. This versatile technique can work with various materials and enables the creation of large-area patterns, which enhances scalability for high-throughput devices. It eliminates the need for expensive UV light systems and simplifies the process compared to methods like electron beam lithography. Moreover, its resolution is limited by Mold size rather than light wavelength, allowing for the production of patterns smaller than the diffraction limit of optical lithography. Additionally, it uses fewer toxic chemicals, making it more environmentally friendly. Recently, Cho et al. [161] developed ZnO nanograting structures on $Cu(In,Ga)Se_2$ (CIGS) solar cells through a simple nano transfer lithography process. These structures featured grating periods of 770 nm and 1400 nm. In their method, ZnO nanoparticles were spin-coated onto a PDMS Mold, which was then utilized in a nanoimprint system to transfer patterns onto the solar cells. The resulting grating structures exploited light diffraction, resulting in short-circuit current density (JSC) losses of 0.38 mA cm^{-2} for the 770 nm gratings and 1.00 mA cm^{-2} for the 1400 nm gratings. Furthermore, these structures improved hydrophobicity, achieving a water contact angle (WCA) of 144° for the 770 nm grating and 136° for the 1400 nm grating, as well as enhanced self-cleaning properties, which improved performance under oblique light. This technique is also applicable to other thin-film solar cells such as CdTe and perovskites.

In another study, Choi et al. [162] used reverse nanoimprint lithography (RIL) and reactive ion etching (RIE) to create superhydrophobic and oleophobic overhang structures on substrates. The static contact angles on a flat substrate measured 109° for water, 84° for diiodomethane, and 66° for hexadecane, while the overhang structures exhibited enhanced contact angles of 164°, 151°, and 114°, respectively, indicating a better fit with the metastable Cassie model. Additionally, Yang et al. [163] produced robust superhydrophobic coatings using PVB/SiO_2 microspheres on wood. The petal-like texture obtained through nanoimprint lithography resulted in a water contact angle (WCA) of 160°, demonstrating excellent durability and improved thermal stability, with an initial decomposition temperature 30.5 °C higher than that of untreated wood. The coated wood effectively repelled various liquids, maintaining WCAs near 150° even after 24 h of ultrasonic rinsing.

3.6. Sputtering method

The sputtering method is nothing but a physical vapor deposition (PVD) technique in which high-energy ions, typically derived from an inert gas plasma, bombard a target material. This process ejects atoms from the target to form a thin film on a substrate [164]. The thickness and uniformity of the film can be controlled by varying parameters such as sputtering power, chamber pressure, and deposition time [165]. This method ensures excellent adhesion and uniformity and is compatible with various substrates, including those with complex shapes. Although it requires advanced equipment, sputtering is widely used for producing high-quality coatings in fields such as electronics, optics, and materials engineering [166].

Ma et al. [167] developed an antireflective and hydrophobic CaF_2 film using magnetron sputtering, for potential applications in outdoor environment. The structural morphology and properties of the CaF_2 films were controlled by adjusting the SF_6/Ar gas flow ratio during sputtering process. The gas flow ratios of SF_6/Ar were adjusted to 0 %, 10 %, and 15 %, to control the film's structure and performance. The transmittance of the 10 % CaF_2 film was 96.2 % at 456 nm, and the average transmittance was higher than that of the uncoated glass, with the 15 % CaF_2 film showing slightly lower transmittance (94.52 %). The 0 % SF_6 film exhibited poor transmittance almost identical to the uncoated glass in the 300–1100 nm range (See Fig. 14a). The wettability of the 10 % CaF_2 film showed the highest WCA of 139.4°, 93° for the 0 % CaF_2 and 132° for 15 % CaF_2 films (Fig. 14b). The film's micro-nano structure contributed to increased surface roughness, enhancing hydrophobicity. Zuo et al. [168] fabricated a transparent superhydrophobic ZnO surface using RF magnetron sputtering, with enhanced wettability and optical properties. The fabrication process involved sputtering Zn at 100 W for varying times (2, 7.5 and 15 min), followed by annealing at 400 °C and surface treatment with a 2 wt % hexadecyltrimethoxysilane (HDTMS) solution. The sputtering time of 2 min provided the best results, with contact angles greater than 160° and sliding angles below 90°. While increasing the film thickness improved the surface's ability to trap air and enhance wettability, it also caused more light scattering, reducing the coating transparency (Fig. 14c-f). The coating shows resistance to acidic and alkaline environments, stable performance across temperatures ranging from −20 °C to 100 °C, and effective water repellence even when subjected to high-velocity water droplets of up to 2.8 m/s. Furthermore, the self-cleaning performance was evaluated by spreading 25 nm sized carbon particles as contaminant. Then 10 μL water droplets were rolled over the surface. During the rolling action, the carbon nanoparticles were collected by water droplets. Also, the prepared sample was tilted at 15° and dusted surface of the sample was readily rolled off from the surface and left it clean behind.

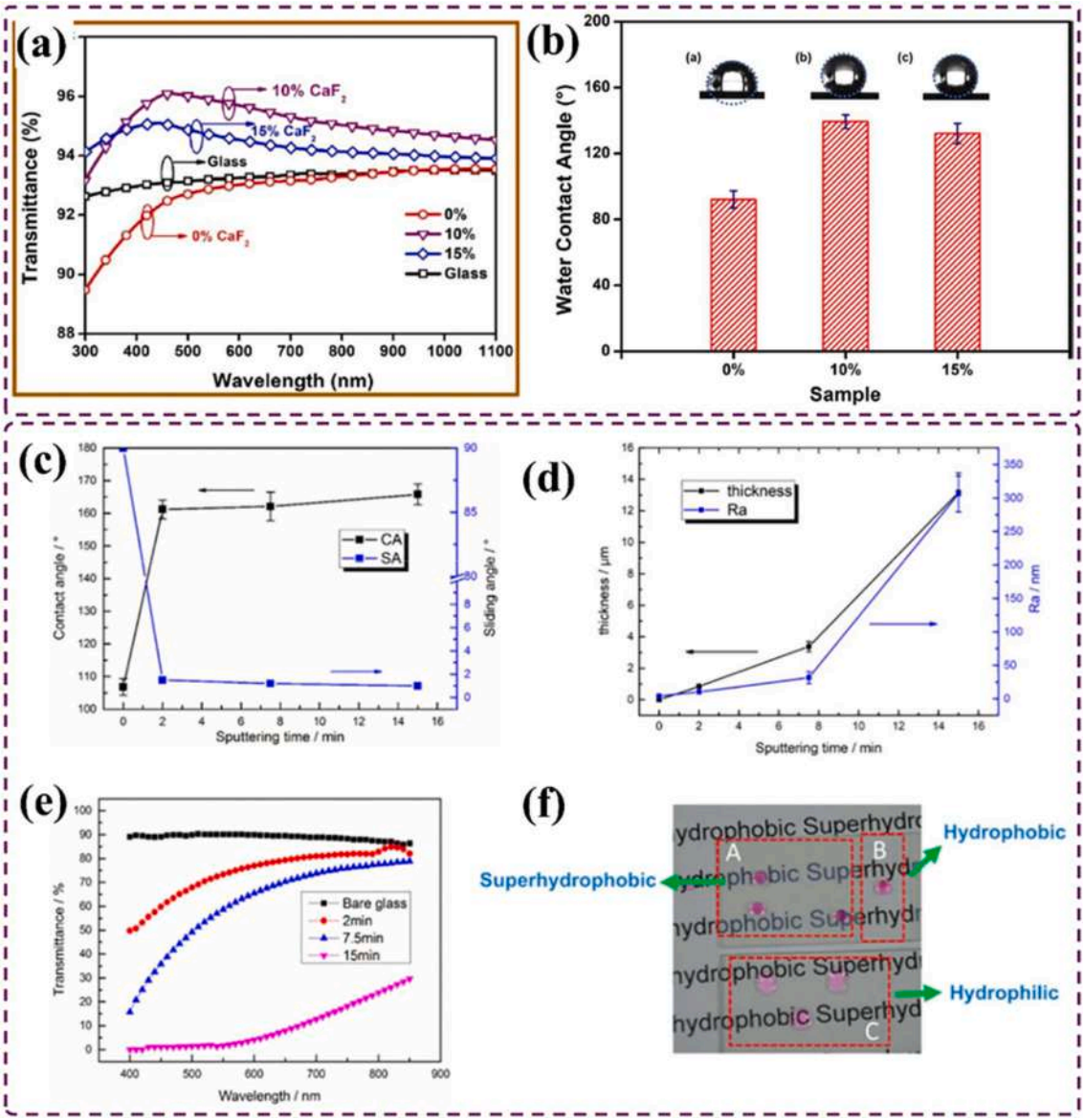

Fig. 14. The (a) transmittance and (b) wettability study of the CF_2 coated samples. (c) Wettability, (d) film thickness & Ra and (e) transmittance curves of the surfaces prepared with various sputtering time and (f) optical images of water droplets on various surfaces. (Add copyright details).

Therefore, had claimed that, the fabrication method is stable and can be applicable for large scale application in solar cells, car windshields and display windows.

For instance, Gupta et al. [169] developed multifunctional superhydrophobic indium tin oxide (ITO) coatings on glass substrates using magnetron sputter deposition and oxidation. These coatings exhibited dual-scale roughness with a WCA of 163° and a minimal hysteresis of 5° when the optimal surface roughness was about 1.1 μm. As the deposition time increased, transparency decreased; a sample deposited for 5 min maintained moderate transparency, while longer deposits resulted in less than 50 % transmittance, and the 40-minute sample exhibited less than 15 % transparency. This highlights a trade-off between hydrophobicity and optical transparency. Additionally, Drábik et al. [170] created fluorocarbon plasma polymer films using RF magnetron sputtering. They found that the WCA increased from 113° to over 170° at higher gas pressures, indicating that a minimal film thickness is crucial for achieving superhydrophobicity due to increased surface roughness. The films transitioned to a PTFE-like structure under specific discharge and pressure conditions and maintained their superhydrophobic properties after 12 months. Kim et al. [171] produced superhydrophobic and transparent PTFE films on glass using RF sputtering and catalytic chemical vapor deposition (Cat-CVD). Their optimized Cat-CVD process improved the WCA to 153 ± 1° while achieving over 90 % optical transparency. This work underscores the importance of micro- and nano-structuring, as well as the role of CF_2 and CF_3 functional groups, in enhancing hydrophobicity.

3.7. Atmospheric pressure plasma spray (APPS)

In contrast to traditional coating methods, the APPS method employs plasma technology for surface treatment and coating applications. This technique has gained prominence due to its ability to enhance surface properties not only adhesion, hardness but also wear resistance. APPS operates by generating a high-temperature plasma jet from a gas (typically air, Argon, or Nitrogen) which is ionized via an electric discharge. The resultant plasma jet is directed towards the substrate at atmospheric pressure, where it interacts with the coating material-usually in powder form. Upon impact, the high-energy plasma melts the powder particles, causing them to be accelerated toward the surface of substrate. As the molten particles impact, they solidify and adhere, forming a cohesive

coating layer. The process parameters, such as plasma temperature, gas flow rates as well as substrate temperature, can be finely tuned to optimize coating characteristics, including thickness, microstructure, and adhesion strength [172,173]. The APPS method offers several advantages over conventional coating techniques. One significant benefit is its capability to produce coatings with exceptional qualities, including enhanced mechanical properties and resistance to thermal and chemical degradation. Because the process occurs in atmospheric conditions, it eliminates the need for vacuum systems, thereby reducing operational complexity and costs.

Hossain et al. [174] fabricated hydrophobic and mechanically robust coatings on soda-lime glass. In this study, a non-thermal plasma jet generated under atmospheric pressure and ambient conditions. Two chemical precursors were employed: Tetramethylsilane (TMS) for imparting hydrophobicity and (3-Aminopropyl)triethoxysilane (APTES) for enhancing mechanical strength and adhesion due to its amine functional groups. Plasma was generated using an AC high voltage (11.5 kHz), and coating properties were optimized by varying TMS/APTES ratio, applied voltage, treatment duration, and argon flow rate. An optimal condition—TMS/APTES ratio of 4.8, 7.5 kV voltage, and 300 s treatment time—yielded a high WCA of 139°, indicating strong hydrophobicity, along with good mechanical durability. Surface characterization using AFM and SEM revealed that coating roughness and thickness significantly influenced hydrophobic performance. UV–Vis analysis confirmed minimal loss in optical transparency of the coated glass. The coating demonstrated long-term stability under aging and annealing conditions, suggesting that non-thermal plasma jet technology is a viable method for producing durable, transparent, and hydrophobic surface coatings. Mugica-Vidalet al. [175] fabricated a hydrophobic coating that simultaneously enhances the wear resistance of glass surfaces. A non-thermal atmospheric jet plasma-polymerization system was employed using binary mixtures of two silane precursors: (Heptadecafluoro-1,1,2,2-tetrahydrodecyl)trimethoxysilane (FLUSI) and aminopropyltriethoxysilane (APTES). FLUSI, due to its fluorocarbon chain, imparts hydrophobicity, while APTES contributes to wear resistance through improved cross-linking and adhesion. Results indicated that chemical modification via fluorinated groups (CF_x, particularly CF_3) was more effective than increasing surface roughness in achieving hydrophobicity, with a maximum WCA of 123.2° ± 1.5 obtained for the A50/F50 composition. Although superhydrophobicity (WCA > 150°) was not achieved due to insufficient surface roughness, the A50/F50 sample presented the best trade-off, showing high fluorocarbon content, improved CF_3 concentration, and a 50.1 % reduction in wear rate compared to uncoated glass. Wear resistance was found to correlate with coating thickness and Si–O–Si content, both influenced by APTES concentration. However, excessive APTES reduced hydrophobicity without proportionally enhancing durability. Wear mechanisms were attributed to tribofilm formation from coating debris, with APTES content affecting film continuity and, consequently, wear resistance. Saget et al. [176] fabricated biomimetic bilayer thin film by using two precursors hexamethyldisiloxane (HMDSO) and 1H,1H,2H,2H-perfluorooctyltriethoxysilane (pFOTES) by atmospheric pressure plasma method. In the study of pFOTES single-layer coatings, the observed pinning phenomenon may result from a heterogeneous distribution of CFx groups at the surface. For the bilayer coating, it was not possible to measure contact angle hysteresis (CAH) due to its ultrahydrophobic nature, as water droplets rolled off the surface, indicating a nearly zero CAH. The bare stainless steel (SS) exhibited a WCA of 81.9° with no measurable CAH, resulting in a total surface free energy of 34.7 mN/m. In contrast, the H20 coating displayed a significantly higher WCA of 107.7°, indicating a pinned state in the Wenzel model, with a CAH of 19.2° and a total surface free energy of 18.8 mN/m. The F20 coating presented an even steeper WCA of 138.1°, also exhibiting a Wenzel state, characterized by a very low CAH of 4.0° and a total surface free energy of 4.0 mN/m. Finally, the H20F20 bilayer was classified as ultrahydrophobic, showcasing exceptional water repellency. Adhesion tests conducted using the cross-hatch cutter method yielded a 5B grade for all thin films, signifying excellent adhesion to a stainless-steel substrate. This strong adhesion for both HMDSO and pFOTES single layers is likely enhanced by surface plasma activation, which introduces active hydroxyl groups that facilitate hydrogen bond formation. The bilayer also demonstrated good adhesion properties to stainless steel.

3.8. Spray & wipe process

The Spray & wipe process works on straightforward principles. Initially, a coating material is atomized using a spray mechanism [177]. This atomization converts the liquid into fine droplets, which are distributed across the target surface of the substrate [178]. Following this, a wiping apparatus (typically made of cloth or a similar absorbent material) is employed to spread the coating evenly and remove excess material. This dual-action not only coats the surface but also facilitates the removal of contaminants, thereby enhancing surface cleanliness and adhesion properties [179,180]. One of the primary advantages of the spray & wipe process is its adaptability. It can be utilized on various substrates, such as metals, plastics, and glass, making it a versatile choice for multiple industries-ranging from automotive and aerospace to consumer electronics and furniture manufacturing. Additionally, the method allows for localized application, thus minimizing material waste and optimizing resource use. The process is especially valuable in scenarios where aesthetic finish and surface protection are critical, such as in the restoration of antique furniture or the protective coating of sensitive electronic components [181,182].

4. Durability tests for transparent self-cleaning superhydrophobic coatings

The durability of superhydrophobic coatings on solar panels is essential to maximizing its performance, efficiency, and lifespan in real time applications. These coatings effectively repel water and stains, maintain high light transmission, and minimize the frequency of cleaning and maintenance. Additionally, they provide protection against environmental factors and contribute to a lower environmental impact. Ultimately, long-lasting coatings ensure consistent performance, reduced maintenance expenses, extended panel longevity, and a more favourable return on investment for solar panel systems. To-a date, a several standard durability testing methods have been used to evaluate the mechanical durability of transparent superhydrophobic coatings. Fig. 15 represents schematics for general overview of different type of durability tests and these are briefly discussed in this section.

4.1. Adhesive tape peeling test

The adhesive tape peeling test is an essential method in coating research for several reasons. Firstly, it allows for the quantitative measurement of adhesion strength between a coating and its substrate, providing valuable insights into actual performance. Secondly, the test can simulate wear and environmental exposure conditions, offering crucial information on the durability of coatings, especially in demanding environments. Additionally, it facilitates the comparison of different coatings or formulations by establishing standardized test conditions, enabling researchers to assess superior adhesion. Many industries have specific adhesion standards that coatings must meet, and the adhesive tape peeling test provides a direct method for demonstrating compliance. In the process of conducting an adhesive tape peeling test, the tape having specific adhesion can be applied on the coating. As the tape is peeled off, the marginal coating materials will remove with tape, resulting change in surface morphology and a reduction in water contact angle. Researchers are investigating the potential of epoxy materials to improve coating durability by leveraging their outstanding adhesive strength and hydrophobic properties. For example, Li et al. [183] have reported that without epoxy layer, the

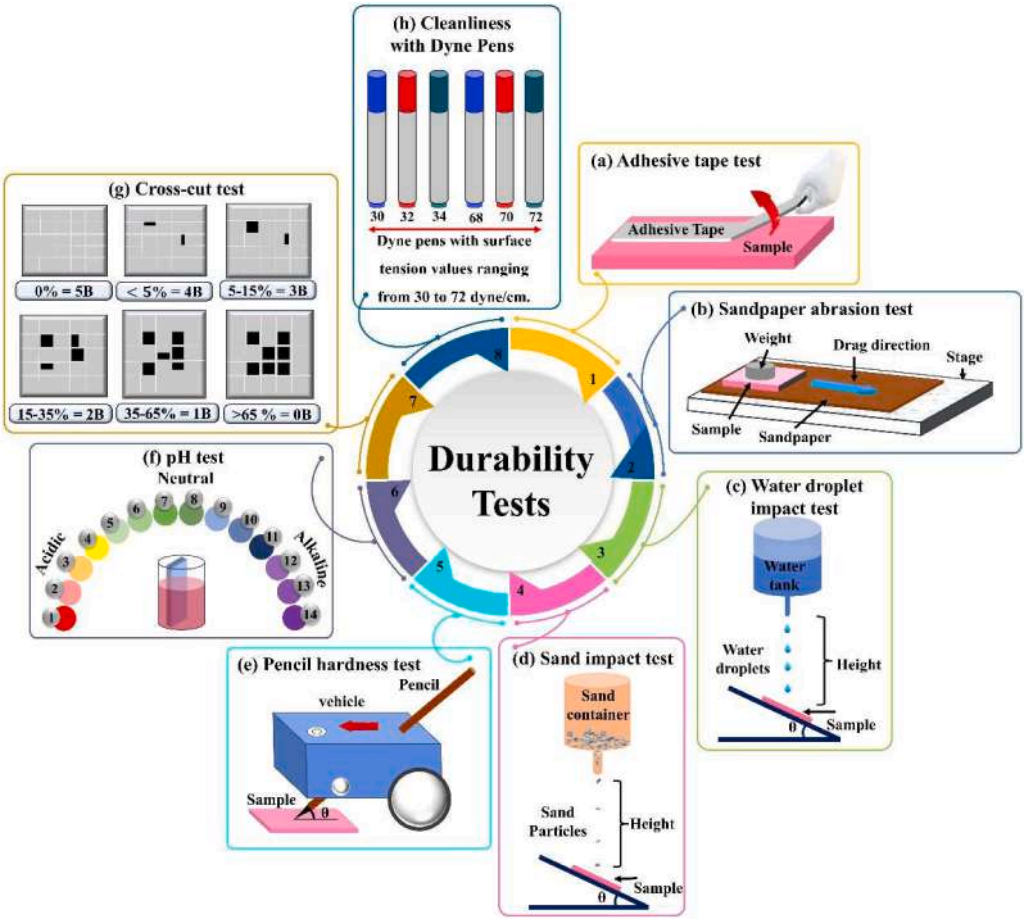

Fig. 15. Schematic illustration of experimental set up of (a) adhesive tape test, (b) sandpaper abrasion test, (c) water droplet impact test, (d) sand impact test, (e) pencil hardness test, (f) chemical stability test, (g) cross-cut test and, (h) cleanliness testing with Dyne Pens.

prepared coating lost superhydrophobic property within 3 cycles, while with epoxy layer the prepared coating sustains superhydrophobic property up to 30 peeling cycles. In another study, Zhao et al. [184] carried out adhesive tape test on the fabricated superhydrophobic coating. A combined solution of epoxy resin with dual-sized nanoparticles were spin coated and modified with 1H,1H,2H,2H-perfluorooctyl-trichlorosilane via CVD method (as depicted in Fig. 16a). The red arrows in Fig. 16b, indicates the detached of nanoparticles from the coating resulted in lowering in WCA from 162° to 160° and SA elevated from 3° to 4°. In this case the epoxy resin was less adhered to nanoparticles. Though, the fabricated sample maintained excellent superhydrophobic property and robustness.

4.2. Sandpaper abrasion test

The sandpaper abrasion test is an essential tool in coating research, providing valuable insights into the mechanical durability of coatings. This test assesses abrasion resistance under friction and contact, simulating real-world conditions. It allows for comparative evaluations of different coatings, aiding in the selection of optimal options for specific applications. Furthermore, it helps for improvement in coating formulation and application techniques by assessing how coatings degrade under abrasive conditions. Additionally, it serves as a standardized method to ensure that coatings meet industry-established benchmarks for abrasion resistance. Sandpaper is commonly used to assess the abrasion resistance of coatings. During this test, the coated material is rubbed against the abrasive surface of sandpaper with a specific grit size, while being subjected to a specific load and dragging velocity. The purpose of this test is to evaluate the adhesion properties of the coating by causing localized damage and progressively removing the coating material. Subsequently, the affected portion of the surface undergoes detailed analysis to examine the nature of the changes that have occurred [185].

For example, Guo et al. [186] have conducted a sandpaper abrasion test on a composite coating consisting of poly(ethyl cyanoacrylate) (PECA), SiO_2, and polydimethylsiloxane (PDMS) to assess its mechanical durability. The coated sample was subjected to abrasion using 600 mesh sandpaper with a 500 g weight at a speed of 5 cm s^{-1} for 20 cm, representing one cycle of abrasion. The study compared the performance of samples with and without the PECA (adhesive material) coating. Results demonstrated that the sample without the PECA coating lost its superhydrophobic property after only two abrasive cycles, while the PECA-coated sample retained its superhydrophobic property for up to 30 cycles. Fig. 16c illustrates the area of the coating that was damaged, with a white arrow indicating the direction of movement on the sample. Continuous abrasion resulted in minimal damage to the rough structure, suggesting that the PECA (adhesive) material contributes to enhancing the durability of the coating by strengthening the interface between the coating and the substrate.

4.3. Water impact test

The water droplet impact test is an essential aspect of coating research due to its ability to evaluate a resistance to water. This test provides valuable insights into the surface properties of coatings, including their potential for self-cleaning and moisture resistance. By simulating real-world conditions involving water impact (rain drops), researchers can gain a comprehensive understanding of how coatings

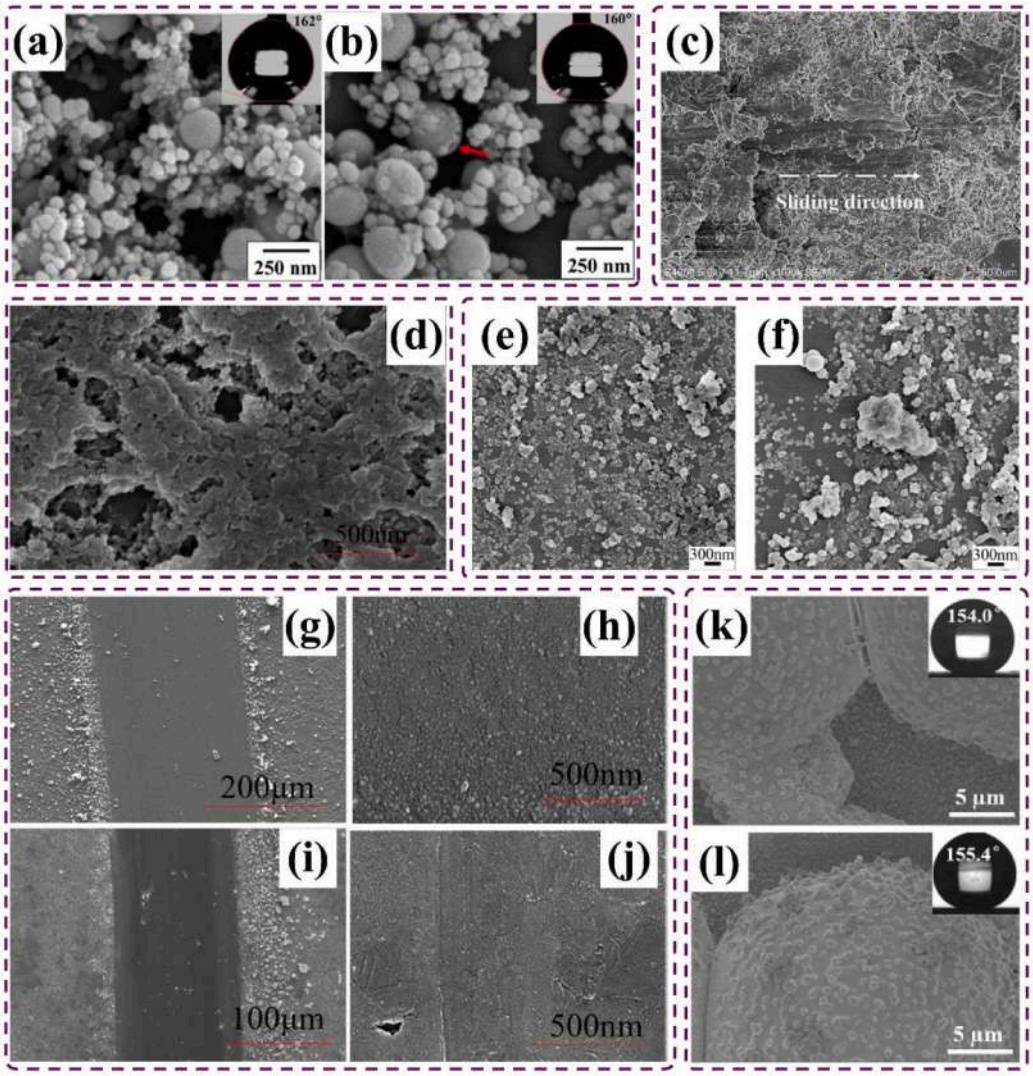

Fig. 16. Surface morphology of (a) before and (b) after adhesive tape test on S200/HS55 film, Reproduced from ref. [184] with permission from Elsevier, © 2020, (c) sandpaper abrasion test on PECA/SiO_2/PDMS, Reproduced from ref. [186] with permission from Elsevier, © 2014, (d) antireflective coating after water droplet impact, Reproduced from ref. [187] with permission from Elsevier, © 2018, (e) before and (f) after sand particle impact, antireflective coating, Reproduced from ref. [189] with permission from American Chemical Society, © 2014, (g) dragged by 4H pencil, (h) magnified area of the 4H pencil dragged area, (i) dragged by 5H pencil, (j) magnified area of the 5H pencil dragged area, Reproduced from ref. [187] with permission from Elsevier, © 2018, P25-P2@Glass samples were immersed in (k) aqueous HCl (pH 2) and (l) aqueous NaOH (pH 12) solutions for 24 h, Reproduced from ref. [191] with permission from Elsevier, © 2020. (inset images depicting WCA for respective test).

withstand mechanical stress caused by water droplets. Additionally, the test can reveal the adhesion strength of a coating to its substrate when exposed to water, identifying potential vulnerabilities that may lead to delamination or deterioration. Furthermore, researchers can use this test to compare the performance of different coatings, identifying formulations that offer optimal resistance to water impact. The results are crucial for determining which coatings are best suited for specific environments, such as outdoor applications, where water exposure is significant.

In this experiment, a sample is inclined at a specific angle to a horizontal surface, with a water tank positioned at a fixed height from the surface and a defined distance from the sample. Water droplets are then released one by one onto a specific area of the sample at a predetermined volume. The volume at which the sample loses its superhydrophobic properties is recorded. Upon impact, the water droplets undergo deformation, flattening due to high pressure at the point of contact, which is caused by the momentum's force. The hierarchical rough surface creates air pockets beneath the droplets, preventing wetting. The droplet's energy causes it to spread and then retract due to surface tension, ultimately causing the droplets to bounce off the coated surface rather than adhere to it. Initially, the water droplets easily roll off the coated surface, but continuous impact in high-pressure zones may lead to a change in the surface morphology of the coating, depending on material's structure. This change could result in dislodgment of nanoparticles or micro-cracks in the coating. For example, Liu et al. [116] conducted a water droplet impact test on a composite coating consisting of ethylene- vinyl acetate copolymer/SiO_2/3-methacrylox ypropyltrimethoxysilane /polytetrafluoroethylene (EVA/SiO_2/PTFE/KH-570). The sample was positioned at 30° angle to the horizontal surface, with the water droplets falling from a height of 40 cm at a rate of 60 droplets per min. After 35,000 water droplet impacts, the WCA decreased from 158.8° to 147.5°, indicating that wetting property slightly changed due to diminish surface structure of coating. Similarly, Zhi et al. [187] have reported that, when the prepared antireflective coating subjected to 60,000 water droplets impact (each with a volume of 25 μL and velocity of 2.7 ms^{-1}), the coating loss their pore structure, leading to reduced wettability of the coating. Additionally, the impacted region experienced a 4 % decrease in transmittance. Fig. 16d illustrates

the surface morphology after the water droplet impact.

4.4. Sand impact test

The sand impact test is of paramount importance in coating research, as it assesses a coating's ability to withstand abrasion and wear from abrasive materials like sand. This test is particularly critical for applications exposed to harsh, abrasive environments. By replicating real-world conditions, the test yields valuable insights into the long-term performance and stability of coatings when subjected to abrasive particles. The results of the test inform decisions regarding the selection of the most appropriate coatings for specific environments, such as outdoor applications where sand and grit are prevalent. In outdoor environments, superhydrophobic solar panels can be damaged by soil and dust particles carried by high-speed winds, leading to a decline in the coating's exceptional properties over time. To assess the coating's resistance to abrasion from sand particles, an impact test similar to the water droplet impact test can be performed. The test involves a container of sand and examining the surface properties after a specific amount of sand particles have fallen on it. During the sand impact test, the sharp edges of the sand can strike the coating, potentially causing dislodgement, cracks, or the formation of small pits. This damage can compromise the superhydrophobic properties of the coating by allowing water droplets to infiltrate the cracked regions. Guo et al. [188] conducted an experiment in which sand particles with an average diameter of 30 to 40 mesh impacted on a composite coating of SiO_2/polydimethylsiloxane/epoxy resin (SiO_2/PDMS/EP). The sample was positioned at a 45° angle to the horizontal surface, and the sand particles were dropped from a distance of 50 cm. After 360 g of sand impacted the surface, the WCA decreased from 163° to 156°, and the SA increased from 3.5° to 7.5°. Similarly, Xu et al. [189] also performed a sand impact test by dropping sand particles sized 100–350 μm with a velocity of 8.7 km/h from a height of 30 cm. The surface morphology of the coating before and after the sand particle impact test is depicted in Fig. 16e and f. After 20 g of sand impacted the surface, the adhered hollow silica nanoparticles (HSNs) and mesoporous silica nanosheets appeared to decrease. This reduction in deposited particles resulted in a slight change in the rough structure and a reduces the WCA to 160° from 162°.

4.5. Pencil hardness test

The pencil hardness test is an essential tool in coating research for quantifying scratch resistance. This property is critical for maintaining the visual and functional quality of coated surfaces. The test assesses a coating's ability to withstand mechanical wear and impact, providing valuable insights into its real-world performance. By comparing the hardness of different coatings, researchers can identify formulations with superior scratch resistance. A higher hardness rating typically indicates better surface protection, making this test particularly valuable for applications in challenging environments. The results obtained from this test can guide researchers in refining coating formulations to achieve the desired hardness characteristics while balancing other properties such as flexibility and adhesion. Furthermore, the pencil hardness test offers a straightforward method for demonstrating compliance. Pencils with different degrees of hardness, typically ranging from B to H, are commonly used in the evaluation of coating scratch. A higher B value indicates a softer pencil, while a higher H value indicates a harder pencil. In the testing process, a pencil is fixed to a testing apparatus so that its tip makes contact with a horizontal surface at a 45° angle. Additional weights can be added to the apparatus to increase pressure. Subsequently, the pencil's tip is brought into contact with the surface of the coating sample, and the apparatus moves at a constant speed in a specific direction. By observing which pencil causes damage to the coating surface, the quality of the coating can be assessed. For example, Zhi and Zhang [187] have performed a pencil hardness test on a dual-scale structure that had been coated with an antireflective layer followed by a layer of hydrophobic silica sol. The coating was able to withstand the pressure of a 4H pencil at a 45° angle with an applied force of 10 N, while still maintaining its antireflective properties (Fig. 16 g-h). However, when subjected to a 5H pencil, the dual-scale structure was completely damaged (Fig. 16i-j). This indicate that coating is stable up to 4H pencil hardness.

4.6. Chemical stability test

Evaluating the corrosion resistance of superhydrophobic coatings in harsh chemical scenarios is crucial for practical application. Exposure to acidic or alkaline conditions can lead to deterioration of the coating surface, resulting in changes in both the chemical composition and surface structure of the coating. A high concentration of H^+ ions characterizes acidic solutions, while alkaline solutions contain OH^- ions. Over time, this degradation can weaken the coating, potentially affecting the composite materials and overall hydrophobic properties. In contrast, neutral solutions with a pH of 7 may have a less significant impact due to the inherent properties of the coating. Therefore, it's crucial to verify the durability of the coating under various pH conditions. One approach to achieve this is by immersing prepared samples in solutions with different pH levels and monitoring the WCA over a specific duration. This comprehensive testing methodology can yield valuable insights into the performance of superhydrophobic coatings in diverse pH environments.

For example, Ji et al. [122] have conducted an experiment to assess the chemical stability of the prepared superhydrophobic samples by immersing them in acidic (pH 1, H_2SO_4), neutral (water), and alkaline (pH 14, KOH) solutions. They performed a wettability study at 10-minute intervals and collected statistical data for up to 40 min of immersion. The results showed that after 40 min, the WCA remained at 145° in neutral and acidic environments, but decreased to 85° in the alkaline solution. This suggests that the surface wettability was influenced by both the pH of the solution and the duration of immersion. Liu et al. [190] found that transparent superhydrophobic samples maintained their superhydrophobic behaviour (with a WCA greater than 150°) and transparency (greater than 90 %) after being immersed in pH solutions of varying pH (1, 3, 5, 7, 9, 11, and 13) for 72 h. This suggests that the coatings are chemically stable under these conditions. Zhu et al. [191] conducted an experiment in which they immersed superhydrophobic P25-P2@Glass samples in aqueous HCl (pH 2) and aqueous NaOH (pH 12) solutions for 24 h to assess the effect on surface morphology of the coatings. They measured contact angles (CAs) and sliding angles (SAs) at 4 h intervals. The results showed that both samples maintained their superhydrophobic properties. Fig. 16k and l illustrate that there was no clear damage to the samples after exposure to pH 2 and 12 solutions, respectively. The authors concluded that the chemical stability was maintained due to the protective layer of PDMS. In addition, Table 1 presents a summary of all discussed durability tests on the superhydrophobic properties as reported in the previous literatures.

4.7. Cross-cut Test

The cross-cut test is a widely accepted method which is employed to assess the adhesion strength and mechanical durability of coatings on various substrates. In this test, a sharp cross-hatch cutting tool is used to produce a grid pattern typically 1 mm × 1 mm squares on the coated surface. The cuts should penetrate through the coating to the underlying substrate. Then a pressure-sensitive adhesive tape is firmly applied over the scribed area and quickly peeled off at a consistent angle. The extent of coating removal is evaluated either visually or under magnification and is classified based on standardized rating scales (e.g., ASTM D3359 or ISO 2409). Areas with weak adhesion may lift or flake upon tape removal. This reveals the localized failure zones. By observing the failure modes whether cohesive (within the coating), adhesive (between coating and substrate), or mixed, researchers gain valuable insights into

Table 1
Summary of the results from durability tests conducted on different transparent superhydrophobic coatings.

Materials	Method	WCA / SA (°)	Transparency (%)	Adhesive tape test (cycles)	Sandpaper abrasion test (cm)	Water impact test (mL)	Sand impact test (g)	Pencil hardness test	Chemical Stability (h)	Refs.
Silica nano particles (~ 50 nm), Bisphenol-A-based epoxy, polyetheramine curing agent (D230) and 1H,1H,2H,2H-perfluorodecyltrimethoxysilane	Spin coating	153.4 ± 1.7/5.1 ± 1.1	97.6 (350–750 nm)	WCA 145.1° after 50 cycles	–	–	–	–	satisfactory water repellency after immersion in 10 vol % HCl aqueous for 3.33 h	[126]
Methoxy functional silicone resin, tetra-n-butyl titanate, methyltriethoxysilane, HMDS-treated fumed silica	Spray coating	163/ 2.3	80 in visible range	WCA 157.8° after 30 cycles	WCA 152.6° after 400 cm	–	–	–	For pH 2, 4, 6, 8, 10, 12 and 14 superhydrophobicity maintained after 24 h immersion	[195]
Phenyltrimethoxysilane, Hydrophilic monodispersed silica microspheres, 1H,1H,2H,2H-Perfluorodecyl-trimethoxysilane, 3-Glycidyloxypropyltrimethoxysliane, Trimethoxy (propyl)silane, N-(2-aminoethyl)-3-aminopropyltrimethoxysilane, Dibutyltin dilaurate	Sol-gel and spin coating	160.1 ± 1/7 ± 1	93.6 (400–800 nm)	WCA 140° after 200 cycles	WCA 128° after 1000 cm	WCA 135° after 300 mL	–	–	WCA 135° after immersion in pH 1, 7 and 14 for 0.667 h	[122]
1H,1H,2H,2H-perfluorodecyltrimethoxysilane, Hydrophobic silica nanoparticles (7–40 nm in diameter), Dupont capstone®FS-3100, Ausbond 92 conformal coating	Spray coating	156.1/ 2	91.5 at 550 nm	–	WCA 150.4° and SA 4.8°after 120 cm	–	–	–	For pH 2, 4, 6, 8, 10 and 12 superhydrophobicity maintained after 24 h immersion	[132]
Hydrophobic SiO_2 nanoparticles (7 − 40 nm), PDMS (prepolymer and curing agent)	Dip coating	164 / 1	91.4 (400–800 nm)	–	WCA 150° and SA 16° after 1200 cm	–	–	–	For pH 1, 3, 5, 7, 9, 11 and 13 superhydrophobicity maintained after 72 h immersion	[190]
TEOS, 1H,1H,2H,2H-Perfluorooctyltriethoxysilane, Silicon dioxide (ANP150)	Sol-gel, dip coating	154	91.6	WCA greater than 150° after 15 cycles	–	WCA greater than 150° after 2000 mL	–	–	–	[196]
PDMS (prepolymer and curing agent), titanium dioxide (P25), SiO_2, tungsten trioxide	Spray coating	168.6	76 (300–800 nm)	–	–	WCA greater than 154.5° after 110 mL	WCA greater than 154°after 50 *g*	–	For pH 2 and 12 superhydrophobicity maintained after 24 h immersion	[191]
TEOS, SiO_2 (40 nm and 15 nm), 1H,1H,2H,2H-per-fluorooctyltrichloro silane	Sol-gel, Dip coating	160.4 ± 4.8/ CAH ~ 7.1 ± 2.0	91 (400–800 nm)	–	–	WCA 156.3 ± 3.1° after 2000 mL	–	withstand by 9H pencil scratch	–	[197]
TEOS, SiO_2 (average diameter 15 ± 5 nm), trimethylchlorosilane, HMDS	Sol-gel, Spin coating	164 ± 2	89.9 at 550 nm	–	–	WCA 154° after 20,000 mL	WCA 152° after 40 *g*	–	From pH 1, 2, 4, 6, 8, 10, 12 and 14 superhydrophobicity maintained for pH 4 to 10 even after 730 h immersion	[198]
TEOS, Diethoxydimethysiliane, dodecyltrichlorosilane, octadecyltrichlorosiliane, Fumed hydrophilic SiO_2 (average diameter 12 nm)	Sol-gel, dip coating	153 / < 5	87.64 in visible range	–	–	WCA 150° after 3000 mL	–	–	–	[199]
Cerakote (MC-156 High Gloss Ceramic Clear), SiO_2 (Aerosil® r8200), parachlorobenzotrifluoride	Spray coating	167.71	Not mentioned	–	–	–	WCA 158.96° after 2.6 *g*	–	–	[200]
Cetyltrimethylammonium bromide, TEOS, 1H,1H,2H,2H-perfluorooctyl-Trichlorosilane, Poly (acrylic acid)	Dip coating and CVD	162	95 (530−1340 nm)	–	–	WCA 160° after 110 mL	WCA 160° after 20 *g*	withstand by 3H pencil scratch	WCAs 162 ± 2° and 153 ± 2° changed respectively after 0.083 h contact for pH 1 and 14	[201]

(*continued on next page*)

Table 1 (*continued*)

Materials	Method	WCA / SA (°)	Transparency (%)	Adhesive tape test (cycles)	Sandpaper abrasion test (cm)	Water impact test (mL)	Sand impact test (g)	Pencil hardness test	Chemical Stability (h)	Refs.
(Heptadecafluoro-1,1,2,2-tetrahydrodecyl) trimethoxysilane	Dip coating	169 / 5	82 in visible range	–	–	–	–	scratched by 9B to 9H pencils	–	[202]
γ-(2,3-epoxypropoxy) propytrimethoxysilane, Hexamethyldisilazane, Poly (ethylene glycol)-2000, octadecylamine, TEOS,	Dip coating	152	93.66 (300 ~ 1200 nm)	–	–	–	–	–	pH (2, 7 and 12): After exposure of 72 h the WCA reduced for pH 2 and 12 was 70° and 58° respectively. Also, remained intact for pH 7	[114]
Ethylene glycol diacrylate, 1H,1H,2H,2H-perfluoro-decyl Acrylate, tert-butyl peroxide and trichlorovinylsilane	iCVD	151 / 2	94.5 (400–800 nm)	–	WCA was greater than 150° after 100 cm	WCA 150° after 200 mL	WCA greater than 150°after 50 *g*	–	pH (1 and 12): WCA was not reduced for pH 1 but slightly changed for pH 12	[81]
TEOS and 1,1,2,2-Tetrahydroperfluorodecyltrimethoxysilane	CVD	166 / 1	80 in visible range	WCA reduced to 160° after 30 cycles	–	–	–	–	pH (1, 2, 3, 4, 5, 6, 7, 8, 9, 10, 11, 12 and 13): After 6 h immersion for acidic condition the superhydrophobicity was maintained but lowered for pH 13. However, for pH values 5 to 8 superhydrophobicity was maintained for 730 h.	[97]
Polytetrafluoroethylene, Alpha- (3,5-dimethyl-1-(2 methylpropyl) hexyl)-omega-poly (oxy-2-ethanediyl), Silica barrier coated glass substrates	AACVD	168 / <1	92.1 (400–760 nm)	–	–	WCA greater than 160° and SA less than 2° after 12 mL	WCA 149° and SA 9° after 10 *g*	–	pH (1, 2, 3, 4, 5, 6, 7, 8, 9, 10, 11, 12, 13 and 14): After 24 h immersion the WCAs greater than 155° while SAs were less than 4°	[100]
TEOS, 3-methacryloxypropyltrimethoxysilane, 1H, 1H, 2H, 2H Perfluorooctyltriethoxysilane, SiO_2 barrier glass	AACVD	165 / 1	90 (200–800 nm)	–	WCA 150° and SA ~3° after 100 cm	–	–	–	–	[99]
Silica glass, 1H,1H,2H,2H-Perfluorodecyl triethoxysilane	Femtosecond laser deposition	161 / 2	92 in visible and near IR region	–	–	–	WCA 155° and SA 30° after 150 g	–	–	[80]
AZP4620 photoresist, PDMS and curing agent, TEOS, Heptadecafluoro-1,1,2,2, -tetrahydrodecyl trichlorosilane,	Lithography	161	77 (400–800 nm)	WCA 146° after 20 cycles	WCA 149° after 5 cm	–	WCA 157° after 20 *g*	–	–	[158]
Hydroxyethyl methacrylate, Sudan Orange G, phenylbis(2,4,6-trimethylbenzoyl) phosphine oxide, tetra (ethylene glycol) diacrylate, diethyleneglycol dibenzoate, Aerosil OX50, tetraethoxysilane and trichloro(1H,1H,2H,2H-tridecafluoro-n-octyl) silane	Microstereolithography	154.3 / 6.8 ± 0.7	Over 90 in visible range	–	–	–	–	–	pH (2, 4, 6, 8, 10, 12 and 14): superhydrophobicity maintained for all pH values even after 2 h exposure	[159]

how the coating system performs under mechanical stress. Beyond adhesion measurement, the cross-cut test also serves as not only an indicator of coating uniformity, durability but also long-term reliability [192].

Luo et al. [193] demonstrated the cross-cut test on poly (ethylene-co-acrylic acid) (EAA)-silica nanoparticles (SiO_2) coating, showing strong adhesion across various substrates. The results show that the coating exhibited less than 5 % peeling, revealing excellent bonding strength. The EAA has significantly improved the adhesion by contributing to a strong bond between SiO_2 and the substrate. Zhao et al. [131] conducted a cross-cut test on SRAC-based superhydrophobic coatings on a glass substrate. These results reveal strong adhesion, with no observable peeling detected after tape removal, indicating Grade 5B adhesion, the highest rating in ASTM D3359. poly(furfuryl alcohol) (PFA) improved the binding strength between the silica nanoparticles layer and substrate, resulting in long-term mechanical durability. Zheng et al. [96] performed the cross-cut test to assess the adhesion strength of SiO_2-based transparent superhydrophobic coating coated on glass substrates. The results demonstrated strong adhesion with less than 5 % of the coating peeling off, with a grade 0–1 adhesion based on ISO 2409–1992 standards, showing excellent interfacial bonding between the coating and the substrate.

4.8. Testing with dyne pens

The dyne pen test is known as rapid test to examine the changes in surface energy of the coatings. It has been used to measure the surface energy of material, which directly influences adhesion performance as well as coating's durability. It contains a series of inks with known surface tension from (30 to 70 dyne/cm). Ink is allowed to apply on the surface, which helps to find out the surface tension by noticing the ink either beads up or wets the surface. The spreading or beading of the ink solution indicates surface energy levels. Higher surface energy after degradation leads to water repellence and a lower CA. This test supports the development of a durable, low-energy surface for long-term superhydrophobic property of coating [35].

Wu et al. [194] conducted dyne pen testing on hexafluorobutyl methacrylate (HFMA)-modified core–shell polyacrylate latex pressure-sensitive adhesives (PSAs) applied to the glass substrate. The results reveal a decrease in surface tension from 42 mN/m to 34 mN/m as HFMA content increases from 0 to 20 wt %, showing improved hydrophobicity and reduced wettability. Surfaces with higher Dyne levels above 40 mN/m showed excellent adhesion (Grade 0–1), confirming strong bonding between the coating and the substrate.

5. Photovoltaic study with transparent superhydrophobic self-cleaning glass

In addition to developing transparent superhydrophobic self-cleaning coatings for cover glass and evaluating their mechanical durability in extreme conditions, it is essential to investigate the performance of solar cells for practical applications. Environmental factors can diminish the efficiency of solar cells, making it imperative to assess the performance of solar cells when shielded with transparent superhydrophobic self-cleaning coatings in outdoor conditions. The efficiency of solar cells after being protected with a transparent superhydrophobic cover glass was studied by Sutha et al. [203]. They fabricated a transparent superhydrophobic coating on glass substrates by spinning aluminium oxide sol in a nitrogen atmosphere. Multiple layers were spin-coated on different glass slides as single, double, triple, and quadruple, with each layer being heated to 150 °C for 60 s. Subsequently, all samples were annealed at 400 °C for 1 h to obtain aluminium oxide films. To obtain superhydrophobicity, the prepared samples were dipped in hot water for 20 min and modified by spinning 1H, 1H, 2H, 2H – perfluorooctyl trichlorosilane-toluene solution on them. Finally, all samples were annealed and the modified samples were denoted as B1, B2, B3, and B4, respectively. Such samples reveal transparency of 86 %, 92 % and 95 %, and WCA of 121°, 146° and 161°, respectively. The photovoltaic study was carried out on spin-coated B1, B2, and B3 samples. Photovoltaic parameters such as open circuit voltage (V_{OC}), short circuit current (I_{SC}), maximum power, fill factor (FF), and efficiency (η) were measured for various situations, including standard solar cells, uncoated substrates, and the as-fabricated substrates (B1, B2, and B3), as well as under dust contamination and after cleaning. The efficiency of the solar cell decreased from 1.5 ± 0.05 to 1.2 ± 0.05 after placing a bare cover glass on it. However, after replacing the bare samples with B1, B2, and B3 samples, the efficiency improved to 1.32 ± 0.04, 1.32 ± 0.03, and 1.4 ± 0.04, respectively. Furthermore, the authors conducted a photovoltaic study under dust contamination and after self-cleaning performance. An increase in the efficiencies was observed from 0.43 ± 0.03, 0.65 ± 0.009, and 0.71 ± 0.009 to 1 ± 0.012, 1.19 ± 0.014, and 1.23 ± 0.015 for B1, B2, and B3 samples, respectively. Therefore, it is concluded that the prepared samples exhibited good transparency and self-cleaning performance.

In another study, Liang et al. [204] developed a transparent superhydrophobic coating for a glass substrate by applying three layers of coatings. First, they applied an antireflective silica layer using the plasma-enhanced CVD method, which had a large number of hydroxyl groups on its surface. Then, they created a middle layer by depositing glycidoxypropyltrimethoxysilane, forming a 3D structure with hydroxyl groups at both ends. Finally, they achieved a stable superhydrophobic surface by spin-coating a top layer of superhydrophobic silica. Three layered coating has showed WCA and transparency of 153° and 94 %, respectively. They conducted a 60-day photovoltaic study in 12-day intervals (1 cycle), measuring the photovoltaic parameters after cleaning with water to remove environmental pollutants. The results showed a 21 % reduction in solar efficiency for the bare covered solar cell, while the efficiency of the superhydrophobic coated solar cell decreased to 14.81 %. These findings indicate that the prepared transparent superhydrophobic cover glass exhibited superior photovoltaic conversion efficiency compared to bare glass. Lee et al. [205] developed antireflective superhydrophobic films using two methods. The first method involved a hot-embossing procedure using PET film coated with fluororesin, while the second method employed nanoprint lithography on UV-curable methacryloxypropyl-terminated polydimethylsiloxane (M-PDMS) resin and PET film. To increase the low surface energy of the M-PDMS sample, heptadecafluoro-1,1,2,2-tetrahydrodecyl trichlorosilane was coated by dipping for 10 min. The I-V characteristics were evaluated by illuminating incident light with a solar simulator on a monocrystalline Si solar cell (20 × 20 mm in size). The bare glass exhibited an efficiency of 21.14 %. In contrast, the fluororesin and M-PDMS coated samples exhibited efficiencies of 21.43 % and 21.58 %, respectively.

Torun et al. [206] utilized a process involving spin coating of end-grafted polymers on a glass substrate, followed by spray deposition of tridecafluoro-1,1,2,2-tetrahydrooctyltrichlorosilane-functionalized silica nanoparticles to create an antireflective superhydrophobic coatings (SHPARCs). The resulting SHPARCs cover glass displayed a WCA of 168° and a SA of 2°, showcasing exceptional water repellence as shown in Fig. 17a. The cover glass effectively repelled water, as depicted by the inset image. In a photovoltaic study, a solar cell (156 × 156 mm^2) with the superhydrophobic antireflective coating exhibited J-V characteristics similar to those of an uncoated solar cell. The efficiency of the solar cell was 16.87 % and 16.64 % before and after applying the SHPARC cover glass, respectively. Wang et al. [207] fabricated double-layer antireflective superhydrophobic coating on glass surface via dip coating method. The bottom layer solution consisted of γ-(2,3-epoxypropoxy) propyltrimethoxysilane in ethanol, high-purity water, octadecylamine, and polyethylene glycol-1000. The top layer solution involved a combination of hydrophobic particulate silica sol and long-chain silica sol. Glass substrates were dipped and withdrawn at a speed of 1500 μm/s for 14 s in the bottom layer solution, followed by

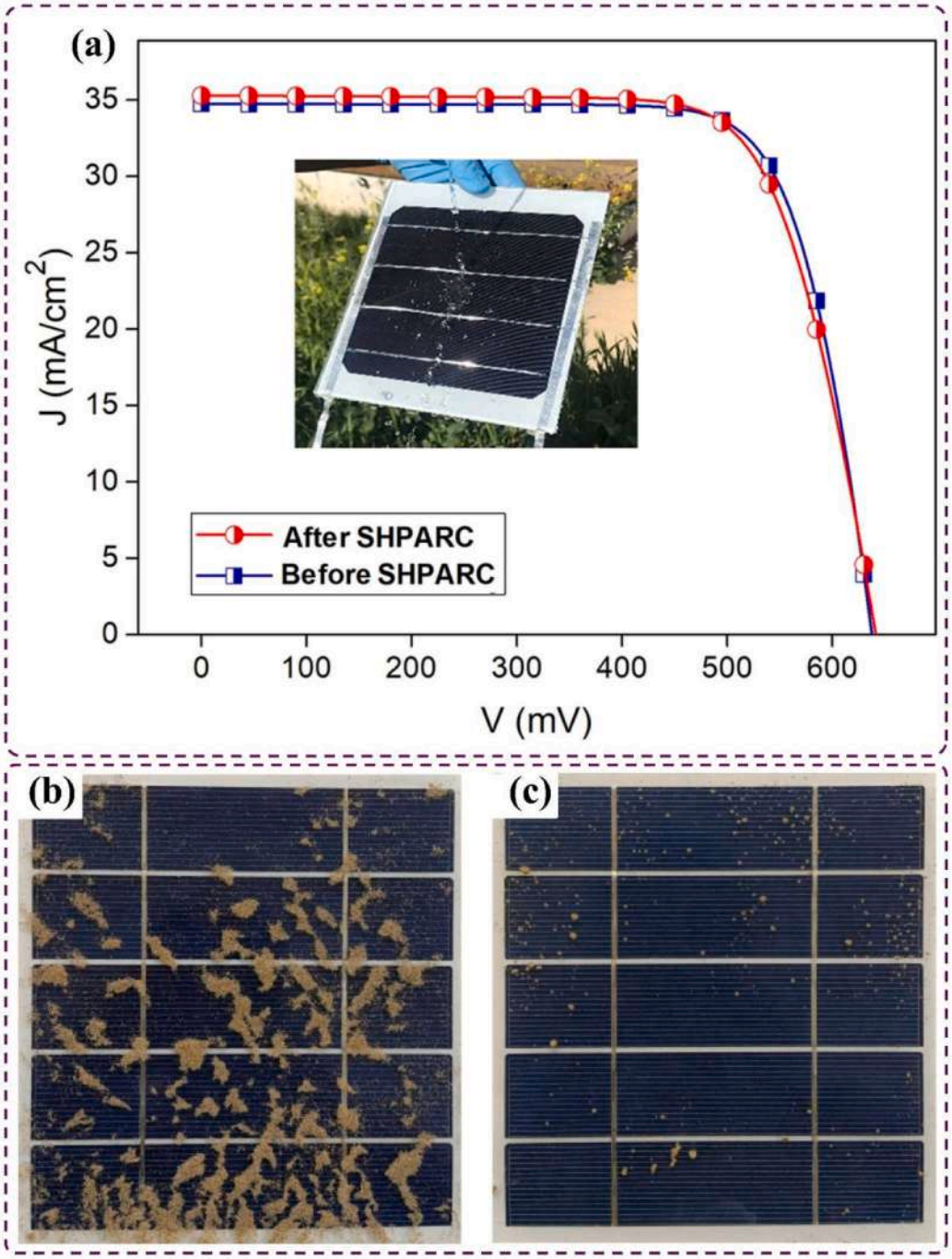

Fig. 17. (a) J-V characteristics of solar cell before and after application of SHPARC. Inset image depicting the self-cleaning effect on solar cell. Reproduced from ref. [206] with permission from American Chemical Society, © 2018. Optical images of solar cell after simulation experiment of rainfall on (b) bare and (c) superhydrophobic coated cover glass. Reproduced from ref. [207] with permission from Elsevier, © 2022.

calcination at 500 °C for 3 h. Subsequently, the substrates were dipped in the top layer solution for 5 h and dried at 80 °C for 30 min. Authors have carried out a simulated experiment of rainfall on the bare as well as superhydrophobic coated solar cell as depicted in Fig. 17b-c. A 2.1 mL volume of water was sprayed on the solar cell of size 180 mm × 150 mm to examine self-cleaning as well as photovoltaic study. After self-cleaning performance, the output power restored for bare and coated cover glass was 83 % and 96.6 %. The minimal rough structure on the bare glass led to strong adhesion, causing dust particles to adhere to the glass surface (Fig. 18b). Conversely, a higher rough structure resulted in reduced adhesion on the superhydrophobic coated glass, enabling water droplets to easily collect and remove dust particles from the surface (Fig. 18c). The authors observed that the bare cover glass had a dust particle density of 2.7 mg/cm^3, while the coated cover glass had a density of 0.28 mg/cm^3. This demonstrates that the prepared superhydrophobic sample exhibited excellent self-cleaning properties and resulted in higher output power. In Table 2, we have compiled data on the efficiency of solar cell that is protected by a transparent superhydrophobic-coated cover glass, as reported in the literature.

Apart from the previous discussion, some commendable studies have explored the application of self-cleaning technology on a large scale. Recently, Walz et al. [212] a team from the Faculty of Renewable Energy and Automotive Technology at Madison College, USA developed a spray technique in collaboration with the college's collision repair facility. It is

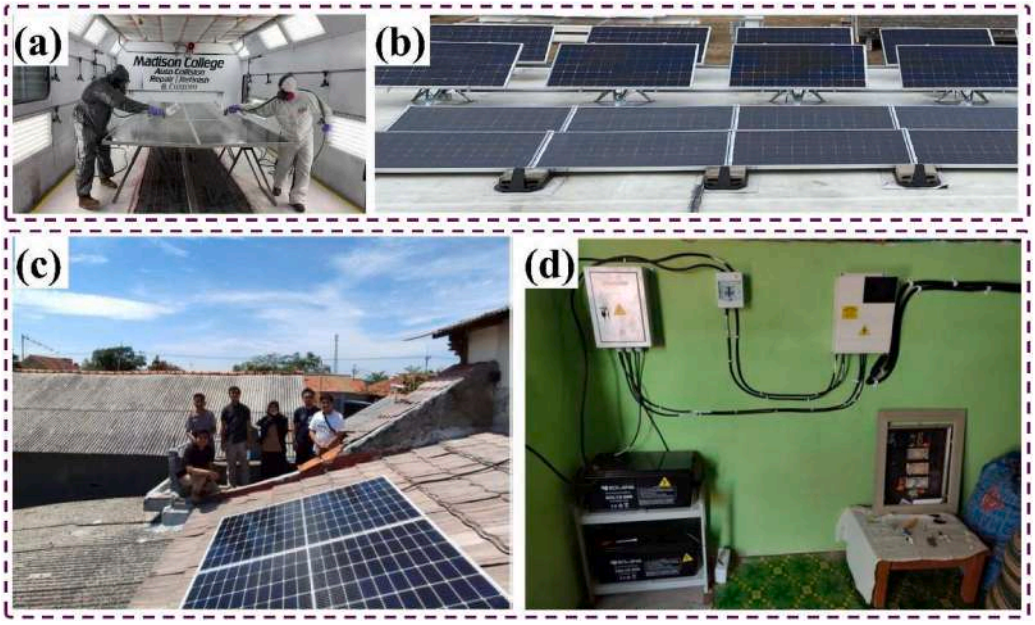

Fig. 18. (a) Spray deposition on solar modules in Medison college collision repair facility centre. (b) Installed solar module at test side of rooftop of Medison college campus (Front eight modules are coated and rear eight modules are uncoated). Reproduced from ref. [212] with permission from Elsevier, © 2023. (c) PV panels installed on the roof of SME's house. (d) An installed electrical system in a room dedicated to solar system. Reproduced from ref. [213] with permission from Green Publisher Indonesia, © 2024.

Table 2
The performance of transparent superhydrophobic glass-protected solar cells.

Materials	Fabrication method	WCA / SA (°)	Transparency (%)	Target Surface	Area of Cover Glass	Solar cell efficiency η (%)				Change in η after coating	Refs.
						Before coating	After coating	Before self-cleaning (under dust)	After self-cleaning		
Glycidoxypropyltrimethoxysilane, Hexamethyldisilazane, Octadecylamine, Tetraethoxysilica	CVD	153	94 (300–780 nm)	Glass	2.5 cm × 2.5 cm	16.47	16.16	–	–	η elevated by 0.31 % after fabrication	[204]
TEOS, Polyethylene glycol-1000, Octadecylamine, γ-(2,3-poxypropoxy) propytrimethoxysilane, Trimethylethoxysilane	Dip coating	151.2/ 4.5	95.9 at wavelength of 507 nm	Glass	18 cm × 15 cm	Power (mW) 1094	Power (mW) 1156	Power (mW) 929.7	Power (mW) 1117	Power was elevated by 107 mW	[207]
Hexamethyldisilazane, Tetraethylorthosilicate		169.7 / 3	93.1 (350−900 nm)	Glass	2 cm × 1 cm	11	11.9	–	–	η elevated by 0.9 % after fabrication	[208]
γ-(2,3-poxypropoxy) propytrimethoxysilane (KH-560), Octadecylamine, Polyethylene glycol-2000, Ethylsilicate,1,1,3,3,3-Hexamethyldisilazane		159	93 (350−800 nm)	Glass	18 cm × 15 cm	Power (mW) 196.3	Power (mW) 206.2	Power (mW) 160.8	Power (mW) 199.1	Power was elevated by 9.9 mW	[209]
Methyl tetra-hydro phthalic anhydride, Epoxy-modified silicone resin, Tetraethoxysilane, hexamethyldisilazane, nanofumed silica (HS, Hydrophobic-100, 7–40 nm), ethyl acetate		155.1 / 0.1	95.5 in visible range	Glass	–	~ 0.9	~ 0.95	~ 0.8	~ 0.9	η elevated by 0.05 % after fabrication	[210]
Hexamethyldisilazane, Trimethyl (1H, 1H, 2H, 2H-decyl) silane, Tetraethylorthosilicate		145	97.4 (350−900 nm)	Glass	–	11.04	11.81	–	–	η elevated by 0.77 % after fabrication	[211]
Aluminium nitrate nonahydrate, 2-methoxyethanol, monoethanolamine, 1H, 1H, 2H, 2H - perfluorooctyltrichlorosilane	Spin coating	161	95 (400–700 nm)	Glass	–	1.2 ± 0.05 At 30 ° inclined angle	1.4 ± 0.02	0.71 ± 0.009	1.23 ± 0.015	η elevated by ~ 0.2 % after fabrication	[203]

clear that a controlled environment free from environmental challenges such as wind velocity, humidity, sprayer control, and safety precautions is required to develop the desired coatings for commercial applications. Therefore, they fabricated coatings on solar modules in a temperature and humidity controlled, dust-free environment provided by the facility centre (Fig. 18a). In addition, a professional controlled spray deposition system was utilized. Approximately 33 mL of the coating solution was sufficient to coat one module, accounting for an estimated 10 % loss of volume due to overspray. The applied coating exhibited a roughness of around 350 nm. The module was dried for 30 min, and it was observed that the thin deposition of coating was visible to the naked eye and showed no removal during a fingertip dragging test. A total of 16 modules were installed on the rooftop of Madison College, with 8 modules coated and 8 uncoated (Fig. 18b). The authors conducted real-world performance tests on both coated and uncoated modules, assessing the impact of bird droppings and soiling at different tilt angles of 10° and 30° They found that the solar specific yield increased by 3.52 % and 3.05 % for the coated modules compared to the uncoated modules over a period of 12 months. The authors claim that large-scale fabrication could reduce costs through bulk purchasing of materials, control over overspray due to the use of an ultrasonic spray system, and minimal waste produced due to an inline mixing system. In this study, the total materials cost was $80 per liter for small batches, which adds approximately $2.60 per solar panel or $0.0070 per watt of power. Consequently, the panel cost increases by about 1.4 %. However, the coated panels generate 3–3.5 % more energy, making the additional cost worthwhile.

In another study, Wahyuono et al. [213] focused on enhancing the solar power efficiency of a rooftop solar power system with a self-cleaning coating made using ZnO and TiO_2 nanoparticles. The potential of the solar system was studied by analysing long-term climate data, such as air temperature and sunlight duration. This solar power was used for domestic electricity, including Small and Medium Enterprises (SMEs). They examined the impact of the self-cleaning coating on the performance of an installed rooftop solar power system (depicted in Fig. 18c) using energy billing data from an SME in Indramayu and the corresponding percentage of energy sharing. A separate electrical system was set up to measure the solar system performance, as shown in Fig. 18d. Electricity consumption during the first three months was established as the baseline. In contrast, the subsequent nine months demonstrated energy savings after the installation of the solar power system. The coating maintained solar panel performance at 85 % over nine months. The energy sharing percentage remained consistent during the implementation of the ZnO/TiO_2 coating on the solar power system, maintaining its functionality throughout both dry and wet seasons. The off-grid photovoltaic system had a capacity of 1050 Wp and significant advantages, including a 30 % reduction in electricity costs for small and medium enterprises, as well as domestic applications. The self-cleaning coating enables consistent energy generation year-round, minimizing maintenance requirements.

Guo et al. [214] developed a robust hydrophobic transparent resin composite film on glass substrate by modifying silica components by organic/inorganic method. The coated layer elevated the transparency of the film by 0.69 % compared to uncoated glass. The coating was applied on the PV panel and placed in outdoor for 3 weeks to examine the not only amount of dust accumulation and efficiency of PV panel. To carry out the test, two solar panels, uncoated and coated which had dimensions of 300 cm × 410 cm × 17 cm each. The dust accumulation on the solar panels were lowered due to elevation in PV panels align to wind direction. The optimum tilt angle was set to 60°. The efficiency of the solar panels was gradually lowered for uncoated and coated glass due to density of dust accumulation was elevated to 22.76 g/m^2 and 14.63 g/m^2 from 0 g/m^2 respectively. The coated PV panel exhibited less amount of dust accumulation due to its self-cleaning property. The efficiency of the uncoated and coated PV panels was almost same at the beginning of the testing. After the three weeks of time, the coated PV panel was showed 1.11 % higher efficiency than uncoated PV panel. Interestingly, efficiency of uncoated PV panel was reduced by 3.8 % while coated PV panel was reduced by only 1.48 % individually. It is obvious reason that, the coated PV panel exhibited self-cleaning behavior than uncoated one.

6. Long-term durability and economic viability

Long-term superhydrophobic coatings on solar panels offer significant economic advantages by enhancing energy efficiency and reducing maintenance costs. These coatings repel water, and preventing dirt, contaminants, debris accumulation that can obstruct sunlight. This leads to optimal energy output and better overall efficiency. A key benefit is their self-cleaning capability, allowing water to bead and roll off, which reduces manual cleaning needs and lowers expenses. These coatings also protect against environmental stressors like heavy rainfall and dust, minimizing wear and tear and enhancing the solar panels' longevity, especially in humid or coastal areas where corrosion is a concern. By ensuring clean panels, they maintain higher energy production, translating to improved economic returns. Additionally, the reduced need for cleaning lowers labor costs and environmental impact, promoting a more sustainable approach to maintenance. In Section 5 as disscussed, Walz et al. [212] and Wahyuono et al. [213] have applied superhydrophobic self-cleaning coatings on installed solar panel system and studied their performance. They have reported that, large scale coatings reduces fabrication cost as well as electricity cost. Pop et al. [216] developed not only highly abrasive-resistant but also durable low temperature processed sol-gel antireflective coating for solar module glass. The coating was developed by hydrolysis as well as partial condensation of organo-tri-alkoxy-silanes and tetra-alkoxy-silanes. The homogenous solutions of the high silanol containing co-polymers of silsesquioxane were coated on pre-cleaned substrates by flow coating technique and allowed cured at 300 °C. The final coating had thickness of 70–120 nm with exceptional antireflective properties. The developed coating was denser than other traditional coatings. These coatings were suffered through industry-standard test EN1096.2 and accelerated environmental test IEC61215 from Enki Technology. The developed coating was exhibited four times greater longevity than other existing coatings with comparable optical properties. This helps to not only lowered the risk of handling during manufacturing and installation, operational and maintenance cost, warranty cost but also elevated the energy yield. Schaeffer et al. [217] developed an anti-soiling coating with high transparency and mechanical robustness via simply spray on coating using functionalised silica nanoparticles. In optical transmission measurements of both uncoated and coated glass substrates demonstrated no loss in transmission. The different applied layers were demonstrated elevation in the transmittance which depicts the anti-reflection properties of the coatings. In mechanical durability test, using a Taber® Industries Abraser, single-layer superhydrophobic coatings exhibited significant degradation after 10 cycles of abrasion. A drop in WCA below the acceptable limit of 150°, attributed to the loss of silica particles. On the other hand, multilayer coatings showed only a ~10 % reduction in WCA after 35–40 cycles, maintaining superior performance, and achieving a four-fold increase in durability relative to single-layer coatings even after 100 abrasion cycles. Additionally, simulated UV exposure, which was 12–17 times greater than typical solar UVA exposure was utilised. Results demonstrated that some coatings retained their superhydrophobicity (CA > 150°) after up to 700 h of UV exposure, whereas a polymeric binder and previous formulations showed lower durability, with the latter rapidly declining to marginally hydrophobic levels after 200 h. Overall, the accelerated UV tests equated to 8,000–12,000 h of real-world solar exposure, indicating that with proper formulation. Therefore, the prepared coatings can withstand significant environmental stressors over extended periods, making them viable for practical applications in outdoor settings.

7. Industrial implementation and patented literature

A one of the world's major solar panel manufacturers, Yingli Solar has announced that all its solar products are developed with a new anti-reflective glass coating called CleanARC® [218]. This innovative coating, developed by Enki Technology in California, helps to boost energy of solar panels over time and reduces the need for frequent cleaning. In addition, it exhibits strong resistance to scratches as well as environmental damage. Especially useful in tough climates like deserts, coastal areas, and regions with high humidity or temperature changes. Its hydrophobic surface also supports better self-cleaning and helps to minimise the maintenance costs. Lab and field tests show that CleanARC® panels perform better in challenging environments, making solar energy more practical and reliable in places where it was once difficult to use. A well-known solar energy company named Suntech was established in 2001 with focused on not only research, development but also production of crystalline silicon solar cells and modules [219]. Suntech yet sold their products more than 100 countries as well as regions around the world. So far, they have shipped over 50 GW of solar products. Currently, company manufactures different solar modules in with power generation ranging within the 435–720 W with maximum efficiencies of 21.6 % to 23 %. Intrface Technologies offers advanced atmospheric plasma treatment solutions which help to improve the performance as well as durability of solar panels [220]. Their systems are used for cleaning and activating surfaces like glass, coatings, junction boxes, and mounting structures so that everything bonds properly and lasts longer. This is especially important for antireflective coatings and electrical connections, which need strong adhesion to work well over time. Interestingly, their method does not rely on harsh chemicals or abrasive cleaning. Additionally, it is designed to keep up with fast-paced solar panel production. By ensuring better bonding and surface preparation, Intrface technology supports the long-term reliability of solar panels, especially in harsh weather and demanding environments. Table 3 represents the features various self-cleaning coatings developed by different companies.

Sakthivel et al. [227] patented a file on "A Super Hydrophobic Coating with High Optical Properties having Easy to Clean Property, UV and Corrosion Resistance Properties, a Process of Preparation and Application of the Same". This innovative coating was developed by spray and wipe method in single layer which eligible to produce self-clean properties. The coating exhibited no loss in optical transmittance. This coating addresses key challenges in protecting PV panels from dust, dirt, corrosion, and moisture, while maintaining high transmittance and power conversion efficiency post-deposition. Key features of this technology include not only low-cost production, simple coating techniques that are easily scalable but also ambient-cured, with superhydrophobic properties demonstrated by water contact angles exceeding 110°. The coating also exhibits high weather and mechanical stability, showing reduced dust accumulation compared to conventional coatings. Applications extend beyond PV panels to include optical lenses, video display panels, architectural and automotive glass, textiles, and various surfaces. The technology has been validated through successful deployment in collaboration with NTPC Ltd and has received certification from the Central Power Research Institute (CPRI), making it available for non-exclusive transfer.

Binghai et al. [228] fabricated transparent superhydrophobic spray capable of forming a clear, water-repellent film on various substrates. This spray consists primarily of surface-modified silica (SiO_2) nanoparticles dispersed in a volatile organic medium such as methanol, ethanol, isopropanol, n-hexane, or n-heptane. The modified SiO_2 nanoparticles, with diameters ranging from 10 to 100 nm, are chemically functionalized using agents like trimethyl chlorosilane, triethyl chlorosilane, or hexamethyldisilazane to impart low surface energy and enhance hydrophobicity. The preparation process involves a sol-gel synthesis route wherein tetraethyl orthosilicate (TEOS) is hydrolysed under acidic conditions (pH 1–3) to form silica sol, followed by pH adjustment to alkaline conditions (pH 8–10) to yield a transparent silica gel. This gel is subsequently modified through alkylation by reacting with the silane modifiers in an appropriate solvent mixture at 30–80 °C for up to 24 h. The resulting hydrophobic gel is washed, dispersed, and decanted to obtain a clear superhydrophobic spray with a silica content of 0.01–0.5 % by mass. When applied to clean and dry surfaces such as ceramics, glass, paper, wood, stone, metals, and polymers, the spray forms a transparent coating exhibiting a water contact angle $\geq$150° and a roll-off angle $\leq$10°. Furthermore, the film maintains a high transmittance of 90–99 % at 550 nm, ensuring excellent optical clarity in the visible region. Xuelin et al. [229] developed superhydrophobic coating technology with a highly wear-resistant and highly transparent nanocoating through an organic-inorganic hybrid approach. This technique employs liquid-phase organic-inorganic hybrid molecules, such as cage-like or trapezoidal polyhedral oligomeric silsesquioxane (POSS), combined with cationic photoinitiators (e.g., diaryliodonium or triarylsulfonium salts) to form a UV-curable resin. The coating's functional nanostructure is fabricated using V-shaped nanopore templates composed of anodized aluminum or photolithographically replicated

Table 3
Features of the self-cleaning coatings of different companies.

Sr. No.	Company name	Product name	Features	Refs.
1..	Advanced NanoTech Lab	Hydrasol®	Self-cleaning superhydrophobic coating, thickness less than 1 μm, colourless appearance, room temperature curing	[221]
2.	Sinovoltaics	DIY®	Hydrophobic, self-cleaning, resistant to salty air,	[222]
3.	Diamon-Fusion International	DIAMON-FUSION®	Coating thickness less than 40 nm, Hydrophobic coating repels rainwater, snow, sleet, and debris, increases solar panel energy efficiencies, keeps solar panels cleaner for longer, Helps protect against chips and cracks, UV resistant	[223]
4.	TriNANO Technologies	TriNANO®	Elevated power generation of solar cell by 4 %, anti-reflection and self-cleaning properties, reduces the panel temperature by 2–3 °C, thermally and chemically stable, anti-soiling, 55 % reduction in water use for cleaning, Coating thickness less than 400 nm	[224]
5.	Nanopool	NP®	Application to solar park, easy cleaning, longer lifespan, weather protection, cost reduction	[225]
6.	Electrical Research and Development Association		Self-cleaning Nano-coating, excellent anti-dust properties & decomposes hydrocarbons and prevent organic growth, coated panel conforms to IEC-61215 for evaluation in simulated conditions, reduced cleaning frequency & hence, saving in expenditure for cleaning (A patent has also been filed on this technology. (Indian patent application No. IN 201721041951 – Title "ANTI-DUST / SELF-CLEANING COATING COMPOSITION AND APPLICATION THEREOF".)	[226]

resin molds. These templates, which contain an ordered array of nanocone-shaped pores with diameters ranging from 10 to 200 nm and periods below 200 nm, are first treated with low-surface-energy release agents like perfluoroalkyl or alkyl silanes to enable easy separation after curing. In the coating process, the UV-curable resin is deposited onto the template and pressed with a target substrate to allow the liquid to infiltrate the nanopores. UV irradiation (3 s to 10 min) initiates curing, followed by thermal post-curing at 60–150 °C for up to 3 h in a controlled humidity environment (60–100 %). This results in the formation of a robust and transparent nanocone array coating on the substrate. Subsequently, the surface undergoes oxygen or air plasma treatment (10–50 W for 1–10 min) to enhance chemical reactivity, after which it is functionalized with low-surface-energy, liquid-like molecules such as linear fluoropolyethers or polydimethylsiloxane, typically with molecular weights between 1000 and 10,000 g/mol. The resulting nanocoating exhibits superhydrophobicity, characterized by high water contact angles and low roll-off angles, while maintaining excellent optical transparency due to the sub-wavelength scale of the nanocone structures. Furthermore, the integration of organic–inorganic hybrid materials, nanostructured geometry, and lubricating surface chemistry contributes to significantly improved mechanical durability, making this coating suitable for demanding applications such as optical devices, flexible electronics, and outdoor protective surfaces where both transparency and abrasion resistance are essential.

Qiang et al. [230] fabricated a transparent superhydrophobic coating with enhanced mechanical durability involves a unique three-layer structure comprising a silicone adhesive base, a superhydrophobic silicon dioxide (SiO_2) layer, and a UV-curable protective topcoat. This method enables the formation of a durable and optically clear coating on glass substrates. The process begins with the preparation of a silicone adhesive diluent by dispersing 0.4 *g* of neutral silicone adhesive in 20 mL of ethyl acetate, followed by magnetic stirring and ultrasonic treatment. This solution is then uniformly sprayed onto a pretreated glass substrate and cured at 100 °C for one h to form the base silicone adhesive layer. The glass substrate is precleaned through ultrasonic cleaning in absolute ethanol and distilled water (each for 20 min), followed by drying at 100 °C for 60 min to ensure a contaminant-free surface. Next, a hydrophobic SiO_2 dispersion is prepared by mixing 0.4 *g* of hydrophobic silica in 20 mL of ethyl acetate with thorough stirring and sonication. This dispersion is sprayed over the cured silicone layer and thermally treated at 150 °C for 90 min to create a uniform superhydrophobic SiO_2 layer. For enhanced durability and protection, a UV glue diluent is prepared by mixing 0.4 *g* of UV adhesive with 10 *g* of absolute ethanol and stirred until uniform. This mixture is applied as a topcoat over the SiO_2 layer, followed by drying at 100 °C for one hour and UV irradiation for six hours to achieve full crosslinking and form the final UV-protected superhydrophobic layer. The multilayered architecture offers a synergistic effect-combining the strong adhesion of silicone, the water-repellent nature of SiO_2, and the mechanical robustness of the UV-curable layer-resulting in a transparent, superhydrophobic coating with superior wear resistance suitable for practical glass-based applications. Shaojun et al. [231] developed transparent superhydrophobic coatings using a streamlined and scalable process. The approach involves four main steps. Initially, an adhesive-such as epoxy resin, polydimethylsiloxane, styrene resin, phenolic resin, or polyurethane-is dispersed in an organic solvent like toluene, acetone, or ethyl acetate using ultrasonic agitation to form a homogeneous primary solution. In the second step, a superhydrophobic modified powder is synthesized and added to this solution, followed by further ultrasonic dispersion to create a uniform secondary mixture. The synthesis of the modified powder entails a multi-step sol-gel-assisted electrochemical process. A filler (e.g., kaolin, diatomite, or hydrotalcite) is dispersed in ethanol, followed by the addition of ethyl orthosilicate and hexadecyltrimethoxysilane, with subsequent pH adjustment using acetic acid and the inclusion of a sodium nitrate solution. Electrochemical treatment is carried out using platinum and copper electrodes under a constant voltage of 30 V for 90 min. The resulting material is purified by ethanol washing and centrifugation, then dried at 60 °C to obtain the final superhydrophobic powder. In the third step, a curing agent-compatible with the chosen adhesive is added to the secondary solution and dispersed ultrasonically to produce a stable coating slurry. Finally, the slurry is applied to a substrate (metal, glass, wood, paper, or fabric) via spray coating at a pressure of 0.4 MPa, with a spray distance of 10–20 cm and drying at 60–90 °C to achieve a uniform superhydrophobic film. This method is not only efficient and environmentally sustainable but also significantly reduces the production cost and time required for transparent superhydrophobic coatings, making it suitable for industrial-scale applications.

8. Conclusions, challenges, and future perspectives

In conclusion, this review discusses the significant potential of transparent superhydrophobic self-cleaning coatings for revolutionizing solar cell technology. Performance of solar cells can be adversely affected by natural contaminants such as dust, fine soil particles, fog, and water, particularly in harsh environments. To address this issue, transparent superhydrophobic self-cleaning coatings have been developed for solar panel cover glass using various fabrication techniques such as CVD, spin coating, dip coating, spray coating, electrospinning, laser deposition and lithography. These techniques are crucial for precisely controlling the fine surface structure to enhance transparency and superhydrophobic properties. Additionally, several testing methods including the adhesive tape test, sandpaper abrasion test, water impact test, sand impact test, pencil hardness test, chemical stability testing, cross-cut test, and cleanliness testing with Dyne pens have been utilized to evaluate the quality of these coatings. The results of these tests demonstrate the potential for large-scale application of transparent superhydrophobic self-cleaning coatings. These coatings have been successfully applied to solar panel cover glass, improving the sustainability and performance of solar cells over an extended period. However, certain challenges still need to be addressed, as outlined below.

1) The current research trend focuses on enhancing light transmission and creating superhydrophobic self-cleaning coatings. In the future, it is important to prioritize understanding the fabrication mechanism and developing self-cleaning, multi-functional surfaces with high mechanical strength and abrasion resistance. Emphasizing interdisciplinary collaboration and continuing research on novel materials and coating techniques is essential to enable practical applications.
2) The process of fabricating materials, from initial lab synthesis to large-scale industrial production, presents a several challenges. Achieving consistent quality and reproducibility on an industrial scale necessitates precise control over fabrication parameters, optimization of deposition techniques, uniform coating thickness, and the selection of scalable fabrication methods.
3) The economic feasibility of fabrication processes is a crucial factor for their market adoption. Therefore, researchers and industrialists should focus their efforts on exploring sustainable materials and fabrication processes, especially in the field of solar energy, to reduce environmental footprints.
4) The ongoing exploration of developing novel materials with advanced design structures is driving research in dynamic superhydrophobicity. Researchers are working to create coatings using a simplified one-step methodology to ensure long-lasting durability. This approach offers benefits such as minimized instrumentation and material use, reduced processing time, and cost-effectiveness. The use of spray-coating for self-cleaning glass has been somewhat neglected and needs more attention. Compared to other production methods, this spray-coating approach provides better control.
5) The pursuit of multifunctional properties, such as superhydrophobicity, transparency, anti-fouling, and anti-reflectivity, holds promising prospects for future research. Integrating

optimized research methodologies and blending them to engineer innovative material compositions will significantly enhance solar cell efficiency in the future.

6) To improve the comparibilty across the studies a standardised substrates should be opted to fabricate transparent superhydrophobic coatings. A consistent substrate will help to evaluate the attributions of the coatings such as transparency, durability, and self-cleaning performance under realistic conditions and ensure the reliable comparison. In addition, a standardised protocols can reduce the variability in the results of coatings not only application but also performance.

CRediT authorship contribution statement

Sagar S. Ingole: Writing – original draft, Methodology, Investigation, Conceptualization. **Rajaram S. Sutar:** Writing – original draft, Methodology, Investigation, Conceptualization. **Pradip P. Gaikwad:** Investigation, Data curation. **Akshay R. Jundle:** Methodology, Data curation. **Rutuja A. Ekunde:** Methodology, Data curation. **Shanhu Liu:** Writing – review & editing, Validation, Supervision. **Sanjay S. Latthe:** Writing – original draft, Validation, Supervision, Funding acquisition.

Declaration of competing interest

The authors declare that they have no known competing financial interests or personal relationships that could have appeared to influence the work reported in this paper.

Acknowledgments

We greatly appreciate the support of financial assistance received through Seed Money Scheme from Vivekanand College, Kolhapur (Empowered Autonomous), Ref. No. VCK/3108/2023-24 dated 30/03/2024 and the Chhatrapati Shahu Maharaj National Research Fellowship – 2021, Chhatrapati Shahu Maharaj Research Training and Human Development Institute (Sarthi), Pune, Ref. No. CSMNRF-2021/2021-22/896.

Data availability

Data will be made available on request.

References

[1] Q. Hassan, P. Viktor, T.J. Al-Musawi, B.M. Ali, S. Algburi, H.M. Alzoubi, A.K. Al-Jiboory, A.Z. Sameen, H.M. Salman, M. Jaszczur, The renewable energy role in the global energy Transformations, Renew. Energy Focus 48 (2024) 100545.
[2] H. Islam, Nexus of economic, social, and environmental factors on sustainable development goals: the moderating role of technological advancement and green innovation, Innov. Green Develop. 4 (2025) 100183.
[3] V. Kaushik, S. Sharma, M. Kumar, Role of solar energy for sustainable environment. Renewable Energy Development: Technology, Material and Sustainability, Springer, 2025, pp. 67–89.
[4] A.S. Al-Ezzi, M.N.M. Ansari, Photovoltaic solar cells: a review, Appl. Syst. Innov. 5 (2022) 67.
[5] R.J. Isaifan, D. Johnson, L. Ackermann, B. Figgis, M. Ayoub, Evaluation of the adhesion forces between dust particles and photovoltaic module surfaces, Solar Energy Mater. Solar Cells 191 (2019) 413–421, https://doi.org/10.1016/j.solmat.2018.11.031.
[6] T. Salamah, A. Ramahi, K. Alamara, A. Juaidi, R. Abdallah, M.A. Abdelkareem, E.-C. Amer, A.G. Olabi, Effect of dust and methods of cleaning on the performance of solar PV module for different climate regions: comprehensive review, Sci. Total Environ. 827 (2022) 154050, https://doi.org/10.1016/j.scitotenv.2022.154050.
[7] D. Dahlioui, B. Laarabi, A. Barhdadi, Review on dew water effect on soiling of solar panels: towards its enhancement or mitigation, Sustain. Energy Technol. Assess. 49 (2022) 101774, https://doi.org/10.1016/j.seta.2021.101774.
[8] M.K. Smith, C.C. Wamser, K.E. James, S. Moody, D.J. Sailor, T.N. Rosenstiel, Effects of natural and manual cleaning on photovoltaic output, J. Sol. Energy Eng. 135 (2013) 034505.
[9] N. Najmi, A. Rachid, A review on solar panel cleaning systems and techniques, Energies 16 (2023) 7960.
[10] H.A. Kazem, M.T. Chaichan, A.H. Al-Waeli, K. Sopian, A review of dust accumulation and cleaning methods for solar photovoltaic systems, J. Clean. Prod. 276 (2020) 123187.
[11] G. Aravind, G. Vasan, T.G. Kumar, R.N. Balaji, G.S. Ilango, A control strategy for an autonomous robotic vacuum cleaner for solar panels, in: 2014 Texas Instruments India Educators' Conference (TIIEC), IEEE, 2014, pp. 53–61.
[12] A. Al Shehri, B. Parrott, P. Carrasco, H. Al Saiari, I. Taie, Impact of dust deposition and brush-based dry cleaning on glass transmittance for PV modules applications, Solar Energy 135 (2016) 317–324.
[13] A. Elnozahy, A.K.A. Rahman, A.H.H. Ali, M. Abdel-Salam, S. Ookawara, Performance of a PV module integrated with standalone building in hot arid areas as enhanced by surface cooling and cleaning, Energy Build. 88 (2015) 100–109.
[14] E. Simsek, M.J. Williams, L. Pilon, Effect of dew and rain on photovoltaic solar cell performances, Solar Energy Mater. Solar Cells 222 (2021) 110908.
[15] M.A. Shirakawa, R. Zilles, A. Mocelin, C.C. Gaylarde, A. Gorbushina, G. Heidrich, M.C. Giudice, G.M. Del Negro, V.M. John, Microbial colonization affects the efficiency of photovoltaic panels in a tropical environment, J. Environ. Manage 157 (2015) 160–167.
[16] E. Andenæs, B.P. Jelle, K. Ramlo, T. Kolås, J. Selj, S.E. Foss, The influence of snow and ice coverage on the energy generation from photovoltaic solar cells, Solar Energy 159 (2018) 318–328.
[17] H. Jiang, L. Lu, K. Sun, Experimental investigation of the impact of airborne dust deposition on the performance of solar photovoltaic (PV) modules, Atmos. Environ. 45 (2011) 4299–4304.
[18] M. Ahmadizadeh, M. Heidari, S. Thangavel, E. Al Naamani, M. Khashehchi, V. Verma, A. Kumar, Technological advancements in sustainable and renewable solar energy systems. Highly Efficient Thermal Renewable Energy Systems, CRC Press, 2024, pp. 23–39.
[19] H.A. Kazem, M.T. Chaichan, A.H.A. Al-Waeli, K. Sopian, A review of dust accumulation and cleaning methods for solar photovoltaic systems, J. Clean. Prod. 276 (2020) 123187, https://doi.org/10.1016/j.jclepro.2020.123187.
[20] R.J. Mustafa, M.R. Gomaa, M. Al-Dhaifallah, H. Rezk, Environmental impacts on the performance of solar photovoltaic systems, Sustainability 12 (2020) 608.
[21] Y. Wu, J. Du, G. Liu, D. Ma, F. Jia, J.J. Klemeš, J. Wang, A review of self-cleaning technology to reduce dust and ice accumulation in photovoltaic power generation using superhydrophobic coating, Renew. Energy 185 (2022) 1034–1061.
[22] B. Zhang, X. Xue, L. Zhao, B. Hou, Transparent superhydrophobic and self-cleaning coating, Polymers 16 (2024) 1876.
[23] Y. Chen, Y. Zhang, L. Shi, J. Li, Y. Xin, T. Yang, Z. Guo, Transparent superhydrophobic/superhydrophilic coatings for self-cleaning and anti-fogging, Appl. Phys. Lett. 101 (2012).
[24] L. Cao, A.K. Jones, V.K. Sikka, J. Wu, D. Gao, Anti-icing superhydrophobic coatings, Langmuir 25 (2009) 12444–12448.
[25] R.S. Sutar, S.S. Latthe, A.R. Jundle, P.P. Gaikwad, S.S. Ingole, S. Nagappan, Y. H. Kim, A.K. Bhosale, V.S. Saji, S. Liu, A facile approach for oil-water separation using superhydrophobic polystyrene-silica coated stainless steel mesh bucket, Mar. Pollut. Bull. 198 (2024) 115790.
[26] R.S. Sutar, S.S. Latthe, X. Wu, K. Nakata, R. Xing, S. Liu, A. Fujishima, Design and mechanism of photothermal soft actuators and their applications, J. Mater. Chem. A (2024).
[27] S.P. Dalawai, M.A.S. Aly, S.S. Latthe, R. Xing, R.S. Sutar, S. Nagappan, C.-S. Ha, K. K. Sadasivuni, S. Liu, Recent advances in durability of superhydrophobic self-cleaning technology: a critical review, Prog. Org. Coat. 138 (2020) 105381.
[28] R.S. Sutar, S. Nagappan, A.K. Bhosale, K.K. Sadasivuni, K.-H. Park, C.-S. Ha, S. S. Latthe, Superhydrophobic Al2O3–polymer composite coating for self-cleaning applications, Coatings 11 (2021) 1162.
[29] M. Li, Y. Li, F. Xue, X. Jing, A robust and versatile superhydrophobic coating: wear-resistance study upon sandpaper abrasion, Appl. Surf. Sci. 480 (2019) 738–748.
[30] P.B. Weisensee, J. Tian, N. Miljkovic, W.P. King, Water droplet impact on elastic superhydrophobic surfaces, Sci. Rep. 6 (2016) 30328.
[31] X. Yao, H. Zhang, L. Zhong, W. Zhu, M. Chen, Z. Wu, Y. Wu, Preparation of wood super-hydrophobic coating using the sand-in method, Prog. Org. Coat. 192 (2024) 108498.
[32] K. Zhang, S. Huang, J. Wang, G. Liu, Transparent organic/silica nanocomposite coating that is flexible, omniphobic, and harder than a 9H pencil, Chem. Eng. J. 396 (2020) 125211.
[33] B. Swain, A. Pati, P. Mallick, S. Mohapatra, A. Behera, Development of highly durable superhydrophobic coatings by one-step plasma spray methodology, J. Therm. Spray Technol. 30 (2021) 405–423.
[34] G. Zhang, C. Schmitz, M. Fimmers, C. Quix, S. Hoseini, Deep learning-based automated characterization of crosscut tests for coatings via image segmentation, J. Coat. Technol. Res. (2022) 1–13.
[35] A. Haque, An Exclusive Assessment Of Surface Dyne Testing In Manufacturing Environments Where Materials Are Tested Before Adhesion Processes As Well As Validating Material Surfaces After Surface Treatment Processes Like Corona And Plasma Treatment Where Both The Surface Tension And Surface Free Energy Plays A Key Role, Available at SSRN 5039314, (2024).
[36] I.S. Bayer, Superhydrophobic coatings from ecofriendly materials and processes: a review, Adv. Mater. Interfaces 7 (2020) 2000095.
[37] A. Hooda, M.S. Goyat, J.K. Pandey, A. Kumar, R. Gupta, A review on fundamentals, constraints and fabrication techniques of superhydrophobic coatings, Prog. Org. Coat. 142 (2020) 105557, https://doi.org/10.1016/j.porgcoat.2020.105557.
[38] P. Nguyen-Tri, H.N. Tran, C.O. Plamondon, L. Tuduri, D.-V.N. Vo, S. Nanda, A. Mishra, H.-P. Chao, A. Bajpai, Recent progress in the preparation, properties

and applications of superhydrophobic nano-based coatings and surfaces: a review, Prog. Org. Coat. 132 (2019) 235–256.
[39] B. Nomeir, S. Lakhouil, S. Boukheir, M.A. Ali, S. Naamane, Recent progress on transparent and self-cleaning surfaces by superhydrophobic coatings deposition to optimize the cleaning process of solar panels, Solar Energy Mater. Solar Cells 257 (2023) 112347, https://doi.org/10.1016/j.solmat.2023.112347.
[40] Y. Bai, H. Zhang, Y. Shao, H. Zhang, J. Zhu, Recent progresses of superhydrophobic coatings in different application fields: an overview, Coatings 11 (2021) 116.
[41] R. Kumar, A.K. Sahani, Role of superhydrophobic coatings in biomedical applications, Mater. Today 45 (2021) 5655–5659.
[42] A. Syafiq, V. Balakrishnan, M.S. Ali, S.J. Dhoble, N. Abd Rahim, A. Omar, Application of transparent self-cleaning coating for photovoltaic panel: a review, Curr. Opin. Chem. Eng. 36 (2022) 100801.
[43] M.Z. Khan, J. Militky, M. Petru, B. Tomková, A. Ali, E. Tören, S. Perveen, Recent advances in superhydrophobic surfaces for practical applications: a review, Eur. Polym. J. 178 (2022) 111481.
[44] Y. Zhan, W. Li, A. Amirfazli, S. Yu, Recent advances in shape memory superhydrophobic surfaces: concepts, mechanism, classification, applications and challenges, Polymer 256 (2022) 125193.
[45] E.J. Falde, S.T. Yohe, Y.L. Colson, M.W. Grinstaff, Superhydrophobic materials for biomedical applications, Biomaterials 104 (2016) 87–103.
[46] Q. Xu, Q. Zhao, X. Zhu, L. Cheng, S. Bai, Z. Wang, L. Meng, Y. Qin, A new kind of transparent and self-cleaning film for solar cells, Nanoscale 8 (2016) 17747–17751.
[47] P.A. Levkin, F. Svec, J.M. Fréchet, Porous polymer coatings: a versatile approach to superhydrophobic surfaces, Adv. Funct. Mater. 19 (2009) 1993–1998.
[48] Z. Wang, N. Koratkar, L. Ci, P. Ajayan, Combined micro-/nanoscale surface roughness for enhanced hydrophobic stability in carbon nanotube arrays, Appl. Phys. Lett. 90 (2007).
[49] S. Alexander, J. Eastoe, A.M. Lord, F. Guittard, A.R. Barron, Branched hydrocarbon low surface energy materials for superhydrophobic nanoparticle derived surfaces, ACS Appl. Mater. Interfaces 8 (2016) 660–666.
[50] G.B. Hwang, A. Patir, K. Page, Y. Lu, E. Allan, I.P. Parkin, Buoyancy increase and drag-reduction through a simple superhydrophobic coating, Nanoscale 9 (2017) 7588–7594.
[51] N.X. Zhu, Z.W. Wei, C.X. Chen, D. Wang, C.C. Cao, Q.F. Qiu, J.J. Jiang, H. P. Wang, C.Y. Su, Self-generation of surface roughness by low-surface-energy alkyl chains for highly stable superhydrophobic/superoleophilic MOFs with multiple functionalities, Angew. Chem. 131 (2019) 17189–17196.
[52] K. Liu, L. Jiang, Bio-inspired self-cleaning surfaces, Annu Rev. Mater. Res. 42 (2012) 231–263.
[53] B. Bhushan, Y.C. Jung, M. Nosonovsky, Lotus effect: surfaces with roughness-induced superhydrophobicity, self-cleaning, and low adhesion. Springer Handbook of Nanotechnology, 2010, pp. 1437–1524.
[54] Y.T. Cheng, D. Rodak, C. Wong, C. Hayden, Effects of micro-and nano-structures on the self-cleaning behaviour of lotus leaves, Nanotechnology. 17 (2006) 1359.
[55] J. Li, Z. Zhang, J. Xu, C. Wong, Self-cleaning materials—lotus effect surfaces, Kirk-Othmer Encyclopedia of Chemical Technology (2000).
[56] M. Nosonovsky, E. Bormashenko, Lotus effect: superhydrophobicity and self-cleaning. Functional Properties of Bio-Inspired Surfaces: Characterization and Technological Applications, World Scientific, 2009, pp. 43–78.
[57] B. Karthick, R. Maheshwari, Lotus-inspired nanotechnology applications, Resonance 13 (2008) 1141–1145.
[58] S. Cheng, Z. Yu, Z. Lin, L. Li, Y. Li, Z. Mao, A lotus leaf like vertical hierarchical solar vapor generator for stable and efficient evaporation of high-salinity brine, Chem. Eng. J. 401 (2020) 126108.
[59] M. Guo, L. Liu, Structuring the thermoplastic interleaf with lotus-leaf-like structure and its interlaminar toughening for CFRPs, Compos. Sci. Technol. 183 (2019) 107825.
[60] R. Jiang, L. Hao, L. Song, L. Tian, Y. Fan, J. Zhao, C. Liu, W. Ming, L. Ren, Lotus-leaf-inspired hierarchical structured surface with non-fouling and mechanical bactericidal performances, Chem. Eng. J. 398 (2020) 125609.
[61] Y. Liang, E. Yang, M. Kim, S. Kim, H. Kim, J. Byun, N. Yanar, H. Choi, Lotus leaf-like SiO2 nanofiber coating on polyvinylidene fluoride nanofiber membrane for water-in-oil emulsion separation and antifouling enhancement, Chem. Eng. J. 452 (2023) 139710.
[62] F. Liu, Y. Jiang, J. Feng, L. Li, J. Feng, Bionic aerogel with a lotus leaf-like structure for efficient oil-water separation and electromagnetic interference shielding, Gels 9 (2023) 214.
[63] X. Yun, Z. Xiong, Y. He, X. Wang, Superhydrophobic lotus-leaf-like surface made from reduced graphene oxide through soft-lithographic duplication, RSC Adv. 10 (2020) 5478–5486.
[64] B. Bhushan, Y.C. Jung, K. Koch, Self-cleaning efficiency of artificial superhydrophobic surfaces, Langmuir 25 (2009) 3240–3248, https://doi.org/10.1021/la803860d.
[65] A.R. Siddiqui, W. Li, F. Wang, J. Ou, A. Amirfazli, One-step fabrication of transparent superhydrophobic surface, Appl. Surf. Sci. 542 (2021) 148534.
[66] K.L. Cho, I.I. Liaw, A.H.-F. Wu, R.N. Lamb, Influence of roughness on a transparent superhydrophobic coating, J. Phys. Chem. C 114 (2010) 11228–11233.
[67] R.G. Karunakaran, C.-H. Lu, Z. Zhang, S. Yang, Highly transparent superhydrophobic surfaces from the coassembly of nanoparticles (≤ 100 nm), Langmuir 27 (2011) 4594–4602.
[68] U. Mehmood, F.A. Al-Sulaiman, B.S. Yilbas, B. Salhi, S.H.A. Ahmed, M.K. Hossain, Superhydrophobic surfaces with antireflection properties for solar applications: a critical review, Solar Energy Mater. Solar Cells 157 (2016) 604–623, https://doi.org/10.1016/j.solmat.2016.07.038.
[69] Y. Li, F. Liu, J. Sun, A facile layer-by-layer deposition process for the fabrication of highly transparent superhydrophobic coatings, Chem. Commun. (2009) 2730–2732.
[70] J. Lin, H. Chen, T. Fei, J. Zhang, Highly transparent superhydrophobic organic–inorganic nanocoating from the aggregation of silica nanoparticles, Colloids Surf. A 421 (2013) 51–62.
[71] Y. Liu, Research on a superhydrophobic coating of highly transparent wear-resistant inorganic/organic silicon composite resin, Coatings 11 (2021) 338.
[72] J. Lyu, B. Wu, N. Wu, C. Peng, J. Yang, Y. Meng, S. Xing, Green preparation of transparent superhydrophobic coatings with persistent dynamic impact resistance for outdoor applications, Chem. Eng. J. 404 (2021) 126456.
[73] D. Wang, Z. Zhang, Y. Li, C. Xu, Highly transparent and durable superhydrophobic hybrid nanoporous coatings fabricated from polysiloxane, ACS Appl. Mater. Interfaces 6 (2014) 10014–10021.
[74] H.S. Wei, C.C. Kuo, C.C. Jaing, Y.C. Chang, C.C. Lee, Highly transparent superhydrophobic thin film with low refractive index prepared by one-step coating of modified silica nanoparticles, J. Solgel. Sci. Technol. 71 (2014) 168–175.
[75] W. Luo, M. Li, Recent advances in fabrication of durable, transparent, and superhydrophobic surfaces, Nanomaterials 13 (2023) 2359.
[76] X. Chen, G. Yin, N. Zhao, R. Yang, M. Xia, C. Feng, Y. Chen, M. Dong, W. Zhu, Turbidity compensation method based on Mie scattering theory for water chemical oxygen demand determination by UV–Vis spectrometry, Anal. Bioanal. Chem. 413 (2021) 877–883.
[77] A. Shams-nateri, Scattering behavior of nonabsorbing metallic nanoparticles, Opt. Laser Technol. 44 (2012) 1670–1674.
[78] L. Yu, H. Li, W. Huang, H. Yu, Y. He, In Situ visualizing oxidase-mimicking activity of single MnOOH nanotubes with mie scattering-based absorption microscopy, Inorg. Chem. 60 (2021) 5264–5270.
[79] E.J. Park, J.K. Sim, M.-G. Jeong, H.O. Seo, Y.D. Kim, Transparent and superhydrophobic films prepared with polydimethylsiloxane-coated silica nanoparticles, RSC. Adv. 3 (2013) 12571–12576.
[80] Y. Lin, J. Han, M. Cai, W. Liu, X. Luo, H. Zhang, M. Zhong, Durable and robust transparent superhydrophobic glass surfaces fabricated by a femtosecond laser with exceptional water repellency and thermostability, J. Mater. Chem. A 6 (2018) 9049–9056, https://doi.org/10.1039/C8TA01965G.
[81] X. Huang, M. Sun, X. Shi, J. Shao, M. Jin, W. Liu, R. Zhang, S. Huang, Y. Ye, Chemical vapor deposition of transparent superhydrophobic anti-Icing coatings with tailored polymer nanoarray architecture, Chem. Eng. J. 454 (2023) 139981.
[82] K. Acatay, E. Simsek, C. Ow-Yang, Y.Z. Menceloglu, Tunable, superhydrophobically stable polymeric surfaces by electrospinning, Angew. Chem. 116 (2004) 5322–5325.
[83] A. Bessonov, J.G. Kim, J.W. Seo, J.W. Lee, S. Lee, Design of patterned surfaces with selective wetting using nanoimprint lithography, Macromol. Chem. Phys. 211 (2010) 2636–2641.
[84] J.-M. Lim, G.-R. Yi, J.H. Moon, C.-J. Heo, S.-M. Yang, Superhydrophobic films of electrospun fibers with multiple-scale surface morphology, Langmuir 23 (2007) 7981–7989.
[85] A. Pozzato, S. Dal Zilio, G. Fois, D. Vendramin, G. Mistura, M. Belotti, Y. Chen, M. Natali, Superhydrophobic surfaces fabricated by nanoimprint lithography, Microelectron. Eng. 83 (2006) 884–888.
[86] Y.H. Sung, Y.D. Kim, H.-J. Choi, R. Shin, S. Kang, H. Lee, Fabrication of superhydrophobic surfaces with nano-in-micro structures using UV-nanoimprint lithography and thermal shrinkage films, Appl. Surf. Sci. 349 (2015) 169–173.
[87] A. Cannavale, F. Fiorito, M. Manca, G. Tortorici, R. Cingolani, G. Gigli, Multifunctional bioinspired sol-gel coatings for architectural glasses, Build. Environ. 45 (2010) 1233–1243.
[88] Z. Ranjbar, H. Yari, G. Momen, Tuning up sol-gel process to achieve highly durable superhydrophobic coating, Surf. Interfaces 33 (2022) 102282.
[89] H. Şakalak, K. Yılmaz, M. Gürsoy, M. Karaman, Roll-to roll initiated chemical vapor deposition of super hydrophobic thin films on large-scale flexible substrates, Chem. Eng. Sci. 215 (2020) 115466.
[90] F. Zhang, Z. Shi, L. Chen, Y. Jiang, C. Xu, Z. Wu, Y. Wang, C. Peng, Porous superhydrophobic and superoleophilic surfaces prepared by template assisted chemical vapor deposition, Surf. Coat. Technol. 315 (2017) 385–390.
[91] M. Eseev, A. Goshev, S. Kapustin, Y. Tsykareva, Creation of superhydrophobic coatings based on MWCNTs xerogel, Nanomaterials 9 (2019) 1584.
[92] D.L. García-Ruiz, F.G. Granados-Martínez, C.J. Gutiérrez-García, J.M. Ambriz-Torres, J. de Jesús Contreras-Navarrete, N. Flores-Ramírez, F. Méndez, L. Domratcheva-Lvova, Synthesis of carbon nanomaterials by chemical vapor deposition method using green chemistry principles. Handbook of Greener Synthesis of Nanomaterials and Compounds, Elsevier, 2021, pp. 273–314.
[93] D. Nanda, A. Sinhamahapatra, A. Kumar, Superhydrophobic metal surface, Materials with extreme wetting properties: methods and emerging industrial applications, (2021) 179–193.
[94] A.R. Siddiqui, R. Maurya, P.K. Katiyar, K. Balani, Superhydrophobic, self-cleaning carbon nanofiber CVD coating for corrosion protection of AISI 1020 steel and AZ31 magnesium alloys, Surf. Coat. Technol. 404 (2020) 126421.
[95] M. Vaka, R. Walvekar, S. Yanamadala, Carbon nanotubes and their composites: from synthesis to applications. Contemporary Nanomaterials in Material Engineering Applications, 2021, pp. 37–67.
[96] J. Zheng, J. Yang, W. Cao, Y. Huang, Z. Zhou, Y.-X. Huang, Fabrication of transparent wear-resistant superhydrophobic SiO2 film via phase separation and chemical vapor deposition methods, Ceram. Int. 48 (2022) 32143–32151.

[97] F. Zhang, Z. Shi, Y. Jiang, C. Xu, Z. Wu, Y. Wang, C. Peng, Fabrication of transparent superhydrophobic glass with fibered-silica network, Appl. Surf. Sci. 407 (2017) 526–531, https://doi.org/10.1016/j.apsusc.2017.02.207.

[98] Y. Yuan, Y. Wang, S. Liu, X. Zhang, X. Liu, C. Sun, D. Yuan, Y. Zhang, X. Cao, Direct chemical vapor deposition synthesis of graphene super-hydrophobic transparent glass, Vacuum. 202 (2022) 111136, https://doi.org/10.1016/j.vacuum.2022.111136.

[99] A. Tombesi, S. Li, S. Sathasivam, K. Page, F.L. Heale, C. Pettinari, C.J. Carmalt, I. P. Parkin, Aerosol-assisted chemical vapour deposition of transparent superhydrophobic film by using mixed functional alkoxysilanes, Sci. Rep. 9 (2019) 7549.

[100] A. Zhuang, R. Liao, S.C. Dixon, Y. Lu, S. Sathasivam, I.P. Parkin, C.J. Carmalt, Transparent superhydrophobic PTFE films via one-step aerosol assisted chemical vapor deposition, RSC Adv. 7 (2017) 29275–29283.

[101] M. Poddighe, P. Innocenzi, Hydrophobic thin films from sol–gel processing: a critical review, Materials 14 (2021) 6799.

[102] H. Muramatsu, R. Corriu, B. Boury, Solid state hydrolysis/polycondensation of alkoxysilane: access to crystal-like silicon-based hybrid materials, J. Am. Chem. Soc. 125 (2003) 854–855, https://doi.org/10.1021/ja020975e.

[103] T. Rezayi, M.H. Entezari, Achieving to a superhydrophobic glass with high transparency by a simple sol–gel-dip-coating method, Surf. Coat. Technol. 276 (2015) 557–564.

[104] Y.-T. Peng, K.-F. Lo, Y.-J. Juang, Constructing a superhydrophobic surface on polydimethylsiloxane via spin coating and vapor− liquid sol− gel process, Langmuir 26 (2010) 5167–5171.

[105] M. Espanhol-Soares, L. Costa, M.R.A. Silva, F. Soares Silva, L.M.S. Ribeiro, R. Gimenes, Super-hydrophobic coatings on cotton fabrics using sol–gel technique by spray, J. Solgel. Sci. Technol. 95 (2020) 22–33.

[106] Q.F. Xu, J.N. Wang, K.D. Sanderson, Organic−inorganic composite nanocoatings with superhydrophobicity, good transparency, and thermal stability, ACS Nano 4 (2010) 2201–2209, https://doi.org/10.1021/nn901581j.

[107] C.J. Brinker, G.C. Frye, A.J. Hurd, C.S. Ashley, Fundamentals of sol-gel dip coating, Thin. Solid. Films 201 (1991) 97–108, https://doi.org/10.1016/0040-6090(91)90158-T.

[108] S.S. Latthe, R.S. Sutar, V.S. Kodag, A. Bhosale, A.M. Kumar, K.K. Sadasivuni, R. Xing, S. Liu, Self–cleaning superhydrophobic coatings: potential industrial applications, Prog. Org. Coat. 128 (2019) 52–58.

[109] A. De Ryck, D. Quéré, Inertial coating of a fibre, J. Fluid. Mech. 311 (2006) 219–237, https://doi.org/10.1017/S0022112096002571.

[110] O. Kim, J. Nam, Confinement effects in dip coating, J. Fluid. Mech. 827 (2017) 1–30, https://doi.org/10.1017/jfm.2017.421.

[111] F. Orgaz, F. Capel, A semi-empirical model for coating flat glass by dipping into metal-organic solutions, J. Mater. Sci. 22 (1987) 1291–1294, https://doi.org/10.1007/BF01233123.

[112] L. Champougny, B. Scheid, A.A. Korobkin, J. Rodríguez-Rodríguez, Dip-coating flow in the presence of two immiscible liquids, J. Fluid. Mech. 922 (2021) A26, https://doi.org/10.1017/jfm.2021.541.

[113] D. Adak, R. Bhattacharyya, H. Saha, P.S. Maiti, Sol–gel processed silica based highly transparent self-cleaning coatings for solar glass covers, Mater. Today 33 (2020) 2429–2433, https://doi.org/10.1016/j.matpr.2020.01.331.

[114] M. Luo, X. Sun, Y. Zheng, X. Cui, W. Ma, S. Han, L. Zhou, X. Wei, Non-fluorinated superhydrophobic film with high transparency for photovoltaic glass covers, Appl. Surf. Sci. 609 (2023) 155299, https://doi.org/10.1016/j.apsusc.2022.155299.

[115] R. Xi, Y. Wang, X. Li, X. Zhang, X. Du, A facile strategy to form three-dimensional network structure for mechanically robust superhydrophobic nanocoatings with enhanced transmittance, J. Colloid. Interface Sci. 563 (2020) 42–53, https://doi.org/10.1016/j.jcis.2019.12.049.

[116] M. Liu, X. Tan, X. Li, J. Geng, M. Han, K. Wei, X. Chen, Transparent superhydrophobic EVA/SiO2/PTFE/KH-570 coating with good mechanical robustness, chemical stability, self-cleaning effect and anti-icing property fabricated by facile dipping method, Colloids Surf. A 658 (2023) 130624, https://doi.org/10.1016/j.colsurfa.2022.130624.

[117] D.P. Birnie, Spin coating: art and science, in: T. Schneller, R. Waser, M. Kosec, D. Payne (Eds.), Chemical Solution Deposition of Functional Oxide Thin Films, Springer Vienna, Vienna, 2013, pp. 263–274.

[118] D.P. Birnie, Spin coating technique, in: M.A. Aegerter, M. Mennig (Eds.), Sol-Gel Technologies for Glass Producers and Users, Springer US, Boston, MA, 2004, pp. 49–55.

[119] H.A.M. Mustafa, D.A. Jameel, Modeling and the main stages of spin coating process: a review, J. Appl. Sci. Technol. Trends 2 (2021) 91–95, https://doi.org/10.38094/jastt203109.

[120] D.B. Hall, P. Underhill, J.M. Torkelson, Spin coating of thin and ultrathin polymer films, Polym. Eng. Sci. 38 (1998) 2039–2045.

[121] Spin coating, Mater. Today 5 (2002) 62, https://doi.org/10.1016/S1369-7021(02)01267-1.

[122] Z. Ji, Y. Liu, F. Du, Rational design of superhydrophobic, transparent hybrid coating with superior durability, Prog. Org. Coat. 157 (2021) 106294, https://doi.org/10.1016/j.porgcoat.2021.106294.

[123] Z. Liang, M. Geng, B. Dong, L. Zhao, S. Wang, Transparent and robust SiO2/PDMS composite coatings with self-cleaning, Surf. Eng. 36 (2020) 643–650.

[124] Y.-J. Choi, J.-H. Ko, S.-W. Jin, H.-S. An, D.-B. Kim, K.-H. Yoon, H.-W. Kim, C.-M. Chung, Transparent self-cleaning coatings based on colorless polyimide/silica sol nanocomposite, Polymers 13 (2021) 4100.

[125] W. Li, Z. Liang, B. Dong, H. Tang, Transmittance and self-cleaning polymethylsiloxane coating with superhydrophobic surfaces, Surf. Eng. 36 (2020) 574–582.

[126] M. Li, W. Luo, H. Sun, M. Zhang, K.W. Ng, F. Wang, X. Cheng, Low-cost preparation of durable, transparent, superhydrophobic coatings with excellent environmental stability and self-cleaning function, Surf. Coat. Technol. 438 (2022) 128367, https://doi.org/10.1016/j.surfcoat.2022.128367.

[127] N. Abu Jarad, H. Imran, S.M. Imani, T.F. Didar, L. Soleymani, Fabrication of superamphiphobic surfaces via spray coating; a review, Adv. Mater. Technol. 7 (2022) 2101702.

[128] K. Fujita, T. Ishikawa, T. Tsutsui, Novel method for polymer thin film preparation: spray deposition of highly diluted polymer solutions, Jpn. J. Appl. Phys. 41 (2002) L70, https://doi.org/10.1143/JJAP.41.L70.

[129] A.G. Leão, B.G. Soares, A.A. Silva, E.C.L. Pereira, L.F.C. Souto, A.C. Ribeiro, Transparent and superhydrophobic room temperature vulcanized (RTV) polysiloxane coatings loaded with different hydrophobic silica nanoparticles with self-cleaning characteristics, Surf. Coat. Technol. 462 (2023) 129479, https://doi.org/10.1016/j.surfcoat.2023.129479.

[130] Z. Hong, Y. Xu, D. Ye, Y. Hu, One-step fabrication of a robust and transparent superhydrophobic self-cleaning coating using a hydrophobic binder at room temperature: a combined experimental and molecular dynamics simulation study, Surf. Coat. Technol. 472 (2023) 129943, https://doi.org/10.1016/j.surfcoat.2023.129943.

[131] S. Zhao, J. Zhao, M. Wen, M. Yao, F. Wang, F. Huang, Q. Zhang, Y.-B. Cheng, J. Zhong, Sequentially reinforced additive coating for transparent and durable superhydrophobic glass, Langmuir 34 (2018) 11316–11324, https://doi.org/10.1021/acs.langmuir.8b01960.

[132] T. Yang, M. Wang, X. Wang, X. Di, C. Wang, Y. Li, Fabrication of a waterborne, superhydrophobic, self-cleaning, highly transparent and stable surface, Soft. Matter. 16 (2020) 3678–3685, https://doi.org/10.1039/C9SM02473E.

[133] C. Ke, C. Zhang, Y. Jiang, Robust transparent superhydrophobic coatings on glass substrates prepared by a facile rapid thermal process, Ceram. Int. 49 (2023) 22718–22725, https://doi.org/10.1016/j.ceramint.2023.03.289.

[134] M. Ahmadi Bonakdar, D. Rodrigue, Electrospinning: processes, structures, and materials, Macromol 4 (2024) 58–103.

[135] W. Han, L. Wang, Q. Li, B. Ma, C. He, X. Guo, J. Nie, G. Ma, A review: current status and emerging developments on natural polymer-based electrospun fibers, Macromol. Rapid. Commun. 43 (2022) 2200456.

[136] A.J. Hijano, I.G. Loscertales, F.J. Higuera, Modelling the electric microdripping from a needle, J. Fluid. Mech. 920 (2021) A47, https://doi.org/10.1017/jfm.2021.467.

[137] W. Yiwei, B. Weijie, W. Fei, Z. Haiyi, W. Zhihai, W. Yaohong, Generation of micro-droplet on demand with reduced sizes by a hybrid pneumatic electrohydrodynamic method, J. Micromech. Microeng. 30 (2020) 035002, https://doi.org/10.1088/1361-6439/ab68b1.

[138] C. Errico, F. Chiellini, N. Detta, A. Piras, D. Puppi, E. Chiellini, A novel electrospinning procedure for the production of straight aligned and winded fibers, Nano Biomed. Eng. 3 (2011) 222–226.

[139] T. Kim, M.G. Song, K. Kim, H. Jeon, G.H. Kim, Recyclable superhydrophobic surface prepared via electrospinning and electrospraying using waste polyethylene terephthalate for self-cleaning applications, Polymers 15 (2023) 3810.

[140] J.-P. Chen, C.-Y. Guo, Q.-J. Zhang, X.-Q. Wu, L.-B. Zhong, Y.-M. Zheng, Preparation of transparent, amphiphobic and recyclable electrospun window screen air filter for high-efficiency particulate matters capture, J. Memb. Sci. 675 (2023) 121545, https://doi.org/10.1016/j.memsci.2023.121545.

[141] D.-H. Youn, K.-S. Lee, S.-K. Jung, M. Kang, Fabrication of a simultaneous highly transparent and highly hydrophobic fibrous films, Appl. Sci. 11 (2021) 5565.

[142] N.A. Shepelin, Z.P. Tehrani, N. Ohannessian, C.W. Schneider, D. Pergolesi, T. Lippert, A practical guide to pulsed laser deposition, Chem. Soc. Rev. 52 (2023) 2294–2321.

[143] I. Milov, V. Zhakhovsky, D. Ilnitsky, K. Migdal, V. Khokhlov, Y. Petrov, N. Inogamov, V. Lipp, N. Medvedev, B. Ziaja, V. Medvedev, I.A. Makhotkin, E. Louis, F. Bijkerk, Two-level ablation and damage morphology of Ru films under femtosecond extreme UV irradiation, Appl. Surf. Sci. 528 (2020) 146952, https://doi.org/10.1016/j.apsusc.2020.146952.

[144] H. Naser, H.M. Shanshool, K.I. Imhan, Parameters affecting the size of gold nanoparticles prepared by pulsed laser ablation in liquid, Brazil. J. Phys. 51 (2021) 878–898, https://doi.org/10.1007/s13538-021-00875-x.

[145] A. Žemaitis, M. Gaidys, P. Gečys, G. Račiukaitis, M. Gedvilas, Rapid high-quality 3D micro-machining by optimised efficient ultrashort laser ablation, Opt. Lasers. Eng. 114 (2019) 83–89, https://doi.org/10.1016/j.optlaseng.2018.11.001.

[146] B. Wang, Y. Hua, Y. Ye, R. Chen, Z. Li, Transparent superhydrophobic solar glass prepared by fabricating groove-shaped arrays on the surface, Appl. Surf. Sci. 426 (2017) 957–964, https://doi.org/10.1016/j.apsusc.2017.07.169.

[147] A. Chakraborty, N.R. Gottumukkala, M.C. Gupta, Superhydrophobic surface by laser ablation of PDMS, Langmuir 39 (2023) 11259–11267, https://doi.org/10.1021/acs.langmuir.3c00818.

[148] D. Zhao, H. Zhu, Z. Zhang, K. Xu, W. Lei, J. Gao, Y. Liu, Transparent superhydrophobic glass prepared by laser-induced plasma-assisted ablation on the surface, J. Mater. Sci. 57 (2022) 15679–15689, https://doi.org/10.1007/s10853-022-07507-y.

[149] D. Baek, S.H. Lee, B.-H. Jun, S.H. Lee, Lithography technology for micro-and nanofabrication. Nanotechnology for Bioapplications, 2021, pp. 217–233.

[150] G. Watson, S. Myhra, J. Watson, Lithography of diamond-like-carbon (DLC) films for use as masters in soft lithography, SPIE (2006).

[151] H. Wang, W. Zhang, D. Ladika, H. Yu, D. Gailevičius, H. Wang, C.F. Pan, P.N. S. Nair, Y. Ke, T. Mori, Two-photon polymerization lithography for optics and photonics: fundamentals, materials, technologies, and applications, Adv. Funct. Mater. 33 (2023) 2214211.
[152] P. Ragesh, V.A. Ganesh, S.V. Nair, A.S. Nair, A review on 'self-cleaning and multifunctional materials, J. Mater. Chem. A 2 (2014) 14773–14797.
[153] T. Li, M. Paliy, X. Wang, B. Kobe, W.-M. Lau, J. Yang, Facile one-step photolithographic method for engineering hierarchically nano/microstructured transparent superamphiphobic surfaces, ACS Appl. Mater. Interfaces 7 (2015) 10988–10992.
[154] S. Martin, B. Bhushan, Transparent, wear-resistant, superhydrophobic and superoleophobic poly (dimethylsiloxane)(PDMS) surfaces, J. Colloid. Interface Sci. 488 (2017) 118–126.
[155] V.R. Shrestha, S.-S. Lee, E.-S. Kim, D.-Y. Choi, Aluminum plasmonics based highly transmissive polarization-independent subtractive color filters exploiting a nanopatch array, Nano Lett. 14 (2014) 6672–6678, https://doi.org/10.1021/nl503353z.
[156] K.-H. Yeon, P.-S. Kang, K.-M. Kim, J.-H. Lim, Fabrication of superhydrophobic molecules nanoarray by dip-pen nanolithography, J. Adhes. Interface 19 (2018) 163–166.
[157] J. Li, W. Wang, R. Zhu, Y. Huang, Superhydrophobic artificial compound eye with high transparency, ACS Appl. Mater. Interfaces 13 (2021) 35026–35037, https://doi.org/10.1021/acsami.1c05558.
[158] C. Rin Yu, A. Shanmugasundaram, D.-W. Lee, Nanosilica coated polydimethylsiloxane mushroom structure: a next generation flexible, transparent, and mechanically durable superhydrophobic thin film, Appl. Surf. Sci. 583 (2022) 152500, https://doi.org/10.1016/j.apsusc.2022.152500.
[159] H. Zhang, Y.-Q. Liu, S. Zhao, L. Huang, Z. Wang, Z. Gao, Z. Zhu, D. Hu, H. Liu, Transparent and Robust Superhydrophobic Structure on Silica Glass Processed with Microstereolithography Printing, ACS Appl. Mater. Interfaces 15 (2023) 38132–38142.
[160] W. Luo, J. Xu, G. Li, G. Niu, K.W. Ng, F. Wang, M. Li, Fabrication of robust, anti-reflective, transparent superhydrophobic coatings with a micropatterned multilayer structure, Langmuir 38 (2022) 7129–7136.
[161] D.-H. Cho, S.-H. Hong, W.-J. Lee, J.Y. Kim, Y.-D. Chung, Colorful solar cells utilizing off-axis light diffraction via transparent nanograting structures, Nano Energy 80 (2021) 105550.
[162] H.-J. Choi, S. Choo, J.-H. Shin, K.-I. Kim, H. Lee, Fabrication of superhydrophobic and oleophobic surfaces with overhang structure by reverse nanoimprint lithography, J. Phys. Chem. C 117 (2013) 24354–24359.
[163] Y. Yang, H. He, Y. Li, J. Qiu, Using nanoimprint lithography to create robust, buoyant, superhydrophobic PVB/SiO2 coatings on wood surfaces inspired by red roses petal, Sci. Rep. 9 (2019) 9961.
[164] A. Baptista, F. Silva, J. Porteiro, J. Míguez, G. Pinto, Sputtering physical vapour deposition (PVD) coatings: a critical review on process improvement and market trend demands, Coatings 8 (2018) 402.
[165] H. Ejaz, S. Hussain, M. Zahra, Q.M. Saharan, S. Ashiq, Several sputtering parameters affecting thin film deposition, J. Appl. Chem. Sci. Int. 13 (2022) 41–49.
[166] R. Garg, S. Gonuguntla, S. Sk, M.S. Iqbal, A.O. Dada, U. Pal, M. Ahmadipour, Sputtering thin films: materials, applications, challenges and future directions, Adv. Colloid. Interface Sci. (2024) 103203.
[167] C. Ma, L. Wang, X. Fan, J. Liu, Broadband antireflection and hydrophobic CaF2 film prepared with magnetron sputtering, Appl. Surf. Sci. 560 (2021) 149924.
[168] Z. Zuo, J. Gao, R. Liao, X. Zhao, Y. Yuan, A novel and facile way to fabricate transparent superhydrophobic film on glass with self-cleaning and stability, Mater. Lett. 239 (2019) 48–51.
[169] N. Gupta, S. Sasikala, D. Mahadik, A. Rao, H.C. Barshilia, Dual-scale rough multifunctional superhydrophobic ITO coatings prepared by air annealing of sputtered indium–tin alloy thin films, Appl. Surf. Sci. 258 (2012) 9723–9731.
[170] M. Drábik, O. Polonskyi, O. Kylián, J. Čechvala, A. Artemenko, I. Gordeev, A. Choukourov, D. Slavínská, I. Matolínová, H. Biederman, Super-hydrophobic coatings prepared by RF magnetron sputtering of PTFE, Plasma Processes and Polymers 7 (2010) 544–551.
[171] H.-M. Kim, S. Sohn, J.S. Ahn, Transparent and super-hydrophobic properties of PTFE films coated on glass substrate using RF-magnetron sputtering and Cat-CVD methods, Surf. Coat. Technol. 228 (2013) S389–S392.
[172] B. Garrido, I. Cano, S. Dosta, Adhesion improvement and in vitro characterisation of 45S5 bioactive glass coatings obtained by atmospheric plasma spraying, Surf. Coat. Technol. 405 (2021) 126560.
[173] Z. Zhou, Z. Zhang, Y. Chen, X. Liang, B. Shen, Composition optimization of Al-Ni-Ti alloys based on glass-forming ability and preparation of amorphous coating with good wear resistance by plasma spray, Surf. Coat. Technol. 408 (2021) 126800.
[174] M.M. Hossain, Q.H. Trinh, M. Sudhakaran, L. Sultana, Y.S. Mok, Improvement of mechanical strength of hydrophobic coating on glass surfaces by an atmospheric pressure plasma jet, Surf. Coat. Technol. 357 (2019) 12–22.
[175] R. Múgica-Vidal, F. Alba-Elías, E. Sainz-García, J. Ordieres-Meré, Atmospheric plasma-polymerization of hydrophobic and wear-resistant coatings on glass substrates, Surf. Coat. Technol. 259 (2014) 374–385.
[176] M. Saget, N. Nuns, P. Supiot, C. Foissac, S. Bellayer, K. Dourgaparsad, P.-A. Royoux, G. Delaplace, V. Thomy, Y. Coffinier, Ultra-hydrophobic biomimetic transparent bilayer thin film deposited by atmospheric pressure plasma, Surf. Interfaces 42 (2023) 103398.
[177] N. Kenters, E.G. Huijskens, S.C. de Wit, J. van Rosmalen, A. Voss, Effectiveness of cleaning-disinfection wipes and sprays against multidrug-resistant outbreak strains, Am. J. Infect. Control 45 (2017) e69–e73.
[178] K. Kaya, M. Khalil, B. Fetrow, H. Fritz, P. Jagadesan, V. Bondu, L. Ista, E.Y. Chi, K. S. Schanze, D.G. Whitten, Rapid and Effective Inactivation of SARS-CoV-2 with a Cationic Conjugated Oligomer with Visible Light: studies of Antiviral Activity in Solutions and on Supports, ACS Appl. Mater. Interfaces 14 (2022) 4892–4898.
[179] M. Mizuno, J. Matsuda, K. Watanabe, N. Shimizu, I. Sekiya, Effect of disinfectants and manual wiping for processing the cell product changeover in a biosafety cabinet, Regen. Ther. 22 (2023) 169–175.
[180] D.G. Prajapati, A. Mishra, Long-term and fast-bactericidal activity of methacrylamide-based copolymer for antibiofilm coatings and antibacterial wipes applications, J. Appl. Polym. Sci. 141 (2024) e54745.
[181] D. Adak, R. Bhattacharyya, H.C. Barshilia, A state-of-the-art review on the multifunctional self-cleaning nanostructured coatings for PV panels, CSP mirrors and related solar devices, Renew. Sustain. Energy Rev. 159 (2022) 112145.
[182] C. Gümüş, E. Çakmakçi, Oxetane-based transparent anti-smudge coatings via solvent-free spray-deposition and cationic photopolymerization, React. Funct. Polym. (2025) 106171.
[183] Y. Li, X. Shi, W. Bai, J.e. Li, S. Zhu, Y. Li, J. Ding, Y. Liu, L. Feng, Robust superhydrophobic materials with outstanding durability fabricated by epoxy adhesive-assisted facile spray method, Colloids Surf. A 664 (2023) 131109, https://doi.org/10.1016/j.colsurfa.2023.131109.
[184] X. Zhao, D.S. Park, J. Choi, S. Park, S.A. Soper, M.C. Murphy, Robust, transparent, superhydrophobic coatings using novel hydrophobic/hydrophilic dual-sized silica particles, J. Colloid. Interface Sci. 574 (2020) 347–354, https://doi.org/10.1016/j.jcis.2020.04.065.
[185] P. Wang, M. Chen, H. Han, X. Fan, Q. Liu, J. Wang, Transparent and abrasion-resistant superhydrophobic coating with robust self-cleaning function in either air or oil, J. Mater. Chem. A 4 (2016) 7869–7874.
[186] X. Guo, Z. Shao, H. Wang, J. Cheng, Z. Jiang, M. Huang, Y. Wu, C. Ma, C.-H. Xue, Mechanically durable superhydrophobic coating of poly(ethyl cyanoacrylate)/SiO2/polydimethylsiloxane with superior abrasion resistance, Prog. Org. Coat. 186 (2024) 108044, https://doi.org/10.1016/j.porgcoat.2023.108044.
[187] J. Zhi, L.-Z. Zhang, Durable superhydrophobic surface with highly antireflective and self-cleaning properties for the glass covers of solar cells, Appl. Surf. Sci. 454 (2018) 239–248, https://doi.org/10.1016/j.apsusc.2018.05.139.
[188] X.-J. Guo, D. Zhang, C.-H. Xue, B.-Y. Liu, M.-C. Huang, H.-D. Wang, X. Wang, F.-Q. Deng, Y.-P. Pu, Q.-F. An, Scalable and mechanically durable superhydrophobic coating of SiO2/polydimethylsiloxane/epoxy nanocomposite, ACS Appl. Mater. Interfaces 15 (2023) 4612–4622.
[189] A.S.A. Almalki, A. Alhadhrami, A.M.A. Adam, I. Grabchev, M. Almeataq, J.Y. Al-Humaidi, T. Sharshar, M.S. Refat, Preparation of elastic polymer slices have the semiconductors properties for use in solar cells as a source of new and renewable energy, J. Photochem. Photobiol. A 361 (2018) 76–85, https://doi.org/10.1016/j.jphotochem.2018.05.001.
[190] Y. Liu, X. Tan, X. Li, T. Xiao, L. Jiang, S. Nie, J. Song, X. Chen, Eco-friendly fabrication of transparent superhydrophobic coating with excellent mechanical robustness, chemical stability, and long-term outdoor durability, Langmuir 38 (2022) 12881–12893.
[191] T. Zhu, Y. Cheng, J. Huang, J. Xiong, M. Ge, J. Mao, Z. Liu, X. Dong, Z. Chen, Y. Lai, A transparent superhydrophobic coating with mechanochemical robustness for anti-icing, photocatalysis and self-cleaning, Chem. Eng. J. 399 (2020) 125746, https://doi.org/10.1016/j.cej.2020.125746.
[192] O. Kovac, P. Lukacs, T. Rovensky, Software evaluation of cross-cut adhesion testing, in: 2018 41st International Spring Seminar on Electronics Technology (ISSE), IEEE, 2018, pp. 1–5.
[193] H. Luo, M. Yang, D. Li, Q. Wang, W. Zou, J. Xu, N. Zhao, Transparent super-repellent surfaces with low haze and high jet impact resistance, ACS Appl. Mater. Interfaces 13 (2021) 13813–13821.
[194] C. Wu, C. Fang, Investigating the influence of hexafluorobutyl methacrylate on the properties of core–shell polyacrylate latex pressure sensitive adhesives and films, Iran. Polym. J. (2025) 1–12.
[195] A. Allahdini, R. Jafari, G. Momen, Transparent non-fluorinated superhydrophobic coating with enhanced anti-icing performance, Prog. Org. Coat. 165 (2022) 106758, https://doi.org/10.1016/j.porgcoat.2022.106758.
[196] C. Ke, C. Zhang, X. Wu, Y. Jiang, Highly transparent and robust superhydrophobic coatings fabricated via a facile sol-gel process, Thin Solid Films 723 (2021) 138583, https://doi.org/10.1016/j.tsf.2021.138583.
[197] W.-H. Huang, C.-S. Lin, Robust superhydrophobic transparent coatings fabricated by a low-temperature sol–gel process, Appl. Surf. Sci. 305 (2014) 702–709, https://doi.org/10.1016/j.apsusc.2014.03.179.
[198] Y. Zhang, B. Dong, S. Wang, L. Zhao, L. Wan, E. Wang, Mechanically robust, thermally stable, highly transparent superhydrophobic coating with low-temperature sol–gel process, RSC Adv. 7 (2017) 47357–47365.
[199] Z. Chen, X. Liu, Y. Wang, J. Li, Z. Guan, Highly transparent, stable, and superhydrophobic coatings based on gradient structure design and fast regeneration from physical damage, Appl. Surf. Sci. 359 (2015) 826–833, https://doi.org/10.1016/j.apsusc.2015.10.150.
[200] G. Polizos, G.G. Jang, D.B. Smith, F.A. List, M.G. Lassiter, J. Park, P.G. Datskos, Transparent superhydrophobic surfaces using a spray coating process, Solar Energy Mater. Solar Cells 176 (2018) 405–410, https://doi.org/10.1016/j.solmat.2017.10.029.
[201] L. Xu, Z. Geng, J. He, G. Zhou, Mechanically Robust, Thermally Stable, Broadband Antireflective, and Superhydrophobic Thin Films on Glass Substrates, ACS Appl. Mater. Interfaces 6 (2014) 9029–9035, https://doi.org/10.1021/am5016777.

[202] S. Liu, X. Liu, S.S. Latthe, L. Gao, S. An, S.S. Yoon, B. Liu, R. Xing, Self-cleaning transparent superhydrophobic coatings through simple sol–gel processing of fluoroalkylsilane, Appl. Surf. Sci. 351 (2015) 897–903.
[203] S. Sutha, S. Suresh, B. Raj, K.R. Ravi, Transparent alumina based superhydrophobic self–cleaning coatings for solar cell cover glass applications, Solar Energy Mater. Solar Cells 165 (2017) 128–137, https://doi.org/10.1016/j.solmat.2017.02.027.
[204] Z. Liang, Z. Zhou, L. Zhao, B. Dong, S. Wang, Fabrication of transparent, durable and self-cleaning superhydrophobic coatings for solar cells, New J. Chem. 44 (2020) 14481–14489.
[205] S.H. Lee, K.S. Han, J.H. Shin, S.Y. Hwang, H. Lee, Fabrication of highly transparent self-cleaning protection films for photovoltaic systems, Progr. Photovolt. 21 (2013) 1056–1062.
[206] I. Torun, N. Celik, M. Hancer, F. Es, C. Emir, R. Turan, M.S. Onses, Water impact resistant and antireflective superhydrophobic surfaces fabricated by spray coating of nanoparticles: interface engineering via end-grafted polymers, Macromolecules 51 (2018) 10011–10020, https://doi.org/10.1021/acs.macromol.8b01808.
[207] P. Wang, X. Yan, J. Zeng, C. Luo, C. Wang, Anti-Reflective superhydrophobic coatings with excellent durable and Self-cleaning properties for solar cells, Appl. Surf. Sci. 602 (2022) 154408, https://doi.org/10.1016/j.apsusc.2022.154408.
[208] S. Kareem, Y. Xie, T. Li, Y. Ding, E.A. Tsiwah, A.S.A. Ahmed, J. Chen, F. Qiao, Z. Chen, X. Zhao, Base-catalyzed synthesis of superhydrophobic and antireflective films for enhanced photoelectronic applications, J. Mater. Res. Technol. 9 (2020) 3958–3966, https://doi.org/10.1016/j.jmrt.2020.02.022.
[209] P. Wang, H. Wang, J. Li, L. Ni, L. Wang, J. Xie, A superhydrophobic film of photovoltaic modules and self-cleaning performance, Solar Energy 226 (2021) 92–99, https://doi.org/10.1016/j.solener.2021.08.018.
[210] C. Li, G. Chang, S. Wu, T. Yang, B. Zhou, J. Tang, L. Liu, R. Guan, G. Zhang, J. Wang, Y. Yang, Highly transparent, superhydrophobic, and durable silica/resin self-cleaning coatings for photovoltaic panels, Colloids Surf. A 693 (2024) 133983, https://doi.org/10.1016/j.colsurfa.2024.133983.
[211] W. Jin, X. Tan, Q. Dai, T. Li, L. Jiang, T. Xiao, W. Chen, Simple synthesis of weather-resistant and self-cleaning anti-reflective coating for enhancing photovoltaic conversion efficiency, Mater. Sci. Semicond. Process. 184 (2024) 108847, https://doi.org/10.1016/j.mssp.2024.108847.
[212] K.A. Walz, T.D. Hoege, J.W. Duensing, W.A. Zeltner, M.A. Anderson, Field tests of a self-sintering, anti-soiling, self-cleaning, nanoporous metal oxide, transparent thin film coating for solar photovoltaic modules, Solar Energy Mater. Solar Cells 262 (2023) 112560, https://doi.org/10.1016/j.solmat.2023.112560.
[213] R.A. Wahyuono, M.M. Julian, Design and implementation of self-cleaning coated rooftop photovoltaic system supporting energy conservation in small-medium enterprises, J. Sos. Teknol. 4 (2024) 516–526.
[214] R. Guo, Y. Wang, H. Lu, S. Wang, B. Wang, Q. Zhang, Micron-smooth, robust hydrophobic coating for photovoltaic panel surfaces in arid and dusty areas, Coatings 14 (2024) 239. https://www.mdpi.com/2079-6412/14/2/239.
[215] L. Yang, J. Yang, D.-Q. Yang, A durable superhydrophilic self-cleaning coating based on TiO2–SiO2-PAA nanocomposite for photovoltaic applications: long-term outdoor study, Solar Energy Mater. Solar Cells 268 (2024) 112731, https://doi.org/10.1016/j.solmat.2024.112731.
[216] S.C. Pop, V. Abbaraju, B. Brophy, Y.S. Yang, S. Maghsoodi, P. Gonsalves, A highly abrasive-resistant, long-lasting anti-reflective coating for PV module glass, in: 2014 IEEE 40th Photovoltaic Specialist Conference (PVSC), IEEE, 2014, pp. 2715–2719.
[217] D.A. Schaeffer, G. Polizos, D.B. Smith, D.F. Lee, S. Rajic, P.G. Datskos, S. R. Hunter, Spray-on anti-soiling coatings that exhibit high transparency and mechanical durability, in: Sensors, and Command, Control, Communications, and Intelligence (C3I) Technologies for Homeland Security and Homeland Defense XIII, SPIE, 2014, pp. 88–93.
[218] CleanARC(R) Coated Solar Panels for Tough Climates and Harsh Conditions, in, YIGLI SOLAR, 2025, Online, https://www.prnewswire.com/news-releases/yingli-introduces-cleanarcr-coated-solar-panels-for-tough-climates-and-harsh-conditions-300022145.html.
[219] Self-Cleaning Hydrophobic and Antireflective Panels By M/S Suntech Solar, in, Suntech Solar, 2025, Online, www.suntech-power.com/about-us/#section-6e437af.
[220] Atmospheric Plasma Treatment of Solar Panels, Coatings, Films, Cells and Mounting Systems, in, Intrface Technologies, 2025, Online, Atmospheric Plasma Treatment of Solar Panels, Coatings, Films, Cells and Mounting Systems |, INTRFACE TECHNOLOGIES.
[221] Hydrasol For Self Cleaning Solar Panels, in, ADVANCED NanoTech Lab, 2025, Online, https://www.antlab.in/hydrasol-solar-nano-coating.php?product=sent.
[222] D.D. Rooij, Solar Panel Nano Coatings, SINO VOLTAICS, 2025.
[223] DIAMON-FUSION® Protective Solar Panel Coating And Cleaner, in, Diamon-Fusion International, 2025, Online, https://dfisolutions.com/surfaces-we-protect/solar-panels/.
[224] S. Harsh, Solar Panel Coating, in, TriNano Technologies Pvt. Lmt., 2025, Online, http://tri-nano.co.
[225] Revolutionise Energy Production With Nanopool coatings in Solar Parks, in, NANOPOOL, 2025, Online, https://www.nanopool.eu/en/solar/.
[226] Anti-dust/Self-Cleaning Nano-Coating Technology For Solar PV Glass, in, Electrical Research and Development Association, 2025, Online, https://www.erda.org/anti-dust-self-cleaning-nano-coating-technology-for-solar-pv-glass/.
[227] S. V, S. Sakthivel, S.V. Joshi, A Super Hydrophobic Coating with High Optical Properties having Easy to Clean Property, UV and Corrosion Resistance Properties, A Process of Preparation and Application of the Same, in, India, 2021.
[228] F.D. Dong Binghai, W. Shimin, G. Zhiguang, L. Jing, Z. Li, L. Weimin, Transparent Super-Hydrophobic Spraying Agent, and Preparation Method and Application Thereof, Hubei Jiaolian Medical Technology Co ltd, 2015.
[229] C.L. Tian Xuelin, D. Yingying, High-Wear-Resistance High-Transparency Super-Hydrophobic Nano Coating and Preparation Method Thereof, Sun Yat Sen University, 2023.
[230] Z.C. Li Qiang, W. Jinpe, A New Preparation Method For Transparent Superhydrophobic Coating With UV Glue Protection, Liaoning Technical University, 2023.
[231] L.X. Yuan Shaojun, W. Yuan, L. Bin, Preparation Method of Environment-Friendly Low-Cost Transparent Super-Hydrophobic Coating, Sichuan University, 2021.